2013

Synthesis and reactivity of pyridinediimine iron complexes: for the breakdown of carbon dioxide

Zachary Thammavongsy
Western Washington University

Follow this and additional works at: https://cedar.wwu.edu/wwuet

Part of the Chemistry Commons

Synthesis and Reactivity of Pyridinediimine Iron Complexes:
For the Breakdown of Carbon Dioxide

By

Zachary Thammavongsy

Accepted in Partial Completion
Of the Requirements of the Degree
Master of Science

Kathleen Kitto, Dean of the Graduate School

Advisory Committee

Chair, Dr. John D. Gilbertson

Dr. Gregory W. O'Neil

Dr. Clint P. Spiegel

Master's Thesis

In presenting this thesis in partial fulfillment of the requirements for a master's degree at Western Washington University, I grant to Western Washington University the non-exclusive royalty-free right to archive, reproduce, distribute, and display the thesis in any and all forms, including electronic format, via any digital library mechanisms maintained by Western Washington University.

I represent and warrant this is my original work, and does not infringe or violate any rights of others. I warrant that I have obtained written permissions from the owner of any third party copyrighted material included in these files.

I acknowledge that I retain ownership rights to the copyright of this work, including but not limited to the right to use all or part of this work in future works, such as articles or books.

Library users are granted permission for individual, research and non-commercial reproduction of this work for educational purposes only. Any further digital posting of this document requires specific permission from the author.

Any copying or publication of this thesis for commercial purposes, or for financial gain, is not allowed without my written permission.

Zachary Thammavongsy

May 31, 2013

Synthesis and Reactivity of Pyridinediimine Iron Complexes: For the Breakdown of Carbon Dioxide

A Thesis
Presented to
The Faculty of
Western Washington University

In Partial Fulfillment
Of the Requirements for the Degree
Master of Science

By
Zachary Thammavongsy
May 2013

Abstract

The increase of greenhouse gases in our atmosphere, particularly carbon dioxide (CO_2), has been recognized by the scientific, industrial, and political communities. The increase in CO_2 concentration has been connected to negative effects on our environment (global warming). Despite the negative associations of CO_2, chemists can synthesize useful organic products and fuel from it. Ideally, the two electron reduction of CO_2 to CO can provide one of the two products of synthesis gas (CO and H_2), which is used in the Fischer-Tropsch process to produce diesel fuel. This thesis aims to convert CO_2 to CO, using a cheap and abundant metal, Fe. The research presented herein focuses on the redox-active capability of pyridinediimine (PDI) ligands and their promotion of the CO_2-to-CO conversion on Fe(II). Furthermore, the chemical and electrochemical release of CO on Fe(II) has shown to complete the CO_2-to-CO cycle. Additional studies with varying Lewis acids and Lewis bases located within the secondary coordination sphere of the PDIFe complex will be discussed. These studies demonstrated the electronic effects on the reduction-oxidation potential of the CO release in $PDIFe(CO)_2$ complexes.

Acknowledgements

There are numerous friends, staff members, mentors and professors whom I would like to thank; however I would like to acknowledge a few people specifically who contributed to the completion of my graduate career, scientifically, financially and emotionally. First and foremost, I would like to thank my parents, who supported my academic career from the very beginning. My family friends (Andrew, Ali, Joe, Jose, Ryan, Russ and Andrea) for their encouragement throughout this two year endeavour. My fab five brothers (Val, Daniel, Randy and Matt) who made Western Washington University a home. My ligand team (Brandon, Seth, Andy Charile, Yubin and Jillian) for their contribution to my scientific success. My non-ligand team (Eddie, Matt and Darren) for keeping me motivated and focused. My two editors (Anne and Andrea) for their numerous edits for the completion of this thesis. The master's court (Bella, Pat, Casey, Jamie and Stas) for their emotional support. My cousin, Eric, for his wisdom. Charles F. Wandler for his unwavering assistance in every aspect of both my project and educational career. And finally my principle investigator, Dr. Gilbertson, for his guidance and mentorship.

Table of Contents

Chapter 1. Introduction

Chapter 2. Redox Active Ligand

Chapter 3. CO_2-to-CO Conversion

Chapter 4. CO Release

Chapter 5. Conclusion

Chapter 6. Experimental

Tables and Figures

Equations and Schemes

Chapter 1: Introduction

1.1 CO_2 Issues

Climate change, as result of global warming has become a major focus of government, public, and corporate debate due to its world-wide consequences. Such consequences include, but are not limited to, adverse effects on agriculture, oceanic wildlife and living conditions of human beings.[1,2] With respect to agriculture, Wilbanks and coworkers believe that severe climate change will negatively affect food productions necessary to sustain the growing population.[3] In terms of oceanic wildlife, a variety of species are suffering from the gradual temperature elevations. For example, reductions in the abundance of two species of pteropod (planktonic marine molluscs) and of bivalve larvae are apparent in large-scale survey data for the northeastern Atlantic over the period 1960–2007.[4] Lastly, for human beings, climate change can mean exposure to more severe weather events (hurricanes, tsunami and droughts). The rise of sea-level can impact the popultation and its distribution, resource consumption and waste disposal, which affect global and regional economies.[2]

The Intergovernmental Panel on Climate Change (IPCC) has placed a 2 ^{o}C increase limit on temperature rise (since the pre-industrial period) in order for human living conditions to be tolerable. However, due to the rising of the average global temperature

(0.74 ± 0.18 °C over the period of 1906 through 2005), the perdicted 2 °C increase limit is projected to pass within this decade (**Figure 1.1**).[5]
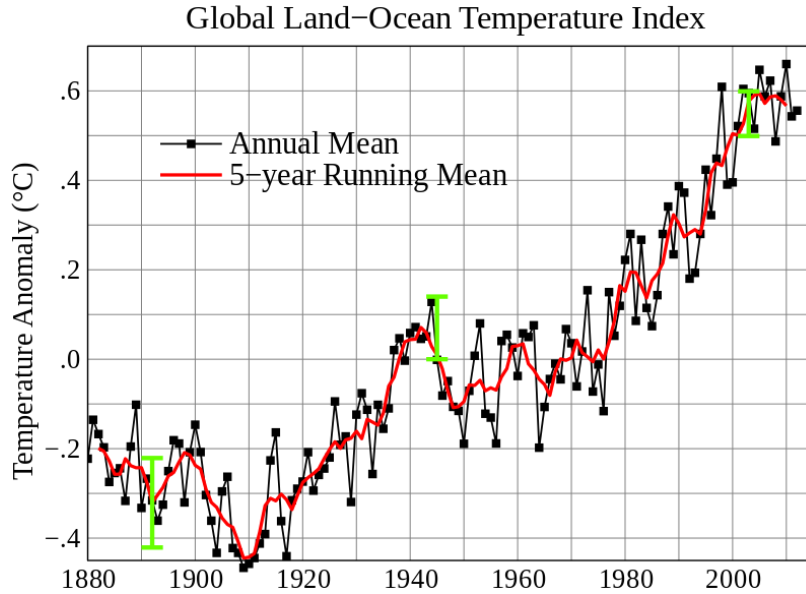
Figure 1.1. Global surface temperature change from 1880 to 2010, reported as a deviation from 1951-1980 average. The black curve shows the globally and annually averaged near-surface temperature derived from a variety of instruments including thermometers, satellites, and various ocean sensors. The green bar indicates the 95% confidence interval. The red curve shows a five year running average.[5]

This increase in temperature has been accompanied by the rise in greenhouse gases such as carbon dioxide (CO_2), water (H_2O), methane (CH_4), and nitrous oxide (NO).[6] This accumulation of greenhouse gases forms a layer between our atmosphere and outer space, preventing infrared (IR) energy (black body radiation from Earth) to escape from our planet, consequently warming the globe. Of the greenhouse gases, CO_2 is considered to play the biggest role in global warming.[7] Although carbon dioxide is not the most effective

2

greenhouse gas, in terms of radioactive trapping, it is by far the most abundant (**Figure 1.2**).[8]

Presently, the amount of CO_2 in our atmosphere has reached 400 parts per million (ppm), which is a historic milestone.[9] The last time the worldwide CO_2 level reached 400 ppm was approximately 10 million years ago, according to the National Oceanic and Atmospheric Administration.[9] Scientists and environmental groups support 350 ppm as a safe level for CO_2, however, due to numerous variables that contribute to this crisis, scientists cannot make a definite prediction of what levels would stop the effects of global warming. Despite the lack of predictability, the underlying message is clear, that the levels of CO_2 and the temperature of our planet are intimately connected.
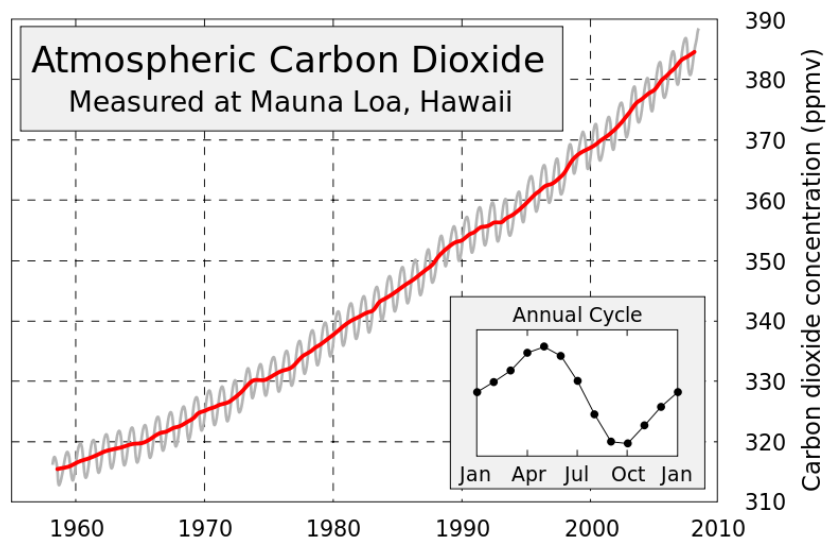
Figure 1.2. The Keeling Curve showing the increase of atmospheric CO_2 concentrations (in ppm by volume) from 1958-2008. The inset figure illustrates monthly CO_2 measurements, displaying seasonal oscillations.[9]

The increase in CO_2 concentration can be directly correlated to human activities. In 2011, the use of electricity in the United States accounted for 35% of all CO_2 emission (2.25 billion metric tons of CO_2) (**Figure 1.3**).[10] Most of the electricity is generated by coal combustion (representing 42% of electricity generated and 80% of all CO_2 emission from the electrical sector). While other energy sources, such as nuclear, generated 19% of all US electricity and produced less greenhouse gas emissions than coal or fossil fuel combustion.[10] The use of coal for electricity, rather than a cleaner source such as nuclear, is driven by cost; consequently, coal power plants will continue to operate.
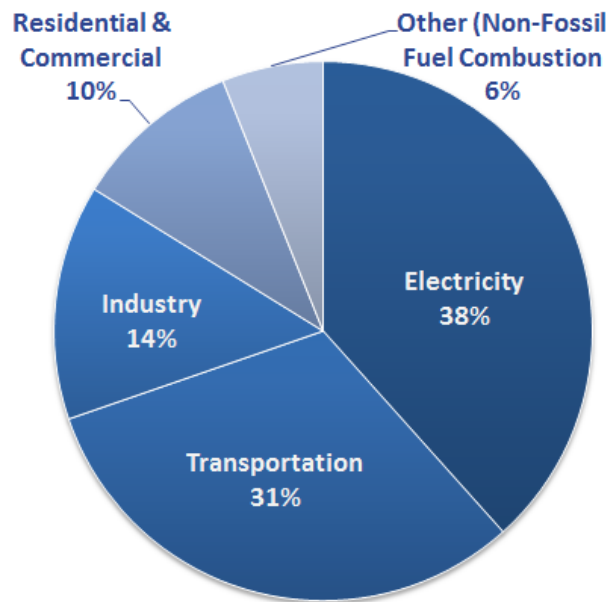
Figure 1.3. A Pie diagram of CO_2 emission from various human activities within the United States of America, in 2011. This diagram was taken from the Environmental Protection Agency.[10]

Coal and fossil fuel are composed of hydrocarbons (C_xH_y), which are long chain organic molecules consisting of carbon and hydrogen. When hydrocarbons combust in the presence of oxygen (O_2), carbon-oxygen (in CO_2) and hydrogen-oxygen (in H_2O) bonds are produced, which releases energy to power our cars and heat our homes (**eq. 1**). Every hydrocarbon burned can be simplified down to a combustion reaction, in which CO_2 is ultimately derived from human beings. Therefore, it is the responsibility of human beings to lessen the impact of CO_2 on the environment.

$$C_xH_y \quad + \quad (x + \frac{y}{4})\,O_2 \quad \longrightarrow \quad xCO_2 \quad + \quad \frac{y}{4}H_2O \quad + \quad Energy \qquad (1)$$
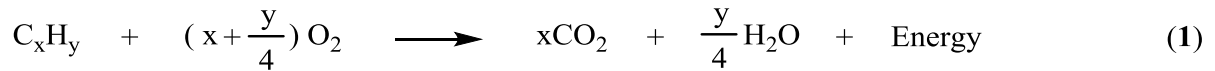
1.2 CO$_2$ Utilization

Despite the mitigation of CO_2 from terrestrial carbon fixation (1/3 of all CO_2 in the atmosphere) by plants, algae and cyanobacteria, and the uptake of CO_2 by the ocean (2 billion metric tons of CO_2 per year), the amount of CO_2 in our atmosphere continues to increase each year (~3 ppm per year, in the last ten years).[11,12] Therefore, methods have been sought and implemented for the recovery and disposal of CO_2 from point-continuous sources, such as power plants and industries for the elimination of large volumes of CO_2.[13] The capture of CO_2 from the flue gases of coal, oil, or gas-fired power plants and from industrial processes use liquids, such as monoethanolamine (MEA), which is commercially

available.[14] MEA is a weak base, which interacts with acidic compounds, such as CO_2 under cold conditions. This interaction occurs in solution to sequester CO_2, and once the solution is heated, CO_2 is re-released. The release of CO_2 is done in natural sites, such as: aquifers, deep geological cavities, spent oil or gas-fields, coal-mines, or the ocean.[15] However, CO_2 capturing technology such as MEA is only implemented at the million metric ton level, while the release of CO_2 from industry operates on the billion metric ton level.

Another method to reduce the amount of CO_2 released into our atmosphere is through the recycling of CO_2 into valuable chemicals, such as urea, methanol and inorganic compounds (pigments). Approximately 110 million metric tons per year of CO_2 is converted into chemicals (roughly 1% of the annual release of CO_2 by the human population). Leading the way is the production of urea (with 70 million metric tons per year), which is a key component of fertilizer for food development, promotion of rehydration of the skin in dermatological products and a primary building block for plastic materials.[16] Inorganic carbonates and pigments use about 30 million metric tons of CO_2 each year for cleaning and preservation, as well as for the manufacture of glass. Carbonates can be synthesized from the reaction of CO_2 and epoxides.[16] A very important chemical, methanol, can also be synthesized from CO_2 with the help of an inorganic catalyst. Methanol production utilizes 6 million metric tons of CO_2 each year and can be used as a fuel or further used for the production of plastics, plywood, paints, explosives and permanent press textiles.[17] CO_2 has also found applications as a fluid in dry-cleaning, refrigerators, air conditioners, fire-

6

extinguishers, separation techniques, water treatment and the food- or agro-chemical industries.[18] These chemicals and others, that are derived from CO_2 are highlighted in **Scheme 1.1**.[19-21] With the exception of methanol, most of the chemicals derived from CO_2 are purely thermal based processes, owning to the thermo-stability of the CO_2 molecule.
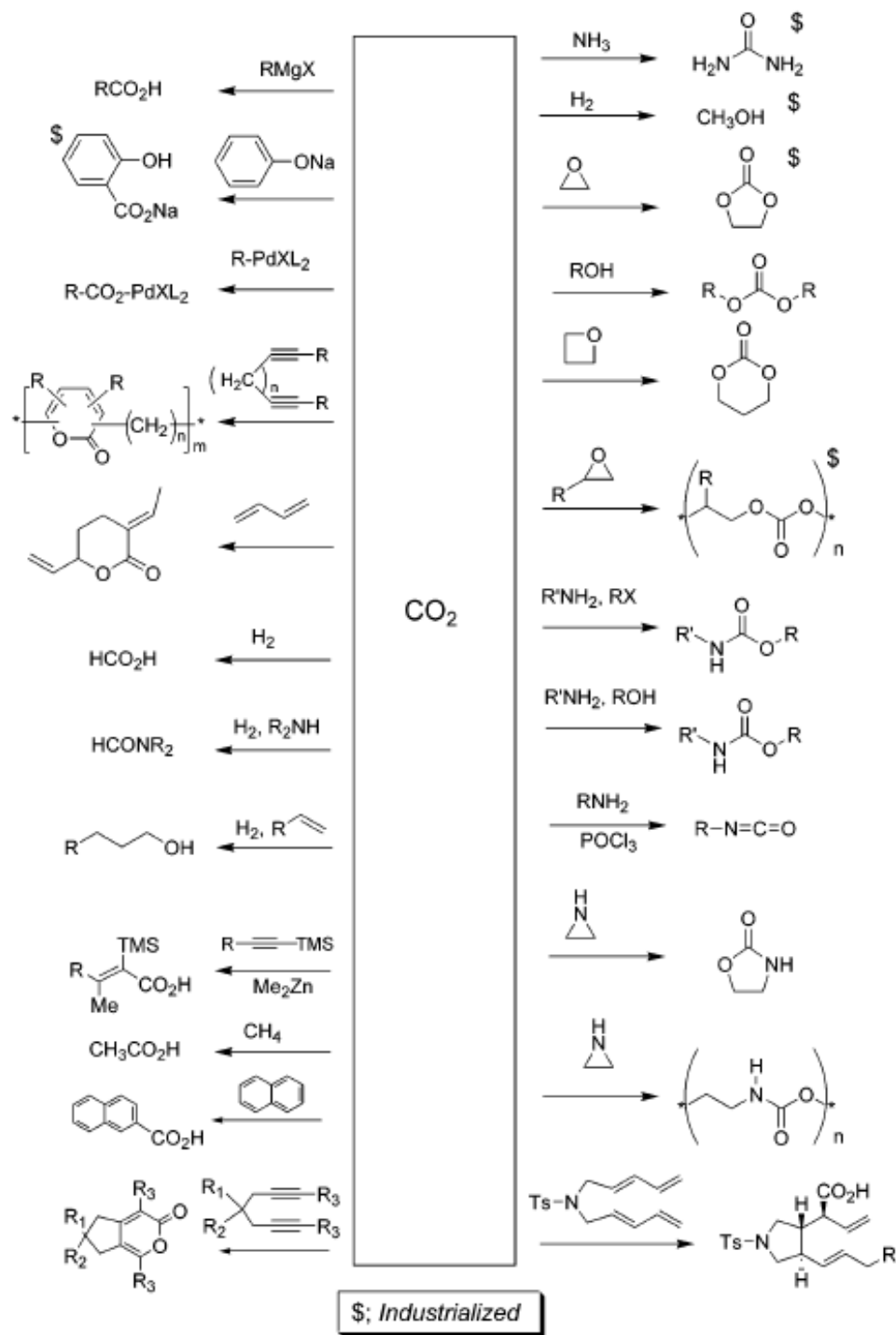
Scheme 1.1. Desirable chemicals derived from CO_2. This scheme was taken from Sakaura and coworkers.[19] The $ symbol in the scheme represents the industrialized chemicals from CO_2.

8

1.3 CO_2: The Molecule

Thermodynamically, CO_2 is very stable, with an enthalpy of formation of gaseous CO_2 of -393.5 kJ/mol at 0 ^{o}C and 100 kPa (STP) (compared to H_2O which is -285.8 kJ/mol at STP). Furthermore, the bond dissociation energy of the double bond (C=O) of CO_2 is even higher, at 532 kJ/mol.[22] CO_2 is also kinetically inert, requiring -1.90 volts to reduce CO_2 by one electron. Therefore, the high activation barrier, coupled with the large bond enthalpy of CO_2 makes the breakdown of CO_2 a difficult task.

CO_2 is a linear, centrosymmetric molecule with a $D_{\infty h}$ symmetry and has a total bond order of four (two σ and π bonds) (**Figure 1.4**).[23] Although CO_2 is non-polar overall, it does have a partial positive carbon center with two partial negative oxygen atoms (**Figure 1.5**). These key features play a vital role towards the reactivity of CO_2, as well as its eventual breakdown and transformation.
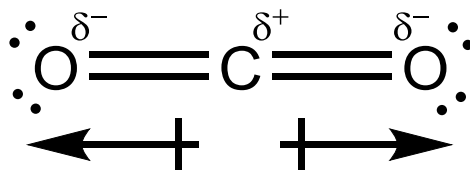
Figure 1.5. The CO_2 molecule displays a partial positive center and negative edge, which allows chemists to access the chemistry of CO_2.

9
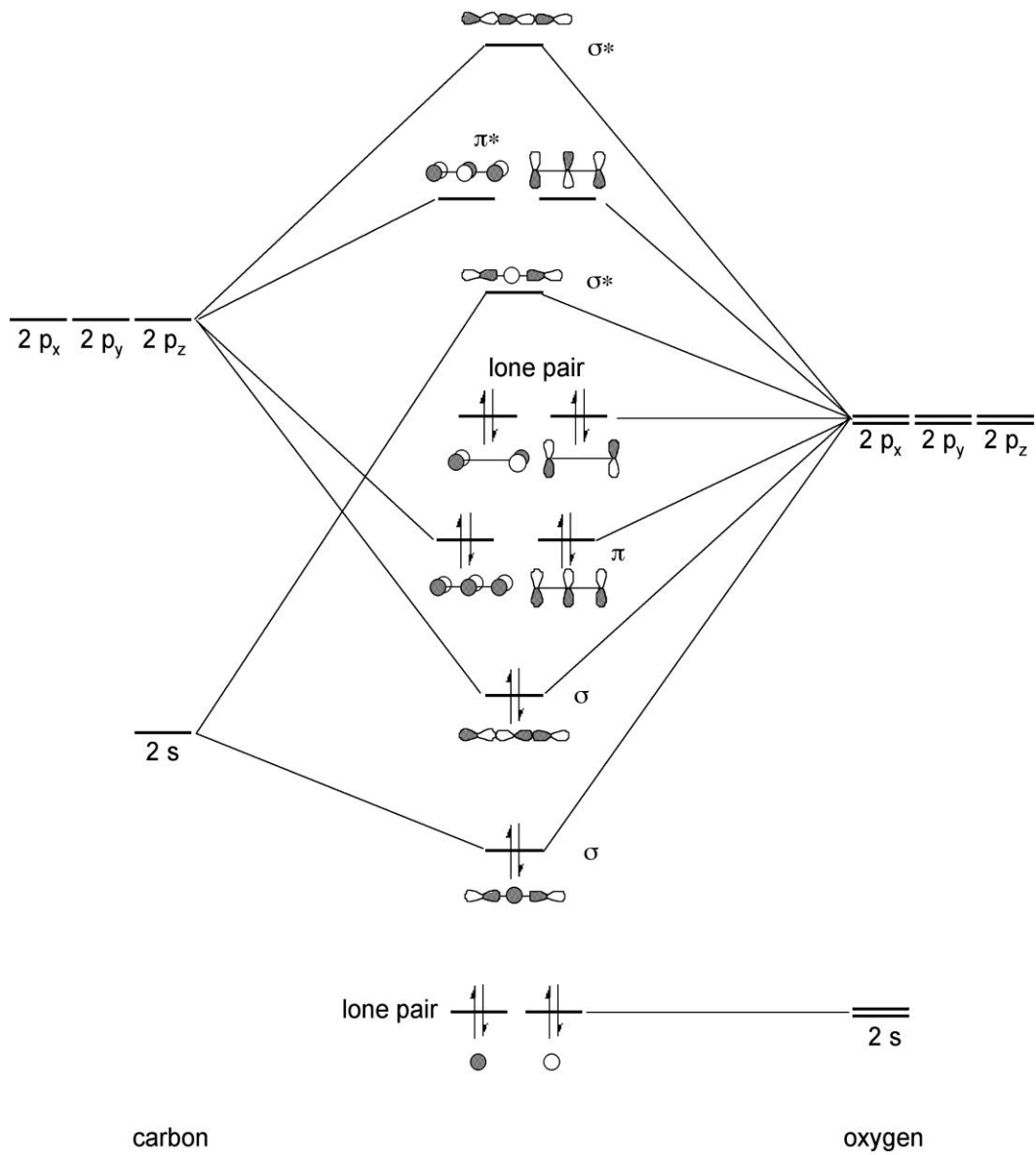
Figure 1.4. The molecular orbital diagram of CO_2, displaying the four lone pair and the four bonding orbitals.[23]

1.4 CO_2 breakdown to CO (Biologically and Industrially)

With the known information regarding the characteristics of the CO_2 molecule, it is clear that the breakdown of CO_2 to CO is rather difficult. However, anaerobic bacteria and archaea (oxygen sensitive) and aerobic bacteria (not oxygen sensitive) have evolved to reversibly catalyze the reaction of CO with H_2O to form CO_2, protons, and electrons with a high turnover frequency (40,000 s^{-1}) and catalytic efficiency (2.0 x 10^9 M^{-1} s^{-1}) (**eq. 2**).[24]

$$CO \quad + \quad H_2O \quad \longleftrightarrow \quad CO_2 \quad + \quad 2\,H^+ \quad + \quad 2e^- \qquad\qquad (2)$$

These bacteria and archaea contain the enzyme carbon monoxide dehydrogenase (CODH), which catalyzes the breakdown of CO_2. The binding of CO_2 takes place within the active site of these enzymes. For example, anaerobic bacteria use a Ni-Fe active site where the nickel acts as a Lewis base and performs a nucleophilic attack at the partial positive carbon center of CO_2. The Fe acts as a Lewis acid and binds to the partial negative charge on the oxygen of CO_2 (**Figure 1.6**). Also, the CO_2 molecule is further stabilized through hydrogen bond interactions with neighboring amino acid residues located on the backbone of the enzyme.[25] The positions of the Ni and Fe are held in place by the Fe_3S_4 framework and are essentially unchanged by the presence or absence of CO_2. The cluster also serves to act as an electronic buffer, stabilizing the electronic charges on Fe and Ni during the catalytic cycle.
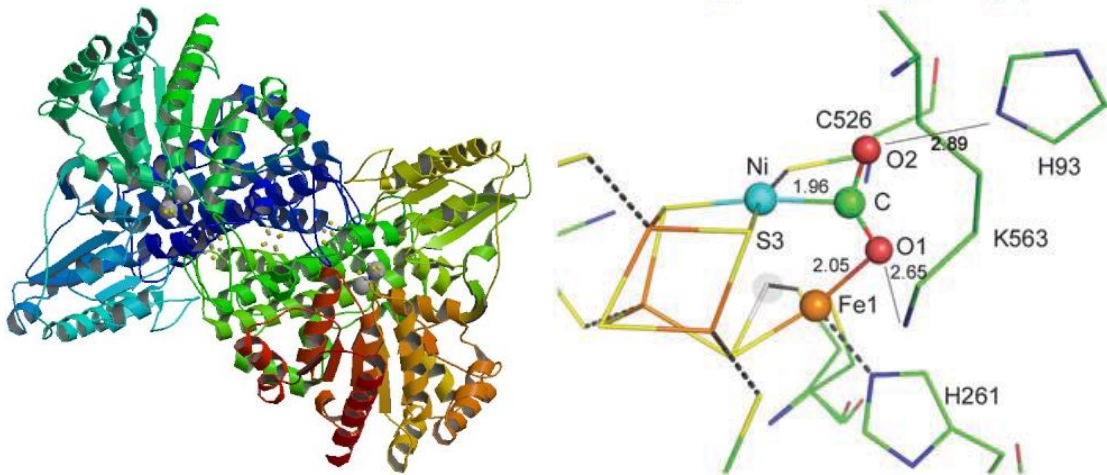
Figure 1.6. Crystal structure of the CODH enzyme (left) and its active site (right), isolated from the bacteria of Rhodospirillium rubrum. The active site shows how the metals bind to CO_2. Images taken from Dobbek and coworkers.[25]

Despite information regarding the biological breakdown of CO_2, industries thermally breaks down CO_2 to CO through the dry reforming process (**eq. 3**). The dry reforming plants require 247.1 kJ per mole of CO_2, in order to produce two molecules of CO. This process produces a mixture of CO and hydrogen gas (H_2), which combined are referred to as synthesis gas (syngas).[26] Syngas is desirable due to its use as an industrial feedstock, particularity in the Fischer-Tropsch (FT) process to produce diesel fuel.[27] Effectively, an efficient way to breakdown the greenhouse gas, CO_2, to a desirable chemical that is a key component to diesel production, CO, would be an ideal scenario for a carbon neutral world. Using the information provided by CODH, chemists can gain insights on how to breakdown CO_2 to CO (one half of syngas).

$$CH_4 \;+\; CO_2 \;\longleftrightarrow\; 2\,CO \;+\; 2\,H_2 \qquad\qquad (3)$$

12

1.5   Fischer-Tropsch Process

Although the ultimate goal of this thesis is on the conversion of CO_2-to-CO, it is worth mentioning the final utility of CO. CO and H_2 gas combined, are the starting materials for the FT process for the production of diesel fuel (**eq. 4**). The FT process is a well-known and well-proven process that utilizes either Fe or Co based catalysts.[27] Currently, the FT process operates in two modes, the high-temperature (300-350 ^{o}C) with an Fe-based catalyst or a low-temperature (200-240 ^{o}C) with either Fe or Co based catalyst. The high-temperature mode is geared towards the production of gasoline and linear low molecular mass olefins, while the low-temperature mode can produce high molecular mass linear waxes.[27] The FT hydrocarbons are also promising alternatives to conventional gasoline and diesel, because they are totally free of sulfur and contain very few aromatics.[28]

$$(2n + 1)\, H_2 + n\, CO \xrightarrow{\text{Fe or Co}} C_nH_{(2n+2)} + n\, H_2O \qquad (4)$$

The FT process is primarily a heterogeneous reaction, where the metal based catalyst is in the solid phase, reacting with high pressurized syngas. Efforts have been made to produce a homogenous catalyst (same phase reaction) for the FT process, largely due to better selectivity and easier modification of the catalyst when compared to heterogeneous catalysts. Early transition metal hydrides, and more recently rare earth polyhydride and actinide complexes, have shown remarkable reactivity towards CO.[29-31] For example, Bercaw

and coworkers have suggested a multi-component system, where their approach involved

the use of two reactive metal centers. A rhenium carbonyl complex with pendant borane

moieties serves as the binding site for CO, while a hydrido-bis(diphosphine) platinum

complex acts to provide the hydride (**Figure 1.7**).[32]
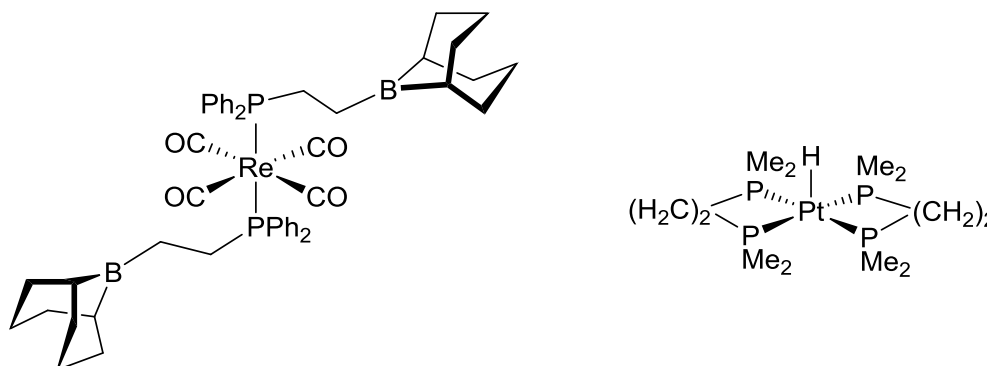
Figure 1.7. Structure of Bercaw's system towards the production of hydrocarbon from CO and hydride.[$12]

1.6 CO_2 breakdown to CO (In the laboratory)

Ultimately, the goal of this thesis is also to make a homogenous catalyst, for the

breakdown CO_2 to CO, utilizing the functionalities of CODH. Inorganic chemists have found

their own route towards utilizing inorganic complexes for the reduction of CO_2 to CO. Some

find inspiration from enzymes[33-35] while others start fresh or build upon older works.[36-38]

There are two classes of reactions which will be discussed within this subchapter, first the

electrochemical reduction of CO_2 to CO, and second, the chemical reduction of CO_2 to CO.

The use of various metals (Ru, Rh, Pd, Fe, Ni, Cu and Co) and ligand scaffolds (bipyridine, macrocyclic and phosphine ligands) have been employed by several groups.[39-44] Of these metal complexes, Savéant and coworkers utilized highly abundant, cheap metal ions for CO_2 reduction, with turnover numbers as high as 350 h^{-1}. However, this system required reduction potentials that are still too negative for practical use (-1.5 V vs. SCE) (**Figure 1.8**).[36] Other notable electrochemical catalysts for the reduction of CO_2 to CO are the polydentate phosphine palladium complexes, which were synthesized by Dubois and coworkers (**Figure 1.8**).[44] This class of complex displayed catalytic rates in the range of 10 to 300 $M^{-1} s^{-1}$ with higher than 90% current efficiencies for CO production. The Pd^I species was proposed to bind the CO_2 molecule, then upon addition of electrons and protons (from acidic acetonitrile solution), the production of CO and H_2O was observed. Lastly, Kubiak and coworkers tested the bipyridine rhenium complexes for the reduction of CO_2 to CO and found the tert-butyl substituents have the best rate constant of 1000 $M^{-1} s^{-1}$ and Faradaic efficiency of 99% (**Figure 1.8**).[45] The tert-butyl group played a role in tuning the electronics of the metal, to prevent Re dimers, which would ultimately discontinue catalytic activity.

Savéant   Kubiak   Dubois
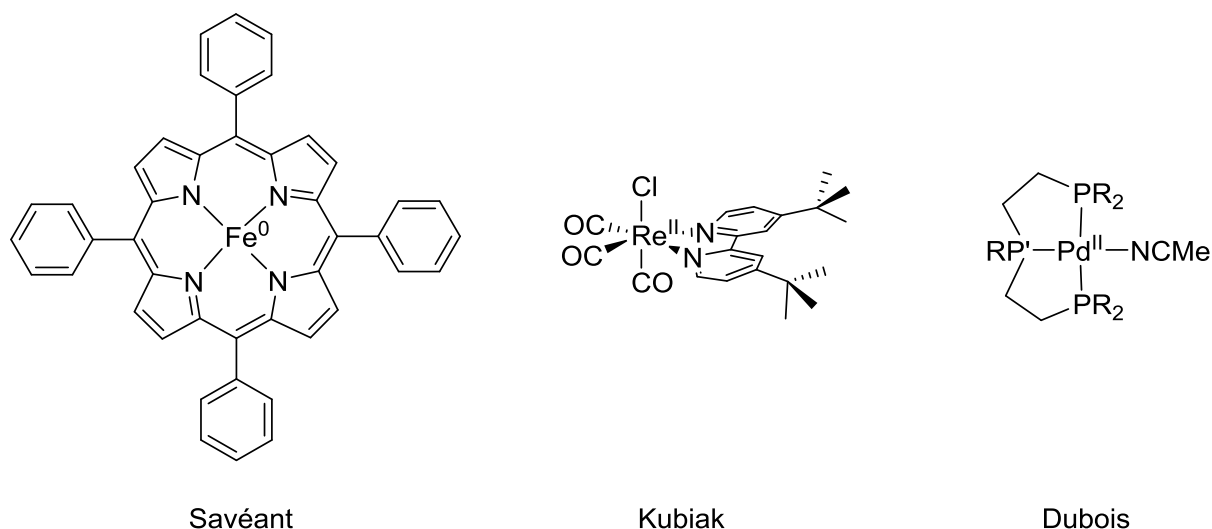
Figure 1.8. Notable electrochemical catalysts that reduce CO_2 to CO.[36,44,45]

Chemical reduction of CO_2 to CO has also been shown, generally for the elucidation of CO_2 binding modes and mechanistic studies. Peters and coworkers has shown a reduction of CO_2 to CO, with minor CO_2 coupling on a tris(phosphine)borate Fe(I) complex (**Figure 1.9**).[46] However, there was no release of CO from Fe in this system. Holland and coworkers also utilized an Fe(I) center for the reduction of CO_2 to CO, with the help of a 2,2,6,6-tetramethyl-3,5-bis-[2,6-diisopropylphenyl)imino]hept-4-yl ligand. They showed that CO_2 can be cleaved to produce two bound products, CO and CO_3^{2-} (**Figure 1.9**).[47] Again, this system does not release CO nor promote CO transformation. Lastly, Cummins and coworkers displayed the conversion of CO_2 to CO by the ligand (nitride), which was bound to a niobium center (**Figure 1.9**).[48] They elaborately designed a system that prevents the CO_2 molecule from binding to the metal center. Instead, their model allowed the CO_2 molecule

16

to bind to the Lewis base, nitride. The importance of the partial positive charge on the carbon of CO_2 allows the nitride's lone pair to perform a nucelophilic attack. Cummins and coworkers also observed the release of CO, with the addition of oxygen atom acceptors. The design of the ligand has proven to affect the chemistry of the CO_2 reduction, which Cummins displayed with his nitride ligand, and also from Kubiak, with his tert-butyl substituents on the bipyridine ligand. Therefore, ligand design will continue to be an integral part of catalysis and inorganic chemistry.

| Cummins | Holland | Peters |
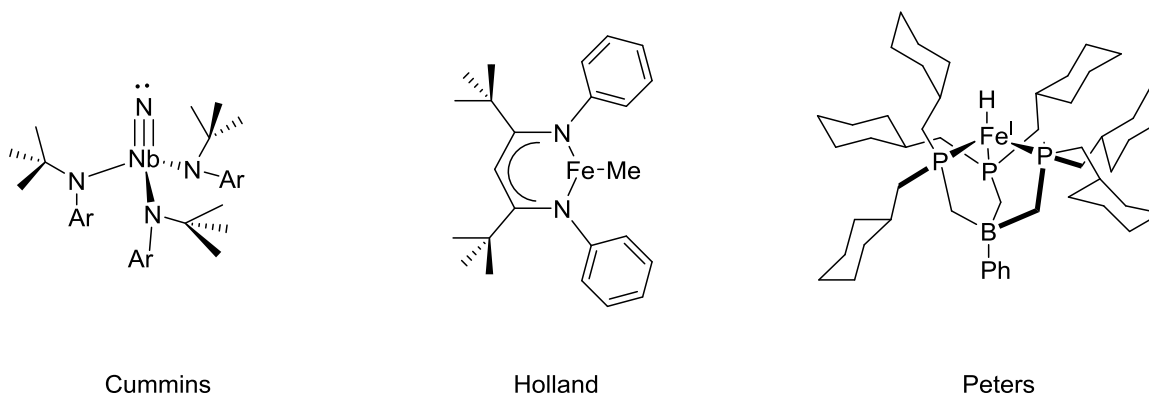
Figure 1.9. Catalysts that reduces CO_2 to CO, chemically.[46-48]

1.7 Ligand Design (Redox Active Ligands)

Although the metal center is key for CO_2 reduction, other factors, such as the ligand (the organic framework that surrounds the metal ion) can also play a big role in the

17

reduction. Functionalizing the secondary coordination sphere of the ligand may affect the binding modes of CO_2, similar to the amino acid residues of the CODH enzyme. Ligands can also tune the electronics of the metal center to affect the overall catalytic rate of the catalyst, similar to Kubiak's bipyridine rhenium catalyst.[46] Ultimately, the reduction of CO_2 to CO requires two electrons, and those two electrons are primarily supplied by the metal center. Cummins and coworkers have proved that the ligand can provide the two electrons necessary for C=O cleavage; this system sets the stage for further investigation into designing ligands that can supply electrons, similar to the FeS cluster of CODH.[25] Redox-active ligands have been intensively researched and have shown to affect the catalytic rates of metal complexes. One such redox-active ligand is the pyridinediimine (PDI), which will be the ligand of focus for this thesis (**Figure 1.10**).
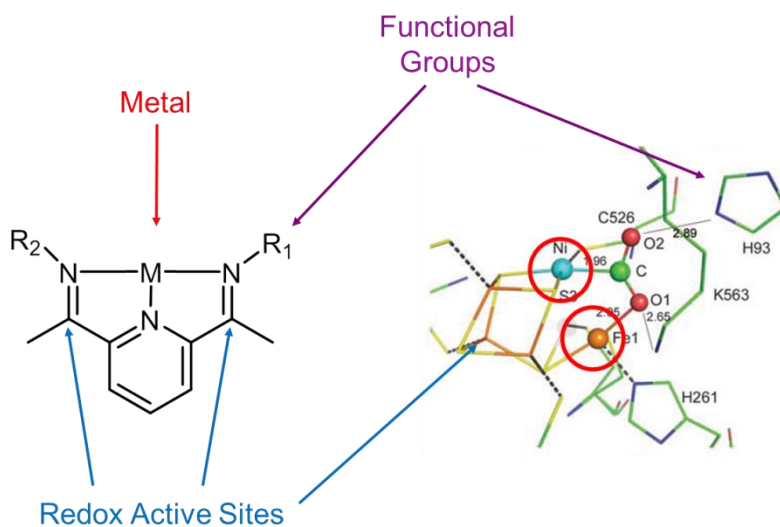
Figure 1.10. The structure (left) represents the pyridinediimine metal complex, showing the versatility of this ligand system to mimic the CODH enzyme (right).[25]

The purpose of this thesis is to contribute to the copious collection of the known CO_2 to CO reductions, utilizing studies on the redox-active PDIFe(II) complex. This work will describe the CO_2 cleavage on a Fe(II) metal ion, through the facilitation of the reduced PDI ligand. The PDI ligand will also incorporate functionalized groups, located within the secondary sphere, in order to influence the binding and releasing of CO on Fe, for the completion of the CO_2-to-CO cycle

1.8 References

1. Folely, J.A.; Defries, R.; Asner, G.P.; Barford, C.; Snyder, P.K. *Science*, **2005**, 309 570-574.
2. Seibel, B.A.; Walsh, P.J. *Science*, **2001**, 294, 319-320.
3. Wilbanks, T.J.; Kates, R.W. *Annals Ass. Am. Geo.* **2010**, 100, 4, 719-728.
4. Economides, M.; Xie, X. *Chem. Enginerring Progress*. **2009**, 105, 6, 20-25.
5. Committee on America's Climate Choices; National Research Council, *Americans Climate Choices*, 2011, The National Academies Press.
6. Marks, T. J. *Chem. Rev*. **2001**, 101, 953-996.
7. The National Academy of Science, *Understanding and Responding to Climate Change*, 2008, The National Academies Press.
8. The National Academy of Science, *Carbom Management: Implications for R & D in the Chemical Sciences and Technology*, 2001, The National Academies Press.
9. U.S. Department of Commerce, "Trends in Atmospheric Carbon Dioxide." National Oceanic and Atmospheric Administration, 28, May, 2013.
10. U.S. Environmental Protection Agency, "Overview of Greenhouse Gases." Environmental Protection Agency, 28, May, 2011
11. Ragsdale, S. W. *Crit. Rev. Biochem. Mol. Biol*. **2004**, 39, 165.
12. Lindahl, P. A. *Biochemistry*. **2002**, 41, 2097.
13. Reay, D.; Hewitt, N.; Grace, J.; Smith, K. A. *Greenhouse Gas Sinks ed*. 2007, CABI Book Inc.
14. Allan, R. J.; Bredesen, R.; Drioli, E.; Aresta, M. *Carbon Dioxide Recovery and Utilization, ed.* 2003, Kluwer Academic Publisher, pp. 53–118.
15. Gale, J.; Kaya, Y. *Greenhouse Gases Technologies*, *ed*. 2002, Pergamon Press.
16. Krase, N.W.; Gaddy, V.L. *Ind. Eng. Chem*. **1922**, 14, 7, 611-615
17. Kim, J.; Henao, C. A.; Johnson, T. A.; Dedrick, D. E.; Miller, J. E.; Stechel, E. B.; Maravelias, C. T. *Energy Environ. Sci*. **2011**, 4, 3122-3132.
18. Vansant, J.; Aresta, M. *Recovery and Utilization of Carbon Dioxide*, ed. 2003, Kluwer Academic Publishers, pp. 3-50.
19. Sakaura, T.; Choi, J.; Yasuda, H. *Chem. Rev*. **2007**, 107, 2365-2387
20. Ricci, M.; Aresta, M. *Recovery and Utilization of Carbon Dioxide, ed*. 2003, Kluwer Academic Publishers, pp. 395–402.
21. Aresta, M.; Galatola, M. J. *Cleaner Prod*. **1999**,7, 181–193.
22. Heats of formation taken from: CRC Handbook, 92nd ed.; http://www.hbcpnetbase.com/.
23. Housecroft, C. E.; Sharpe, A. G. *Inorganic Chemistry, 3rd edition*, 2008, Pearson Education Limited, Edinburgh.
24. Svetlitchnyi, V.; Peschel, C.; Acker, G.; Meyer, O. J. *Bacteriol*. **2001**, 183, 5134.
25. Jeoung, J. H.; Dobbek, H. *Science*, **2007**, 318, 1461.
26. Zhou, H.; Cao, Y.; Zhao, H.; Lin, H.; Pan. W.P. *Energy & Fuels*, **2008**, 22, 2341-2345.
27. Fan, M. S.; Abdullah, A. Z.; Bhatia, S. *Chem. Cat.* **2009**, 1, 192-208.

28. Larson, E.D.; Jin, H. *Proceedings of the Fourth Biomass Conference Americas*, 1999, Kidlington, UK.

29. Wolzanski, P. T.; Bercaw, J. E. Acc. *Chem. Res*. **1980**, 13, 121-127.

30. Matsuo, T.; Kawaguchi, H. *J. Am. Chem. Soc.* **2005**, 127, 17198.

31. Summerscales, O.; Cloke, F.; Hitchcock, P.; Green, J.; Hazari, N. *Science*, **2006**, 311, 829.

32. Miller, A.; Labinger, J. A.; Bercaw, J. E. *J. Am. Chem. Soc*. **2008**, 130, 11874-11875.

33. Pickett, C. J.; Best, S. P. *Coord. Chem. Rev*. **2005**, 249, 1517–1690.

34. Tezuka, M.; Yajima, T.; Tsuchiya, A.; Matsumoto, Y.; Uchida, Y.; Hidai, M. *J. Am. Chem. Soc*. **1982**, 104, 6834.

35. Takuma, M.; Ohki, Y.; Tatsumi, K. *Inorg. Chem*. **2005**, 44, 6034.

36. Bhugun, I.; Lexa, D.; Saveant, J. M. *J. Am. Chem. Soc.* **1996,** 118, 1769.

37. Grodkowski, J.; Neta, P.; Fujita, E.; Mahammed, A.; Simkhovich, L.; Gross, Z. *J. Phys. Chem.* **2002**, 106, 4772.

38. Hawecker, J.; Lehn, J. M.; Ziessel, R. J*. Chem. Soc. Chem. Commun*. **1984**, 328.

39. Meshitsuka, S.; Ichikawa, M.; Tamaru, K. *J. Chem. Soc. Chem. Commun.* **1974,** 158.

40. Fisher, B.; Eisenberg, R. *J. Am. Chem. Soc.* **1980**, 102, 7361.

41. Beley, M.; Collin, J. P.; Ruppert, R.; Sauvage, J. P. *J. Chem. Soc. Chem. Commun*. **1984**, 1315.

42. Ishida, H,; Tanaka H.; Tanaka, T. *Organometallics*. **1987**, 6,181.

43. Bolinger, C. M.; Story, N.; Sullivan, B. P.; Meyer, T. J. *Inorg. Chem*. **1988**, 27, 4582.

44. Raebiger, J. W.; Turner, J. W.; Noll, B. C.; Curtis, C. J.; Miedaner, A.; Cox, B. DuBois, D. L. *Organometallics*. **2006**, 25, 3345.

45. Smieja, J. M.; Kubiak, C. P. *Inorg. Chem*. **2010**, 49, 9283-9289.

46. Lu, C. C.; Saouma, T.; Day, M. W.; Peters, J. C*. J. Am. Chem. Soc*. **2007**, 129, 4-5.

47. Sadique, A. R.; Brennessel, W. W.; Holland, P. L. *Inorg. Chem*. **2008**, 47, 784-786.

48. Silvia, J. S.; Cummins, C. C. *J. Am. Chem. Soc*. **2010**, 132, 7, 2169-2171.

49. Bouwkamp, M. W.; Bowman, A. C.; Lobkovsky, E.; Chirik, P. J. *J. Am. Chem. Soc.* **2006**, 128, 13340–13341.

Chapter 2. Redox Active Ligands

2.1   Ligands (Conventional View)

In coordination chemistry, a ligand is an ion or molecule that binds to the central metal atom to form a coordination complex (metal complex). Nobel prize winner Alfred Werner pioneered the basic concepts of coordination chemistry with his octahedral configuration of transition metal complexes, such as the trans-$[Co(NH_3)_4Cl_2]^+$ and cis-$[Co(NH_3)_4Cl_2]^+$ (**Figure 2.1**). The bonding between the metal and the ligand generally involves dative bonds, where the ligand (Lewis base) donates two electrons to the metal (typically a Lewis acid).
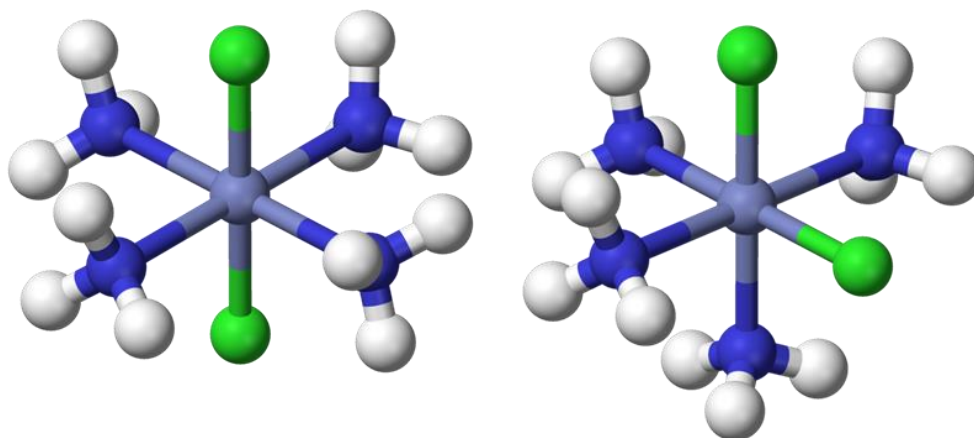
Figure 2.1. Ball and Stick structure of Alfred Werner's trans-$[Co(NH_3)_4Cl_2]^+$ (left) and cis-$[Co(NH_3)_4Cl_2]^+$ (right). The central atom is Co, and the surrounding molecules/atoms are called ligands.

Conventionally, ligands are viewed as having secondary roles in reactivity, such that changing the steric and electronic properties of the ligands can influence the performance of the metal center.[1] A classic example of how ligand steric affects the reactivity of a metal complex can been seen in the "picket fence" iron porphyrin complex. In this case, Robinson and coworkers designed bulky tert-butyl groups on the ends of the porphyrin and an imidazole group on the unhindered side of the porphyrin to close out the binding site of Fe on one end.[2] The picket fence design was intended to discourage bimolecular reactions involving two Fe ions and dioxygen. The bulky picket fence porphyrin permitted only small molecules, such as O_2, to pass through and bind to the Fe center, and prevented another Fe center (from another porphyrin) to complete a bridging oxo complex (**Figure 2.2**).
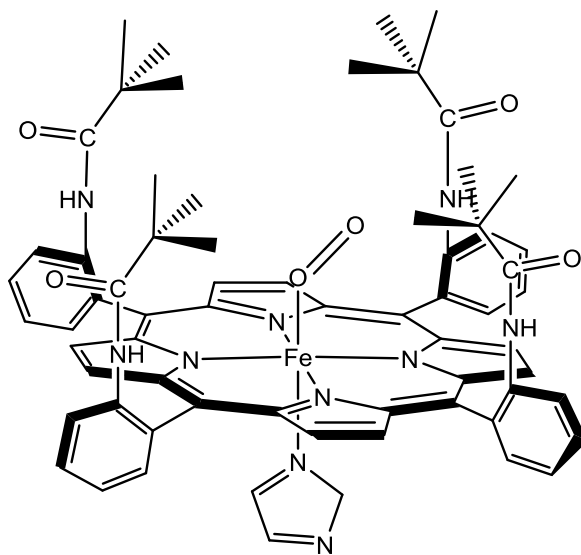
Figure 2.2. Structure of the picket fence iron porphyrin, displaying the steric bulk design of the ligand, meant to prevent iron oxo dimers.[2]

Ligand electronic effects have been well categorized into the spectrochemical series, where ligands are ordered based on their ligand field strength (**Figure 2.3**). The ligand field strength provides insight into how ligands modify the highest occupied molecular orbital – lowest unoccupied molecular orbital (HOMO-LUMO) gap. The HOMO-LUMO gap is the energy gap between the ground state and the next available excited state of the metal complex. This is also called the crystal-field splitting parameter, which can be quantified by measuring the color of the metal complex in Ultraviolet-visible (UV-Vis) spectroscopy.[3] Thus, the overall trend of the spectrochemical series of ligands is that a smaller HOMO-LUMO gap of the metal complex corresponds to weaker field ligands while a larger HOMO-LUMO gap of the metal complex corresponds to stronger field ligands.

$$\xleftarrow{\text{Weak Field (small energy difference)}} \quad \triangle \quad \xrightarrow{\text{Strong Field (large energy difference)}}$$

$$I^- < Br^- < S^{2-} < SCN^- < Cl^- < NO_3^- < N_3^- < F^- < OH^- < H_2O < NH_3 < NO_2^- < PPh_3 < CN^- < CO$$
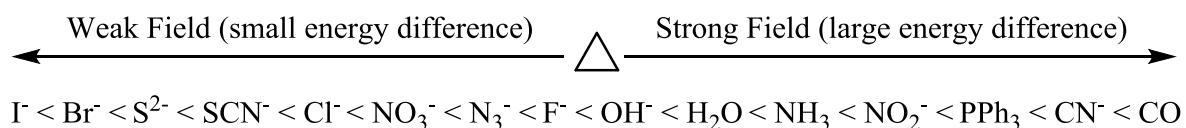
Figure 2.3. Spectrochemical series, showing the field strength of selected ligands.

2.2   Ligands (Non-Conventional View)

Recently, new approaches have emerged that deviate from the conventional concept that ligands predominantly play a secondary role in catalysis. This new approach comes from reactive ligands, which performs a more prominent role in the catalysis of

metal complexes. With reactive ligands, elementary bond-making and bond breaking steps at a rather distant position from the metal can take place and/or ligands can cooperate with metals in a synergistic manner to facilitate chemical processes.[4]

Such ligand involved bond making and bond breaking steps can be seen in Cummins and coworkers example of the nitride ligand, which is bound to a d^0 niobium center and participates in the reduction of CO_2.[5] The design of the niobium complex prevents CO_2 molecules from binding to the metal center, as is normally preferred for small molecules. Due to the electron poor niobium center and the electron rich nitride, the partial positive charge on the carbon of CO_2 binds only to the nitride ligand. With the addition of oxygen atom acceptors, such as acid anhydride, and sacrificial reducing agents, such as sodium amalgam, a closed cycle of CO_2-to-CO was generated (**Scheme 2.1**)
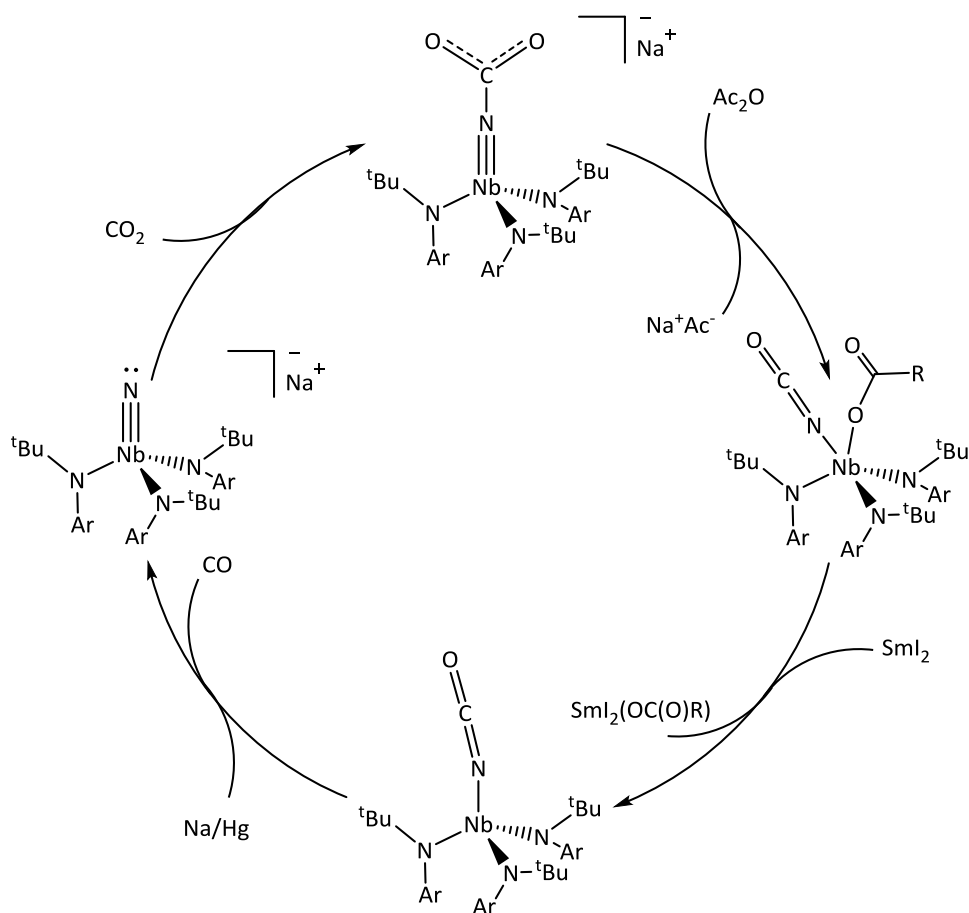
Scheme 2.1. Cummins and coworkers' CO_2-to-CO cycle on a nitride anion ligand.[5]

Additionally, a synergistic approach can be seen in Borovik's catalytic reduction of dioxygen to water using a monomeric Mn(II) complex. Here, the ligand is comprised of carboxyamido groups that can hydrogen bond to the bound dioxgyen molecule. The hydrogen bond interactions, via the ligand, help facilitate the reduction of dioxygen to water by stabilizing the highly reactive monomeric Mn-O complex. Addition of sacrificial reductants, such as diphenylhydrazine or hydrazine, supply the electrons and protons needed to complete the reduction to H_2O (**Scheme 2.2**).[6]

26
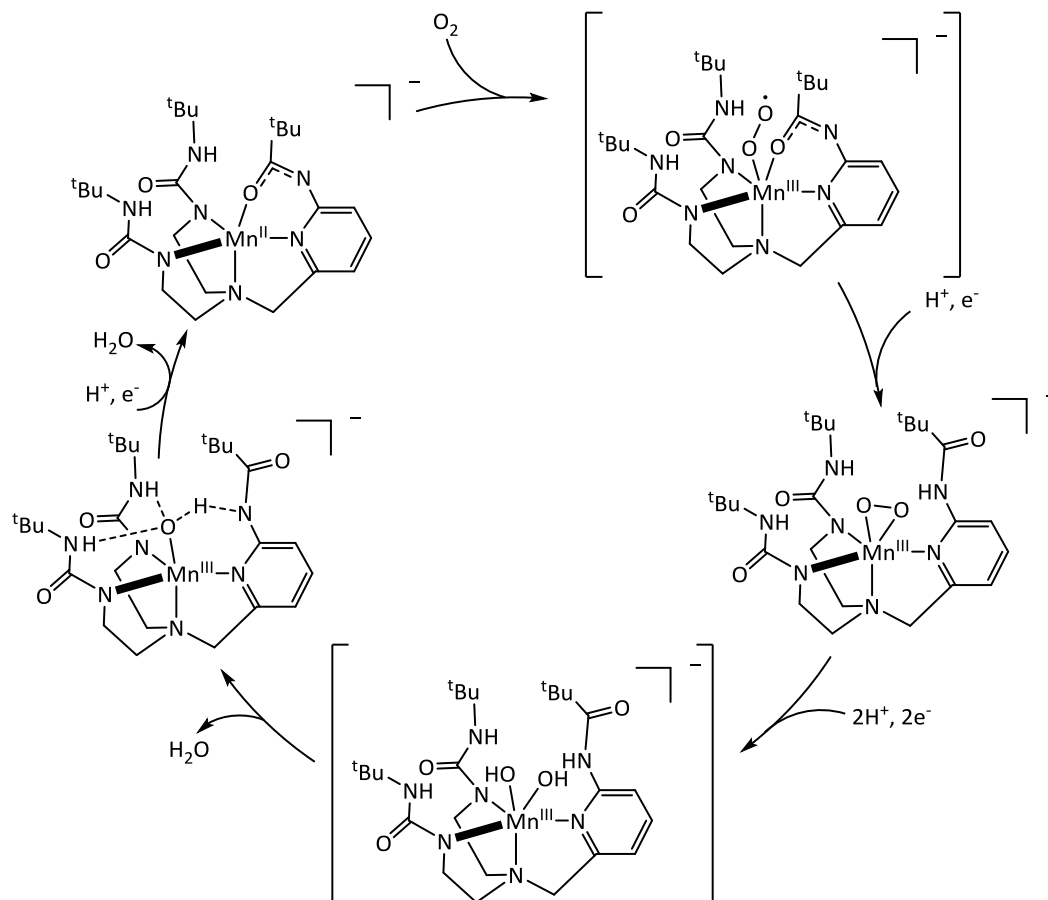
Scheme 2.2. Borovik and coworkers' O_2 to H_2O cycle using a monomeric Mn(II) complex. The mechanism highlights the hydrogen bond between one carboxyamido group from the ligand and the oxygen atom from dioxygen, in order to stabilize the complex for further reduction to H_2O.[6]

Lastly, Wieghardt and coworkers reported a dimer Cu^{II}-thiophenyl complex, which does not only catalyze the oxidation of primary alcohols to aldehydes in the presence of air, but also promotes the formation of diols from secondary alcohols (**Scheme 2.3**).[7] The catalytic cycle involves the oxidation of the Cu complex by O_2, which leads to a ligand-based biradical specie. The coordination of two (deprotonated) secondary alcohols occurs and the α-hydrogen atom is transferred to the oxygen-centered radicals of the aminophenol ligand.

27

The radicals are then positioned on the carbon of the alcohols before radical dimerization

and elimination of the diol. [8]
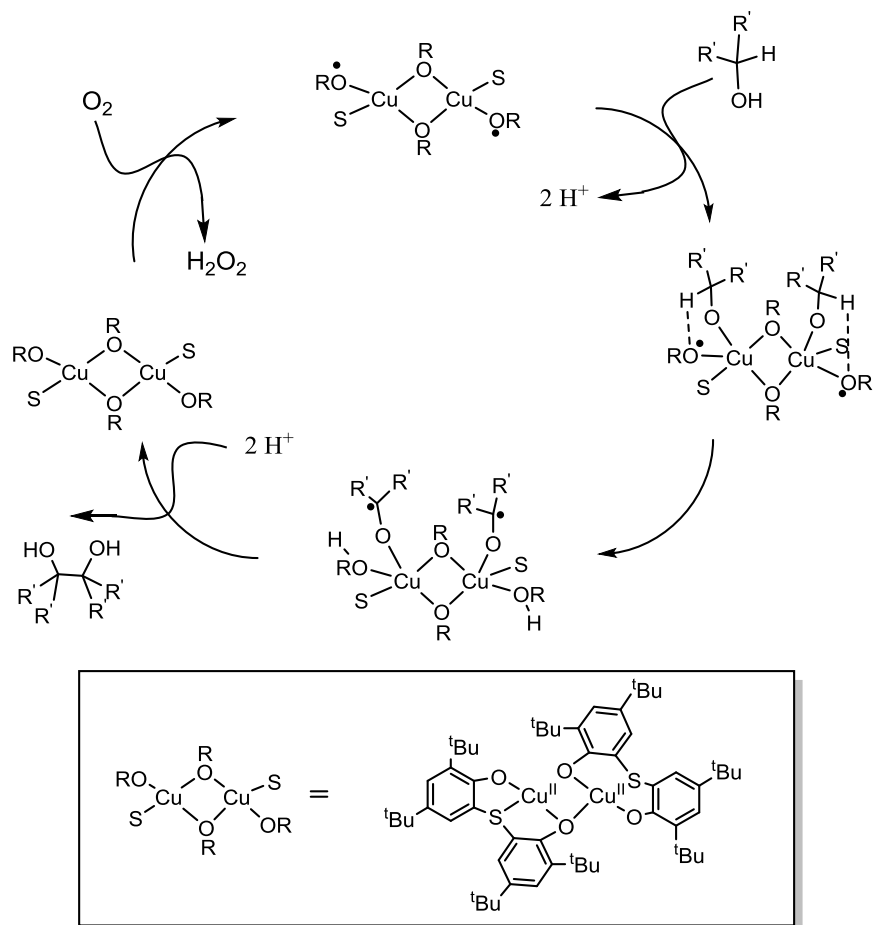
Scheme 2.3. Wieghardt and coworkers' formation of diols from secondary alcohols using a dimer Cu^{II}-thiophenol complex. Hydrogen bonding and radical formation via the thiophenol promote the catalytic cycle.[8]

2.3 Ligands (Redox Active)

With respect to Weighardt's example, the radicals positioned within the oxygen atoms of the thiophenol ligand helped facilitate the last step of the reaction. The thiophenol ligand pertains to a new sub-class of reactive ligands called redox-active ligands. Redox-active ligands are of great interest in the field of catalysis due to their role in facilitating multi-electron transfer reactions. Multi-electron reactions are normally achieved by precious metals, since they typically undergo ± two electron oxidation state changes. However, precious metals are incredibly costly, especially on the industrial scale. Therefore, cheap and abundant first row transition metals that can promote the same types of reactions are fervently sought by chemists. The problem is that first row transition metals tend to undergo ± one electron oxidation state changes.[9] Due to potential radical intermediates and the formation of side products, successive one electron transfers must be avoided. Chirik and Wieghardt have proposed that redox active ligands may be able to confer nobility (act like noble metals) on first row transition metals by combining a one electron redox change at the ligand and a one electron redox change at the metal for an overall two electron change.[9]

The two electron oxidation of alcohols is possible with a redox inactive metal such as Zn(II), when redox active ligands are bound. A prime example is shown with Wieghardt's salen Zn(II) complex, that oxidizes primary alcohols to aldehydes and reduces O_2 to H_2O_2 by

29

two electrons (**Scheme 2.4**).[10] The salen ligand allows the Zn(II) complex to store an oxidizing equivalent in its highly conjugated framework. Futhermore, the compound is able to reversibly coordinate a primary alcohol and participate in a slow H-atom abstraction, followed by the formation of a transient α-hydroxyradical that can go on to eliminate the aldehyde product. The resulting reduced salen Zn(II) complex can be re-oxidized with atmospheric O_2, thus liberating H_2O_2. This same chemistry was also observed with a Cu analogue.[10]
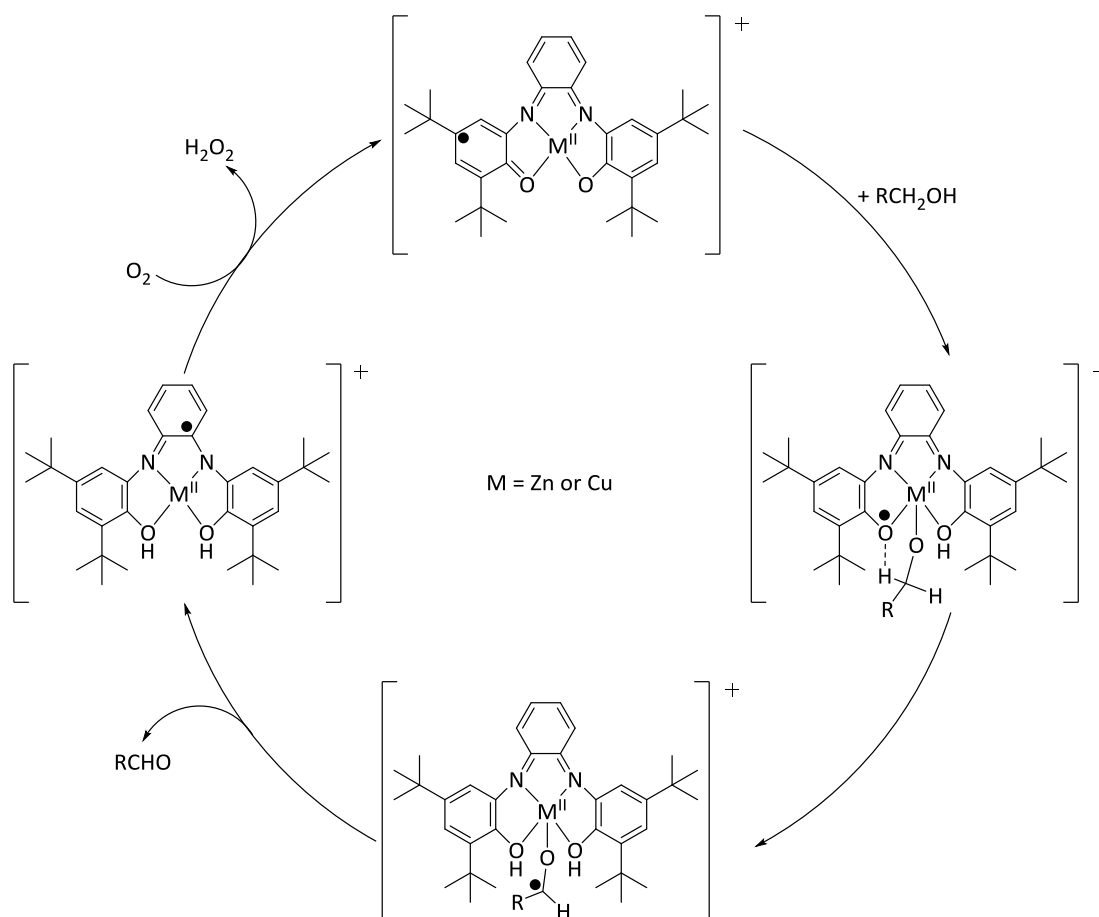
Scheme 2.4. The two electron oxidation of primary alcohols to aldehydes on Wieghardt's redox inactive metal (Zn) with the help of a redox active salen ligand.[10]

Another system that utilized a d^0 metal complex is Heyduk's bis(2-isopropylamido-4-methoxyphenyl)amide ([NNN^{cat}]) Zr(IV) complex, which participate in the catalytic transfer of nitrene.[11] One tert-butyl isocyanide (CN^{t}Bu) dissociates from the [NNN^{cat}]Zr(IV)(CN^{t}Bu)$_2$Cl complex to open up a reactive site in which p-tert-butylphenyl azides can bind. At room temperature, N$_2$ gas is generated as well as the carbodiimide bound [NNN^{cat}]Zr(IV)Cl complex. Addition of one more CN^{t}Bu group completed the nitrene transfer to obtain the product ^{t}BuN=C=N^{t}Bu and the catalyst [NNN^{cat}]Zr(IV)(CN^{t}Bu)$_2$Cl. The two electrons transfer was derived from the [NNN^{cat}] ligand, allowing the Zr metal center to remain in its IV oxidation state (**Scheme 2.5**).
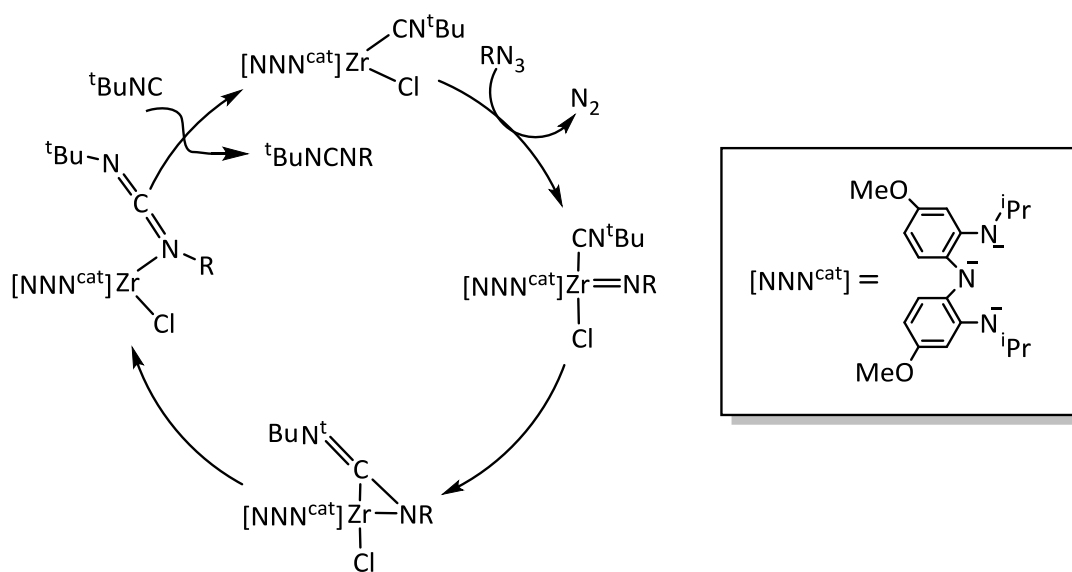
Scheme 2.5. Heyduk's catalytic cycle for nitrene transfer on a Zr(IV) complex.[11] R represents tert-butyl groups.

Another example of how redox active ligands play a prominent role in catalysis is in C-C bond formation. Soper and coworkers have developed a catalytic C-C bond formation using the first row transition metal, cobalt.[12] Their bis-iminophenolate cobalt(III) complex is able to accommodate the formal pseudo-oxidative addition of an alkyl fragment to yield a five-coordinate square pyramidal Co(III) complex. In 2011, Bruin and coworkers highlighted the bis-iminophenolate ligand in Angewandte Chemie's highlight as an electron reservoir, which can store and release electrons without changing the oxidation state of the metal center.[13] Thus, the five-coordinate square pyramidal Co(III) complex has an antiferromagnetically coupled bis-iminophenolate ligand diradical, due to the ligand induced nucleophilic abstraction of the positive alkyl fragment by the Co center. The reaction is followed by a group transfer reaction, either to aryl or alkyl zinc halides to yield the C-C coupled products (**Scheme 2.6**). This reaction showcases the rich chemistry of redox-active ligands that can access first row transition metal catalysis in catalytic cross coupling reactions, a process which has been dominated by expensive metal catalyst, such as Negishi's zinc-based palladium catalyzed cross-coupling.[14]
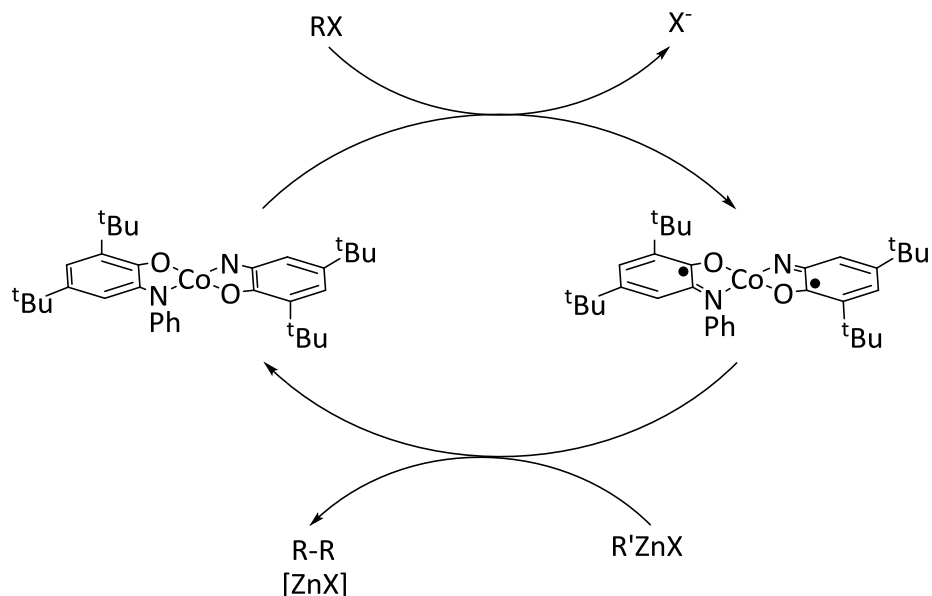
Scheme 2.6. Soper and coworkers' catalytic cycle for C-C bond formation by a redox-active bis-iminophenolate Co(III) complex. The bis-iminophenolate ligand assists the cobalt center to accommodate the formal pseudo-oxidative addition of an alkyl fragment.[12]

2.4   Pyridinediimine Ligands

Chirik and coworkers made significant advancement in the application of Fe(II) catalyzed [2 + 2] cycloaddition reactions using redox active 2,6-pyridinediimine (PDI) ligands.[15] As shown in **Scheme 2.7,** the bis-dinitrogen Fe(II) complex binds the diene substrate in an end-on fashion to form a π-complex. Both complexes contain a diradical dianionic PDI ligand.[16,17] The bound diene Fe(II) complex undergoes a two electron oxidative addition to produce an oxidized PDI Fe(II) complex. The electrons required for this transformation come from the ligand rather than the Fe center, allowing for Fe to maintain

a +2 oxidation state. Subsequently, the oxidized PDI Fe(II) complex undergoes a two electron reductive elimination reaction to liberate the product. The two electrons are again positioned within the PDI ligand, leading to the regeneration of the starting material. Once more, the electron-storage capacity of the PDI ligand allows the metal to maintain its stable Fe(II) oxidation state (avoiding the less favorable Fe(IV) oxidation state).
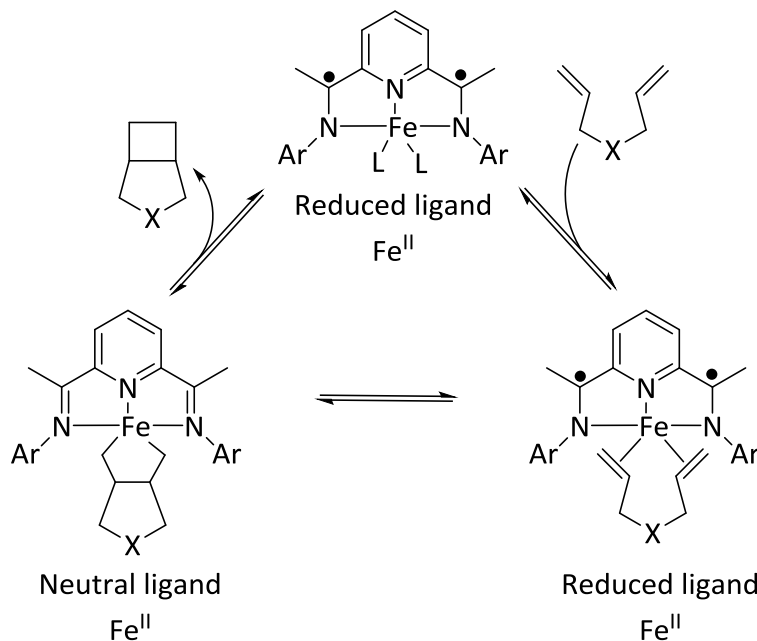
Scheme 2.7. Chirik and coworkers [2 + 2]- cycloaddition reactions using a redox active pyridinediimine Fe(II) complex.[15]

Related pyridinediimine Fe(II) complexes have also been studied for catalyzing enyne cyclization, intermolecular [2 + 2] cycloadditions of alkenes to butadienes, and olefin polymerization.[18-21] The PDI system has been extensively studied with various ligands (weak

and strong field ligands) and it has been found that the PDI Fe complex can access up to three electrons (**Scheme 2.8**).[22]
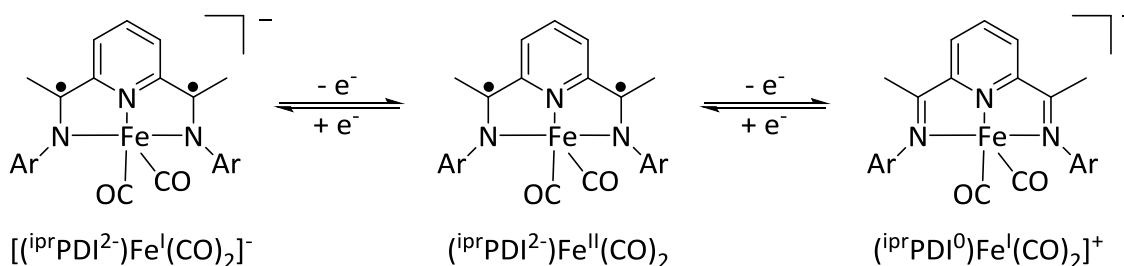
Scheme 2.8. ^{ipr}PDIFe(CO)$_2$ complex displaying its three, two and one electron reduced state.

In this thesis, the study of PDI Fe(II) complexes will be applied to the two electron reduction of CO$_2$ to CO and the chemical/electrochemical redox events involved in the release mechanism of CO. The PDI ligand system was employed due to the ease of its synthesis, high modification and production of high product yields. The main PDI ligand used within this thesis is the [(2,6-^{i}PrC$_6$H$_3$)N=CMe)(2-MeO-6-MeC$_6$H$_3$)N=CMe)C$_5$H$_3$N] (^{MeO}PDI) compound and will be discussed in greater detail.

35

2.5   Synthesis and Characterization of ^{MeO}PDI Ligand

The synthesis of the ^{MeO}PDI ligand started with the commercially available chemicals, diacetylpyridine and 2,6-diisopropyl aniline. These starting materials were mixed (in a 1:1 mole ratio) together and dissolved in methanol. Formic acid was then added under an ice bath, to catalyze the Schiff base condensation reaction. After 1 hour of stirring in an ice bath, the solution was placed in the refrigerator for 2 days to yield yellow precipitates of compound **1**, [(2,6-^{i}PrC$_6$H$_3$N=CMe)(O=CMe)C$_5$H$_3$N] (^{MeO}PDI) (**eq. 5**).[19] The work-up involved filtering the yellow solid of **1** through a buchner funnel and washing with dry methanol, to obtain an 80% yield of **1**.

(5)
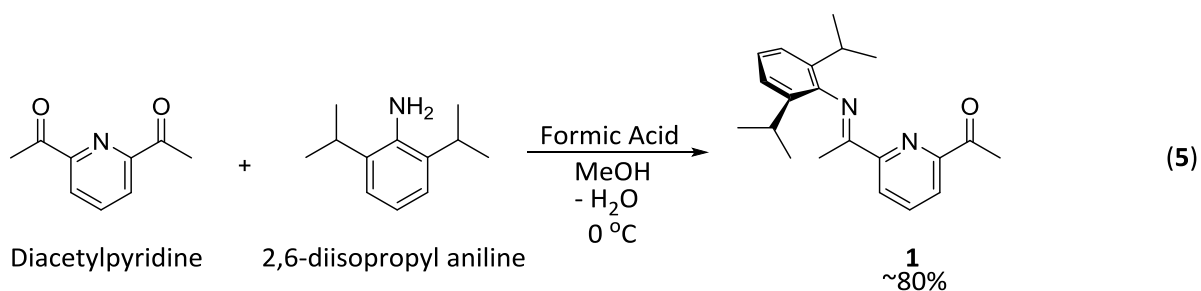
Infrared (IR) and nuclear magnetic resonance (NMR) analysis of compound **1** confirmed the identity. IR displayed a carbonyl (C=O) stretching frequency at 1698 cm^{-1} and an imine (C=N) stretching frequency at 1647 cm^{-1}, owing to the Schiff based reaction (**Figure 2.4**)
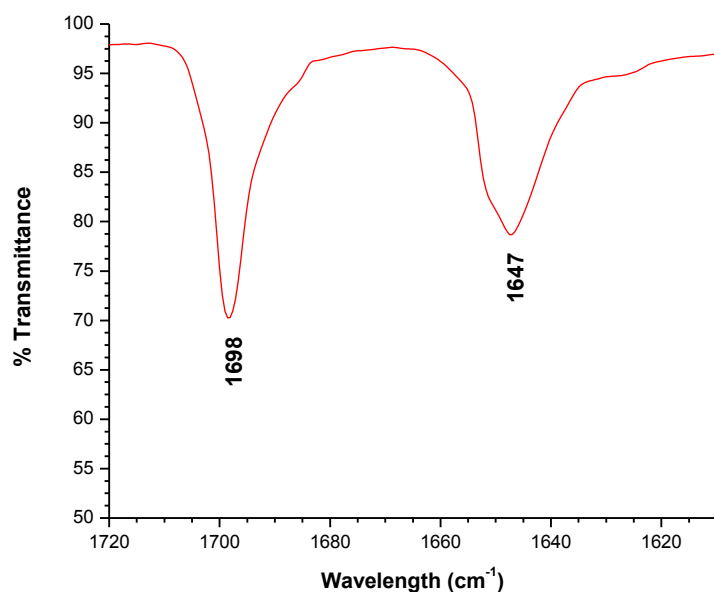
Figure 2.4. IR spectrum of compound **1**. Highlighting the C=O and C=N stretching frequencies.

The ^{1}H NMR showed the appearance of a septet at 2.69 ppm, with an integration of 2 protons (**Figure 2.5**). This resonance was due to the protons from the isopropyl group, which suggested the completion of the Schiff based reaction. Furthermore, the aromatic protons from the 2,6-diisopropyl aryl group were shown at 7.15 ppm (meta positioned protons) and 7.09 ppm (para positioned protons).

37
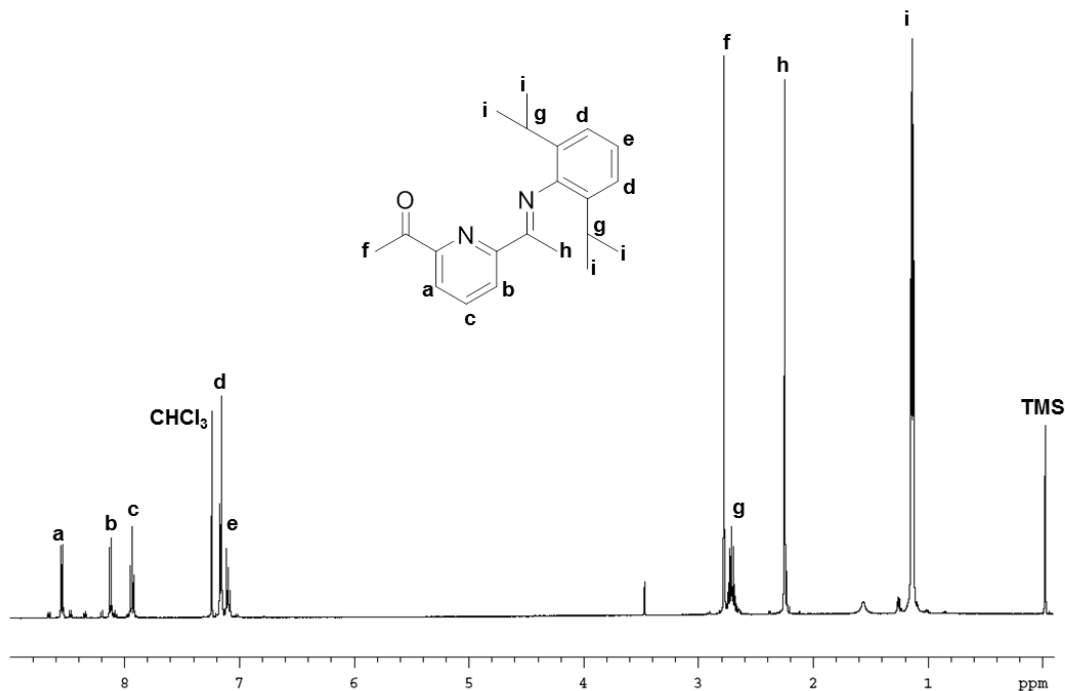
Figure 2.5. ^{1}H NMR spectrum of compound **1**. 500 MHz, CDCl$_3$.

The ligand [(2,6-[i]PrC$_6$H$_3$)N=CMe)(2-MeO-6-MeC$_6$H$_3$)N=CMe)C$_5$H$_3$N] ([MeO]PDI) (**2**) was also synthesized via a Schiff base condensation, with starting materials [(2,6-[i]PrC$_6$H$_3$N=CMe)(O=CMe)C$_5$H$_3$N] and 2-methoxy-6-methylaniline in a Dean-Stark apparatus. The color changed from a pale yellow as a result of [(2,6[i]PrC$_6$H$_3$N=CMe)(O=CMe)C$_5$H$_3$N], to a dark yellow of **2** (**eq 6**). Water was also collected in the Dean-Stark trap to confirm the condensation reaction. Purification of **2** involved periodic wash with acetone, to remove the minor products of the reaction (2,6-diacetylpyridine and the double addition of 2,6-diisopropyl aniline).

38

(6)

1

2-methyl-6-methoxy aniline

2
~60%
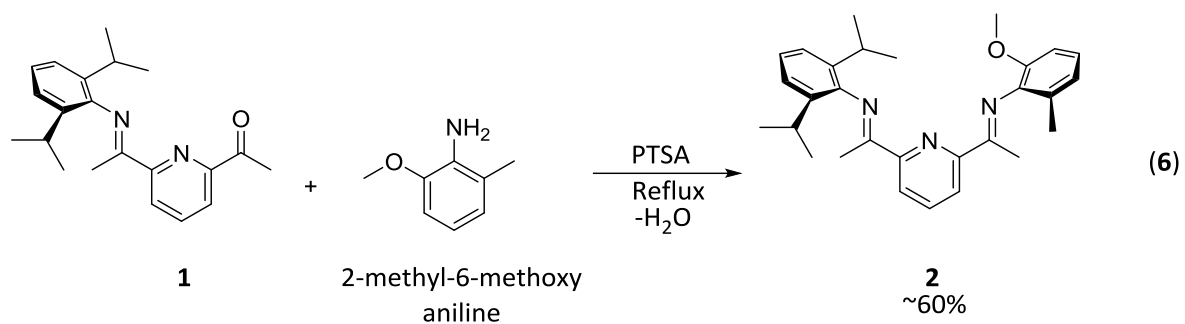
IR and ^{1}H NMR spectroscopy confirmed the structure of **2**. In the IR spectrum, the disappearance of the C=O stretching frequency at 1698 cm^{-1} is prominently noted, owing to the completion of the Schiff based reaction (**Figure 2.6**). Only the C=N stretching frequency at 1641 cm^{-1} is present, due to both C=N, from the 2,6-diisopropyl and 2-methoxy-6-methyl aryl groups.
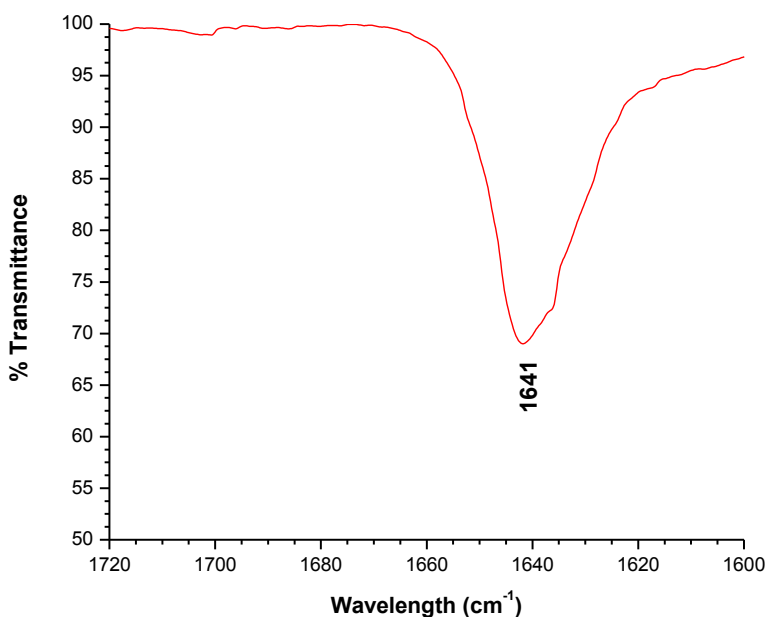
Figure 2.6. IR spectrum of compound **2**. Highlighting the C=N stretching frequency.

39

The ^{1}H NMR showed the appearance of two singlet resonances at 3.76 and 2.09 ppm. These resonances corresponded to the protons of the methoxy and methyl group, respectively, off of the meta position on the 2-methoxy-6-methyl aryl group. The integration displayed 3 protons for each resonance. Furthermore, the aromatic protons from the 2-methoxy-6-methyl aryl group are shown at 7.01 (para), 6.87 (meta) and 6.83 (meta) ppm (**Figure 2.7**).
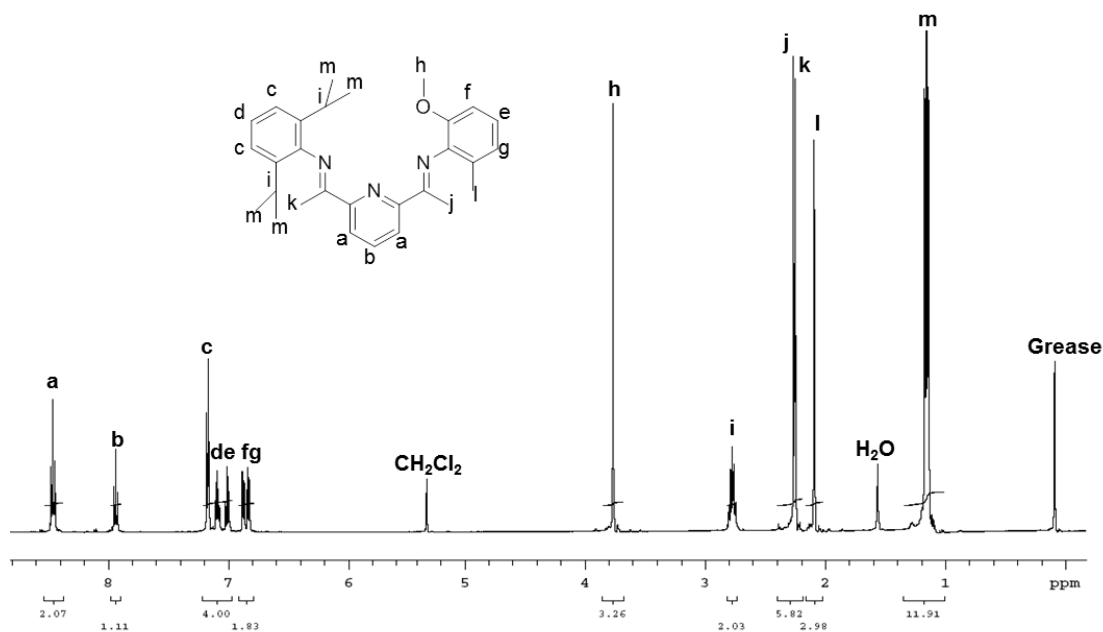
Figure 2.7. ^{1}H NMR spectrum of compound **2**. 500 MHz, CD_2Cl_2.

Compound **2** is highly conjugated and redox active; similar to other PDI ligands.[15] Electrochemical studies confirmed **2** as an electron reservoir, owing to the fact that 2 electrons can be held within the highly conjugated system, to create a diradical dianionic

species of **2** (**Scheme 2.9**). The electron is likely delocalized throughout the conjugated system; therefore the dot (which represents an electron) can be positioned elsewhere within the [MeO]PDI ligand.[22]
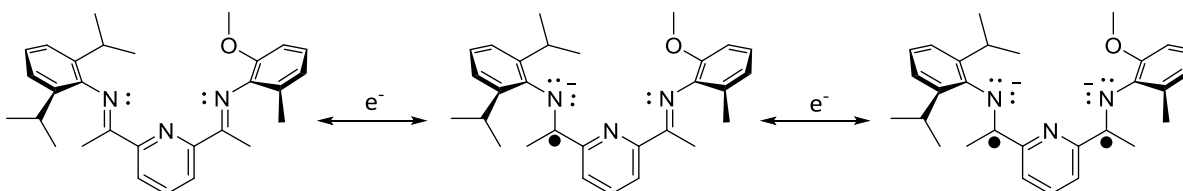
Scheme 2.9. Compound **2** can hold up to 2 electrons within its highly conjugated system.

Cyclic voltammetry (CV) studies of compound **2** (0.1 M) in tetrahydrofuran with ammonium hexafluorophosphate electrolytes (1 M) showed the two electron reduction events of **2** at -1.08 and – 1.63 V, and two electron oxidation events at -0.498 V and -1.26 V (**Figure 2.8**). The voltage split is beyond the reversible value of 59 mV, however, the general shape and stability of **2** after 25 scans support a quasi-reversible status. Lastly, a third oxidation event at 0.68 V suggests compound **2** can undergo an oxidation event, starting from the neutral state, similar to Soper's bis-iminophenolate ligand.[12]

41
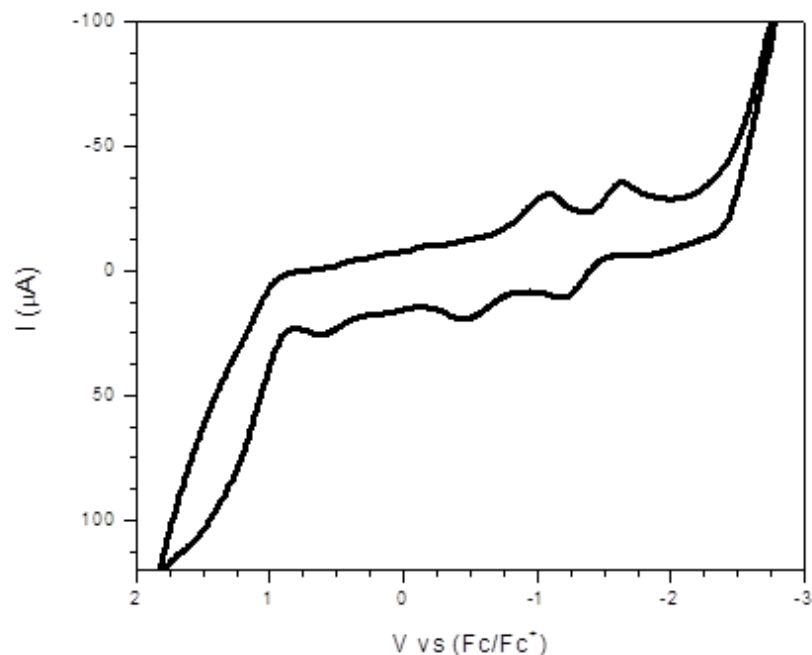
Figure 2.8. Cyclic voltammogram of compound **2**, with a scan rate of 100 mV/sec and a total of 25 scans.

The CV study provided evidence of the redox capabilities of **2**, similar to other well defined PDI ligands.[15] Similarly to other PDI ligands, **2** can store the 2 electrons required for the reduction of CO_2 to CO. However, CO_2 requires a binding site before electrons can transfer. Therefore, the next step before reactivity with CO_2 molecules is the insertion of the Fe metal within the binding pocket of compound **2**.

42

2.6   References

1.   Constable, E. C.; Housecroft, C. E. *Chem. Soc. Rev*. **2013**, 42, 1429-1439.
2.   Collman, J. P.; Gagne, R. R.; Reed, C. A.; Halbert, T. R.; Lang, G.; Robinson, W. T. *J. Am. Chem. Soc.* **1975**, 97, 6, 1427-1439.
3.   Shriver, D. F.; Atkins, P. W. *Inorganic Chemistry*, 3rd edition, Oxford University Press, 2001. pg. 227-236.
4.   Luca, O. R.; Crabtree, R. H. *Chem. Soc. Rev.* **2013**, 42, 1440.
5.   Silvia, J.S.; Cummins, C.C*. J. Am. Chem. Soc.* **2010**, 132, 7, 2169-2171.
6.   Shook, R. L.; Peterson, S. M.; Greaves, J.; Moore, C.; Rheingold, A.L.; Borovik, A. S. *J. Am. Chem. Soc.* **2011**, 133, 5810-5817.
7.   Chaudhuri, P.; Hess, M.; Florke, U.; Wieghardt, K. *Angew. Chem*. *Int. Ed.* **1998**, 37, 2217- 2220.
8.   Chaudhuri, P.; Wieghardt, K.; Weyhermuller, T.; Paine, T. K.; Mukherjee, S.; Mukherjee, C. Biol. Chem. **2005**, 386, 1023-1033.
9.   Chirik, P. J.; Wieghardt, K. *Science*, **2010**, 327, 794.
10.   Chaudhuri, M.; Hess, J.; Muller, J.; Hildenbrand, K.; Bill, E.; Weyhermuller, T.; Wieghardt, K. *J. Am. Chem. Soc*. **1993**, 115, 3239.
11.   Nguyen, A. I.; Zarkesh, R. A.; Lacy, D. C.; Thorson, M. K.; Heyduk, A. F. *Chem. Sci*. **2011**, 2, 166-169.
12.   Smith, A. L.; Hardcastle, K. I.; Soper, J. D. *J. Am. Soc.* **2006**, 128, 8410.
13.   Dzik, W. I.; van der Vlugt, J. N.; Reed, H.; de Bruin, B. *Angew. Chem. Int. Ed.* **2011**, 50, 15,   3356.
14.   Bara, S.; Negishi, E. I. *J. A. Chem. Soc*. **1976**, 98, 6729.
15.   Bouwkamp, M. W.; Bowman, A. C.; Lobkovsky, E.; Chirik, P. J. *J. Am. Chem. Soc.* **2006**, 128, 13340-13341.
16.   de Bruin, B.; Bill, E.; Bothe, E.; Weyhermueller, T.; Wieghardt, K. *Inorg. Chem*. **2000**, 39,   2936-2947.
17.   Budzelaar, P. H. M.; de Bruin, B.; Gal, A. W.; Wieghardt, K. E.; van Lenthe, J. H. *Inorg. Chem*. **2001**, 40, 4649-4655.
18.   Sylvester, K. T.; Chirik, P. J. *J Am Chem. Soc.* **2009**, 131, 8772-8774.
19.   Russell, S. K.; Lobkovsky, E.; Chirik, P. J. *J. Am. Chem. Soc*. **2011**, 133, 8858-8861.
20.   Russell, S. K.; Lobkovsky, E.; Chirik, P. J. *J. Am. Chem. Soc*. **2010**, 132, 15046-15059.
21.   Bouwkamp, M. W.; Lobkovsky, E.; Chirik, P. J. *Inorg. Chem*. **2006**, 45, 2-4.
22.   Tondreau, A. M.; Stieber, C. E.; Milsmann, C.; Lobkovsky, E.; Weyhermuller, T.; Semproni, S. P.; Chirik, P. J. *Inorg. Chem*. **2013**, 52, 635-646.

Chapter 3. CO$_2$-to-CO Conversion

3.1 Binding of CO$_2$

Although the reduction of CO$_2$ by transition metal catalysts is in many ways nascent, the field has gained more attention as well as importance over the past forty years. It was in 1975 that Aresta and Nobile first ascertained that CO$_2$ activation by transition metal complexes was possible, via the crystal structure of a CO$_2$ bound (Cy$_3$P)$_2$Ni complex. It was reported in the crystal structure that an η^2-bidentate binding mode is involved in the carbon and oxygen atom of CO$_2$, with significant bending (**Figure 3.1**).[1] This discovery suggested that the large enthalpy associated with that of the C=O double bond in CO$_2$ (532 kJ/mol), can be activated, and ultimately lead to reduction.[2] Since that discovery, various CO$_2$ binding modes have been observed (**Table 3.1**).
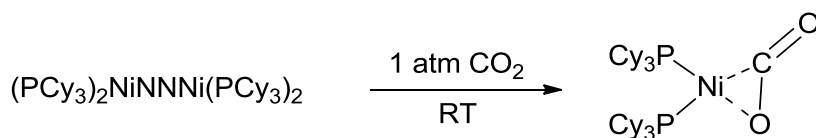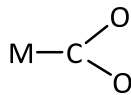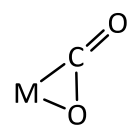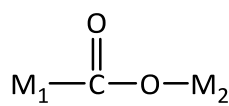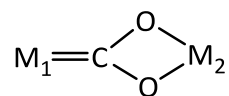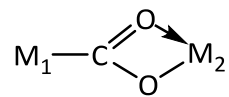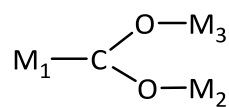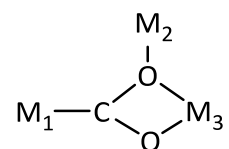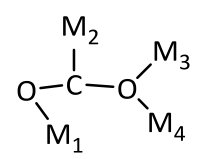
Figure 3.1. Reaction involving the insertion of CO$_2$ gas into a Ni(0) center, affording the first reported crystal structure of CO$_2$ activation by a transition metal complex.[1]

Table 3.1. Modes of bonding CO_2 to metal centers

Bonding Modes	Structural Features of the Adduct	Observed in Metal [Ref]
η^1-O	M—O—C=O	U[3]
η^1-C	M—C(=O)(O)	Rh[4], Ir[5]
η^2-C,O	M bonded to C and O of C=O (three-membered ring)	Ni[6], Rh[7], Fe[8], Pd[9]
μ_2-η^2	M_1—C(=O)—O—M_2	Pt[10], Ir/Zr[11], Ir/Os[12], Rh[13], Ru[14]
μ_2-η^3 (class I)	M_1=C(—O—)(—O—)M_2	Re/Zr[15], Ru/Zr[16], Ru/Ti[16], Fe/Zr[16], Fe/Ti[17]
μ_2-η^3 (class II)	M_1—C(—O→)(—O—)M_2	Re/Sn[18], Fe/Sn[19]
μ_3-η^3	M_1—C(—O—M_3)(—O—M_2)	Os[20], Re[21]
μ_3-η^4	M_1—C(—O—M_2)(—O—M_3)	Co[22]
μ_4-η^4	O(M_1)—C(M_2)—O(M_3)(M_4)	Ru[23]

3.2 Breakdown of CO$_2$ (Electrochemically)

A series of studies involving various other metal catalysts ensued shortly thereafter, regarding the electrocatalytic reduction of CO$_2$ to CO, primarily employing highly expensive and low abundant metals such as Ru and Pd. In 1987, Tanaka and coworkers used the bipyridine complexes of Ru, (bipy)$_2$Ru(II)(CO)$_2$ to electro-catalytically reduce CO$_2$ to CO.[24] The (bipy)$_2$Ru(II)(CO)$_2$ complex displayed a reduction potential of CO$_2$ at -1.40 V vs. SCE, which is 0.5 V less than the one electron reduction of CO$_2$ (without a catalyst). According to Tanaka's mechanism, a two electron reduction of the complex displaced one CO from the Ru, to form a five coordinate neutral complex. In the presence of CO$_2$, the neutral complex forms an η^1-CO$_2$ adduct of Ru(0). The addition of protons from the acidic solution (pH 6.0) produce a H$_2$O molecule and regenerate the catalyst, (bipy)$_2$Ru(II)(CO)$_2$ (**Scheme 3.1**).
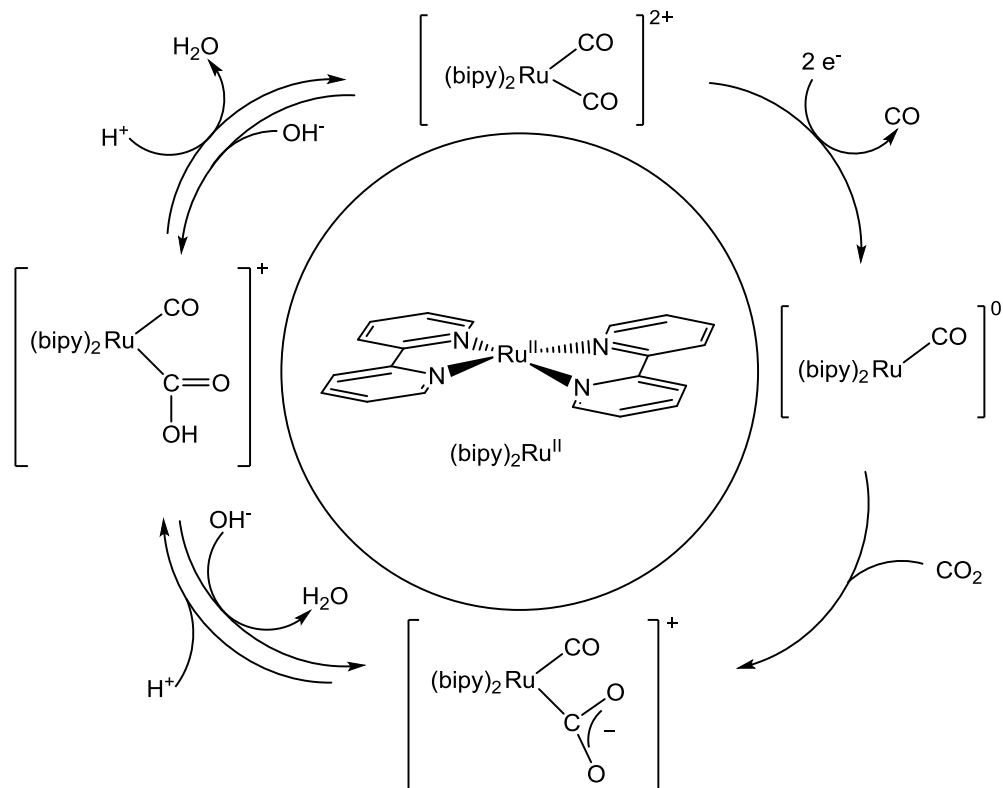
Scheme 3.1. Tanaka and coworkers' catalytic reduction of CO_2 to CO with a (bipy)$_2$Ru(II)(CO)$_2$ complex.[24]

Also, Dubois and coworkers have shown extensive studies of CO_2 reduction to CO on polydentate phosphine Pd complexes.[25-27] The starting, Pd(II) complex gains an electron to form a Pd(I) intermediate, which then binds CO_2 to form the five-coordinate CO_2 adduct. Upon transfer of the second electron, the Pd(0) intermediate dissociates the solvent (acetonitrile) and protonation (from acidic solution) of one of the O atom of the coordinated CO_2 affords the metallo-carboxylic acid intermediate, Pd-COOH. Another protonation occurs to form a dihydroxy carbene intermediate, and through the dehydration of the dihydroxy carbene, CO is released. Acetonitrile once again binds to the open site of Pd, to regenerate the catalyst (**Scheme 3.2**).

47
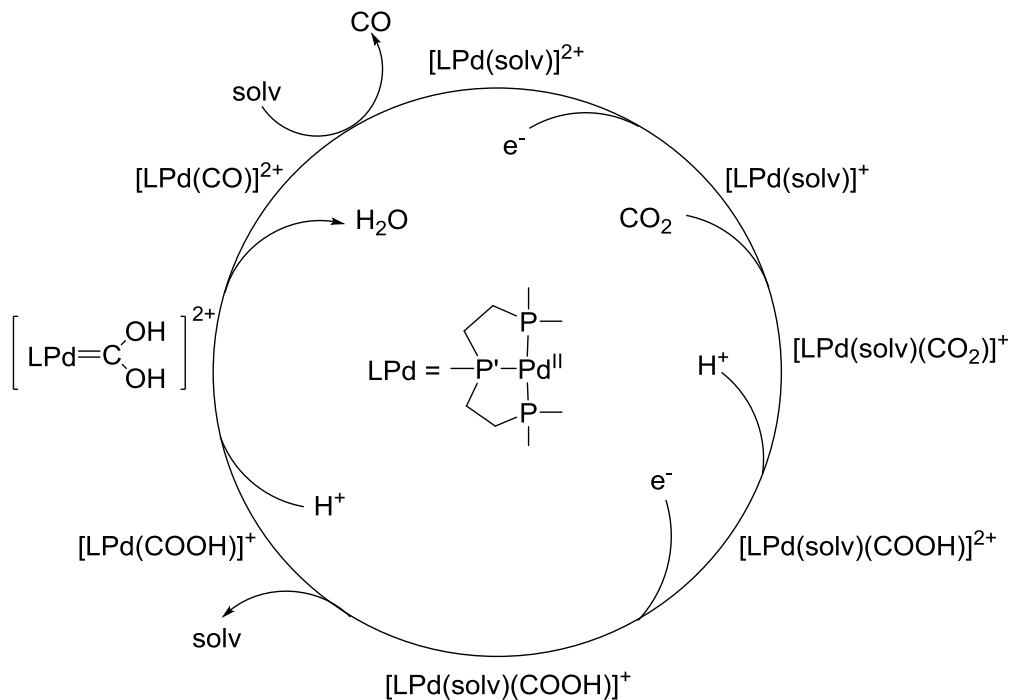
Scheme 3.2. Dubois and coworkers catalytic reduction of CO_2 to CO on a polydentate phosphine Pd complex.[25]

Fe, the most abundant metal on Earth, has also been utilized for the reductive cleavage of CO_2 to CO and O^{2-}. This was demonstrated electrochemically in 1991 by Savéant and coworkers by means of an Fe(0) porphyrin; however the porphyrin ring degraded after several catalytic cycles, due to carboxylation or hydrogenation of the ring.[28] Other notable electro-catalytic Fe complexes include Fe(I) corroles[29], 19-electron Fe Cp complexes[30], and Fe(I) complexes of 2,9-bis(2-hydroxyphenyl)-1,10-phenanthroline.[31] However, for a fair comparison to the work presented within this thesis, chemical studies (electrons derived from chemical reductants) on the reduction of CO_2 to CO must be compared.

48

3.3 Breakdown of CO$_2$ (Chemically)

Fe(I) complexes have shown to chemically reduce CO$_2$ to CO, as shown independently by Holland and Peters. Holland and coworkers have reported the reductive disproportionation of CO$_2$ to CO and carbonate (CO$_3^{2-}$) with a L^{tBu} = 2,2,6,6-tetramethyl-3,5-bis [(2,6-diisopropylphenyl)imino]hept-4-yl Fe(I) complex.[32] The treatment of L^{tBu}FeNNFeL^{tBu} with two mole equivalents of dry CO$_2$ in pentane afforded a mixture of the dicarbonyl Fe(I) (L^{tBu}Fe(CO)$_2$) and the bridging carbonato dimer Fe(II) (L^{tBu}Fe(II)(μ-OCO$_2$)-Fe(II)L^{tBu}) complex (**Scheme 3.3**).
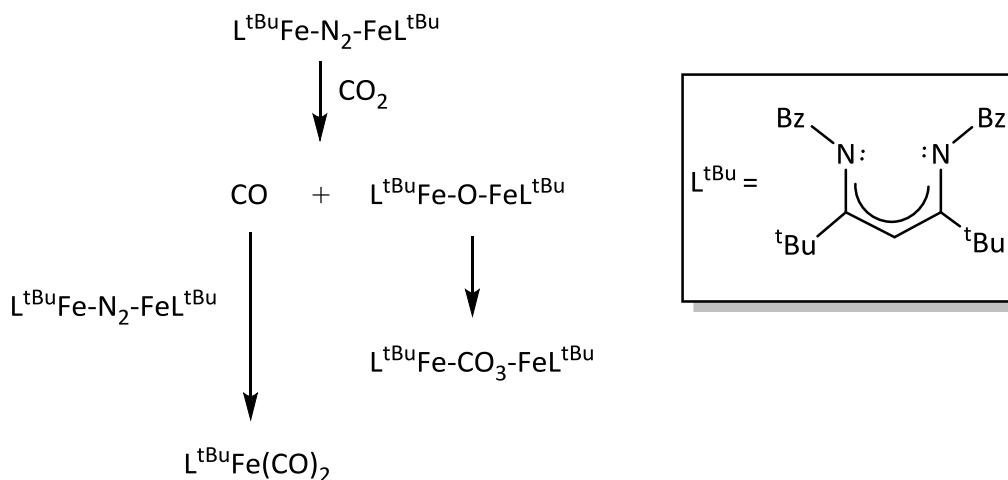
Scheme 3.3. Holland and coworkers reductive disproportionation of CO$_2$ to CO and CO$_3^{2-}$.[32]

49

Peters and coworkers saw a chemical reduction and coupling of CO_2, on a tris(phosphine)borate Fe(I) complex.[33] Two products were identified, one major product, the unprecedented bimetallic μ-carbonyl/μ-oxo (Fe(μ-CO)(μ-O)Fe) complex and the minor product, bimetallic oxalate (Fe(μ-η^2: η^2-oxalato)Fe) complex (**Figure 3.2**).
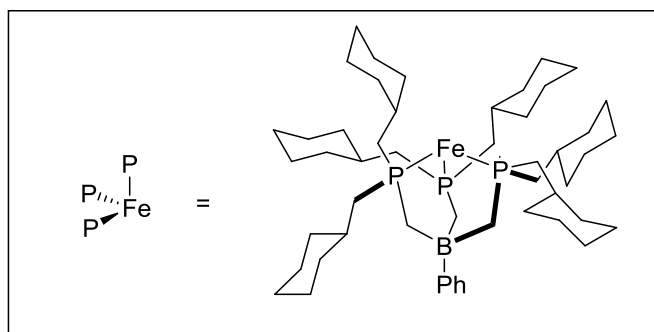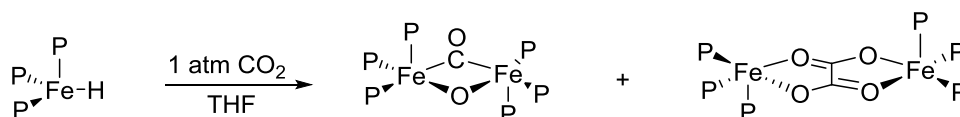
Figure 3.2. Peters and coworkers reductive cleavage of CO_2 to CO using a tris(phosphine)-borate Fe(I) complex.[33]

Only one system known in literature, prior to this work, displayed a CO_2-to-CO reduction on an Fe(II) center. Field and coworkers have shown the reductive disproportionation of CO_2-to-CO and the bicarbonate anion (HCO_3^-).[34] The addition of 3 - 4 atmosphere of CO_2 to Fe(dmpe)$_2$H$_2$ (dmpe = 1,2-bis(dimethylphosphino)ethane) at 70 ^{0}C afforded two products, the iron carbonate Fe(dmpe)$_2$CO$_3$ and the iron carbon monoxide bound [Fe(dmpe)$_2$(CO)H][HCO$_3$] with a bicarbonate counter anion (**Scheme 3.4**).

50
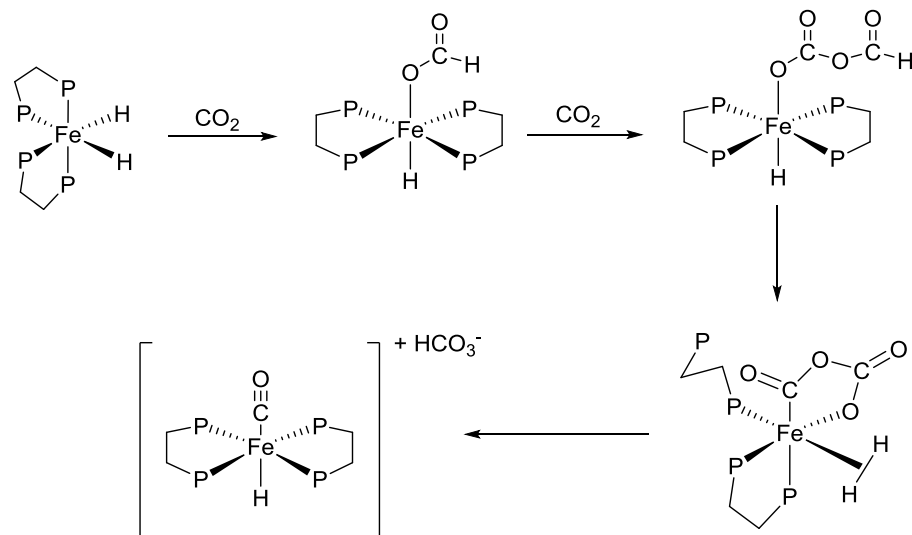
Scheme 3.4. Field and coworkers proposed mechanism for the reductive disproportionation of CO_2 to CO.[34]

The examples shown above employed either reactive hydride (Field) or electron rich Fe(I) centers (Holland and Peters) for the reduction of CO_2 to CO. As eluded to in chapter 2, redox active ligands can confer nobility to first row transition metals, such as Fe, Cu and Zn, in order to explore multi-electron transfer reactions with cheaper and more abundant metals. Instead of rich electron centers or highly reactive hydrides, redox active ligands can assist in the electron transfer reaction needed to complete the reduction of CO_2-to-CO. Redox active ligands such as the PDI ligand system have been extensively studied by Chirik, especially on Fe(II) centers.[35,36] Also, it is important to note that all of the CO_2 to CO reduction cycles shown above are not catalytic. Hence, the PDI Fe(II) system presented herein will demonstrate a complete CO_2 to CO cycle with the help of the redox-active ^{MeO}PDI ligand **2**.

51

3.4 Metallation of ^{MeO}PDI

The PDI ligand **2** has been shown to be redox active (chapter 2). Now a metal center (Fe) must be incorporated within the binding pocket of **2** for the CO_2 molecule to bind. A solution of **2** in dichrolomethane (DCM) was slowly added to a solution of $FeBr_2$ (tetrahydrofuran) in a N_2 filled glove box to produce a color change from dark yellow to dark blue (**eq. 7**). The solution was allowed to stir for 1 day before filtering through a pipette filled with celite, to filter out impurities. The filtered solution was then layered with diethyl ether to produce blue single crystals of **3**.

$$ \textbf{2} \xrightarrow[\text{DCM/THF}]{FeBr_2} \textbf{3} \tag{7} $$
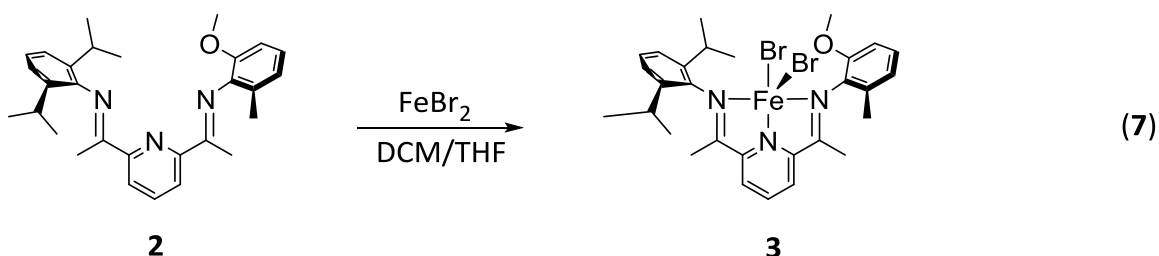
IR analysis showed the shift in the imine stretching frequency from 1643 cm^{-1} in **2** to 1579 cm^{-1} in **3**, due to the dative bond between the imine N and the Fe center (**Figure 3.3**). The new dative bond caused a slight reduction in the imine bond, which lowers the force constant and in turn shifts the frequency to a lower wavenumber.
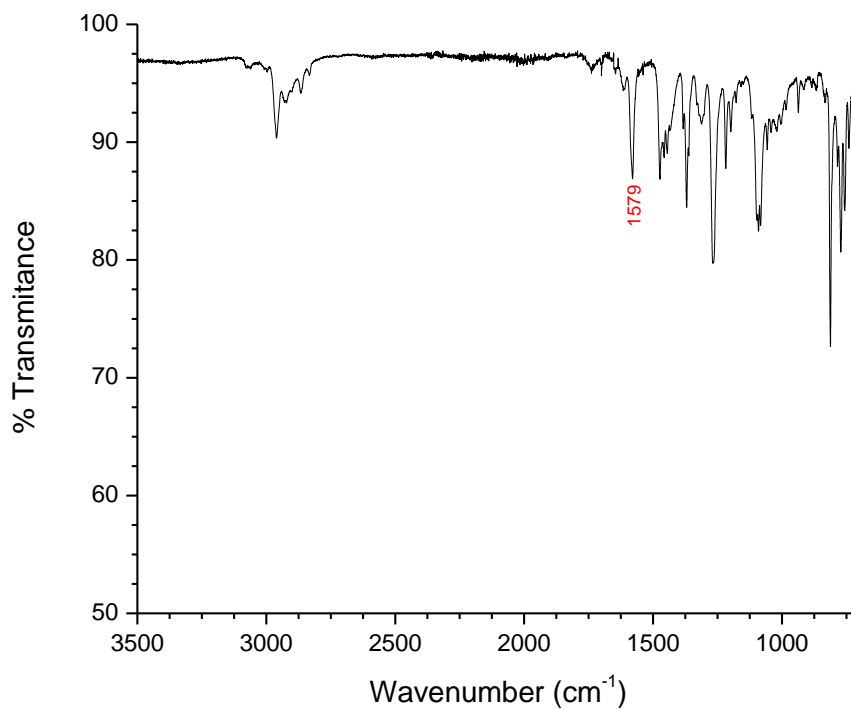
Figure 3.3. IR spectrum of **3**.

Due to the paramagnetic nature of **3**, the ^{1}H NMR spectrum span from 100 to - 50 ppm (**Figure 3.4**). However, the important resonances are assigned from comparing the well analyzed PDI FeCl$_2$ complex from Gibbon and coworkers.[37] It is important to note, that the prominent solvents displayed within the ^{1}H NMR spectrum are from adventitious solvents in the N$_2$ glove box, that are used daily.
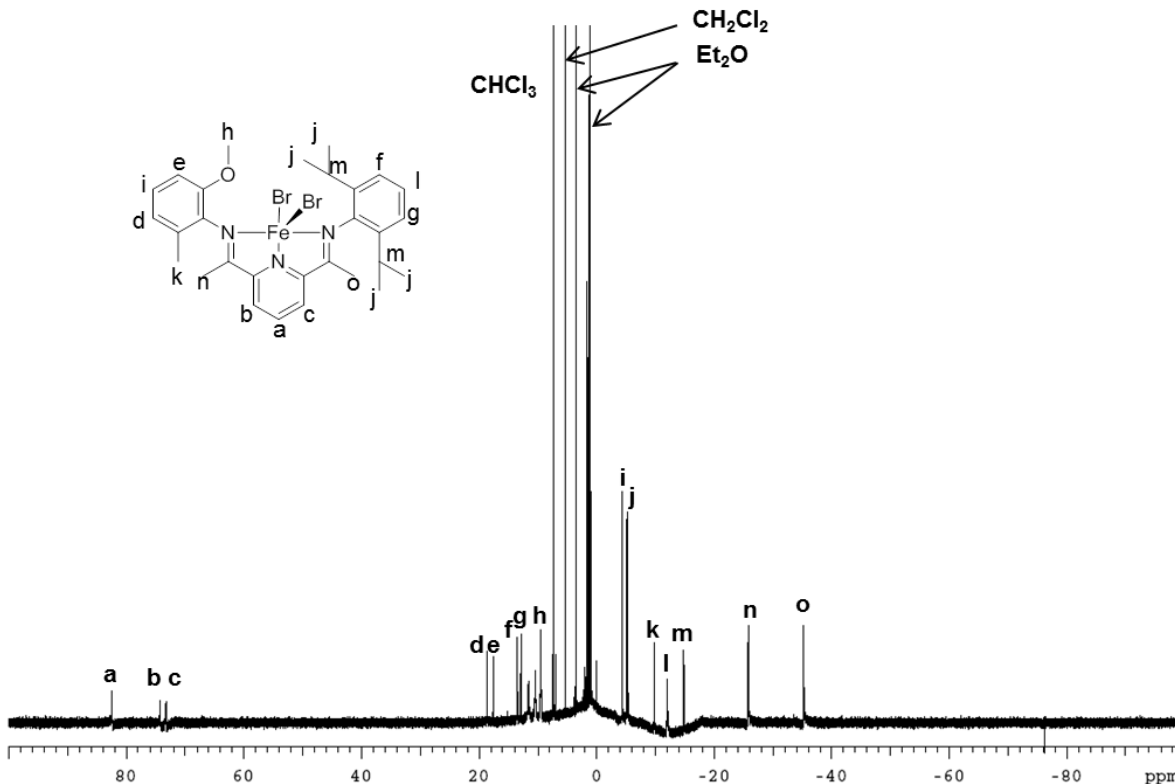
Figure 3.4. ^{1}H NMR spectrum of **3**, 500 MHz, CDCl$_3$.

X-ray crystallographic analysis was also taken of the blue single crystals of **3** (which contained two independent molecules in the unit cell). An Oak Ridge Thermal Ellipsoid Plot (ORTEP) view of a molecule of **3** is shown in **Figure 3.5**. The Fe center is five-coordinate with a distorted square-pyramidal geometry (average τ = 0.28). A τ value of 1 corresponds to an ideal trigonal-bipyramidal geometry, while a τ value of 0 corresponds to an ideal square-pyramidal geometry.[38] The bond lengths and angles are similar to other structurally characterized PDIFe(II) complexes by Chirik and coworkers.[39-42]

54
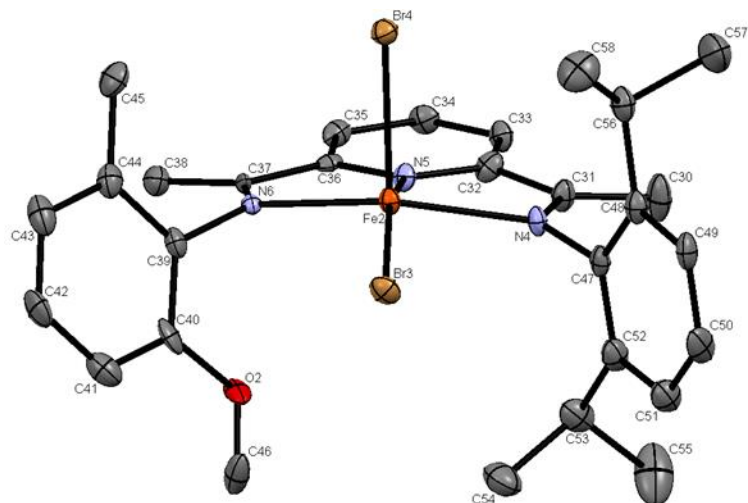
Figure 3.5. Solid-state structure (30% probability) of **3**. H atoms have been omitted for clarity. Selected bond lengths (Å) and angles (deg) for one independent molecule in the unit cell: Fe(1)–Br(1) 2.4062(16), Fe(1)–Br(2) 2.5048(16), Fe(1)–N(1) 2.268(8), Fe(1)– N(2) 2.089(7), Fe(1)–N(3) 2.224(7), C(2)–N(1) 1.308(13), C(8)–N(3) 1.299(11); Br(1)–Fe(1)–Br(2) 108.38(6), N(2)–Fe(1)–Br(1) 158.3(2), N(1)–Fe(1)–N(3) 140.2(3).

The measured effective magnetic moment (μ_{eff}) of **3** yielded values of 5.49 (in the solid state) and 4.89 μ_B (in solution), with magnetic susceptibility balance and Evan's method NMR measurements, respectively.[43] These values are consistent with a high-spin (S = 2) square-pyramidal Fe(II) center.[39] Another technique that confirms the oxidation state of the Fe center is Mössbauer spectroscopy.[44] When **3** was analyzed in a room temperature, zero-field Mössbauer, the isomer shift (δ) and quadruple splitting parameters are 0.644(9) and 1.13(2) mm/s, respectively (**Figure 3.6**). These values are in agreement with the assignment of a high-spin Fe(II) center.[42]

55
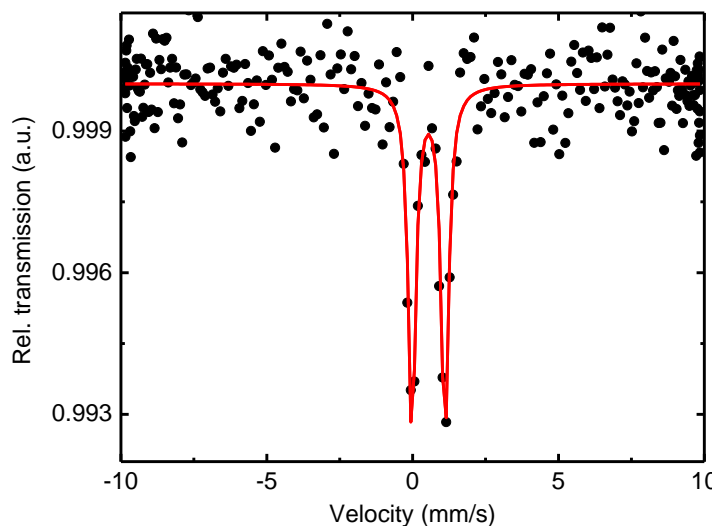
Figure 3.6. Zero-field ^{57}Fe Mössbauer spectrum of **3** recored at room temperature. The isomer shift and quadruple splitting parameters are 0.644(9) and 1.13(2) mm/s, respectively.

3.5 Reduction of ^{MeO}PDIFeBr$_2$ (3).

Once the Fe center is incorporated into the binding pocket of ligand **2** to obtain complex **3**, the complex must be reduced by two electrons to perform the reduction of CO_2-to-CO. From previously reported data on PDI Fe complex, the two electron reduction of the PDIFe(II) complex can be accomplished by the addition of two equivalents of sodium triethylborohydride (NaBHEt$_3$) in a N_2 filled glove box to obtain a dinitrogen complex (PDI)FeN$_2$.[45] As shown in **eq. 8**, a blue suspension of **3** in either diethyl ether or pentane reacts with two equivalents of NaBHEt$_3$ in an N_2 filled glove box, to form the green (^{MeO}PDI)FeN$_2$ complex (**4**).

56

$$(8)$$
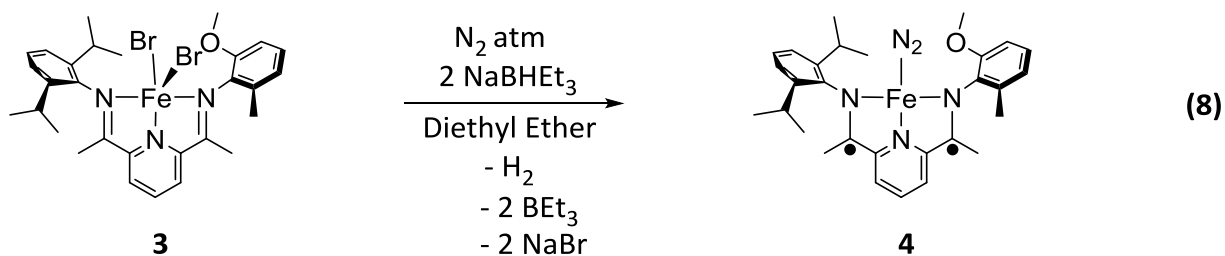
Multiple attempts to isolate **4** in a crystalline form for solid state characterization were unsuccessful, due to degradation (from the removal of solvent or standing in room temperature for two hours). Therefore, complex **4** was unambiguously characterized in solution. As shown in **Figure 3.7**, the liquid Fourier Transform (FT) IR spectrum of **4** in pentane displayed a single bound N_2 stretch at 2045 cm^{-1}, which is not normally seen if N_2 is not bound because of the non-net dipole moment of N_2 gas. Also, the appearance of two N_2 molecules bound to Fe is shown at 2130 and 2071 cm^{-1}, due to previously reported data on the equilibrium between mono and bis-N_2 Fe complexes.[45]
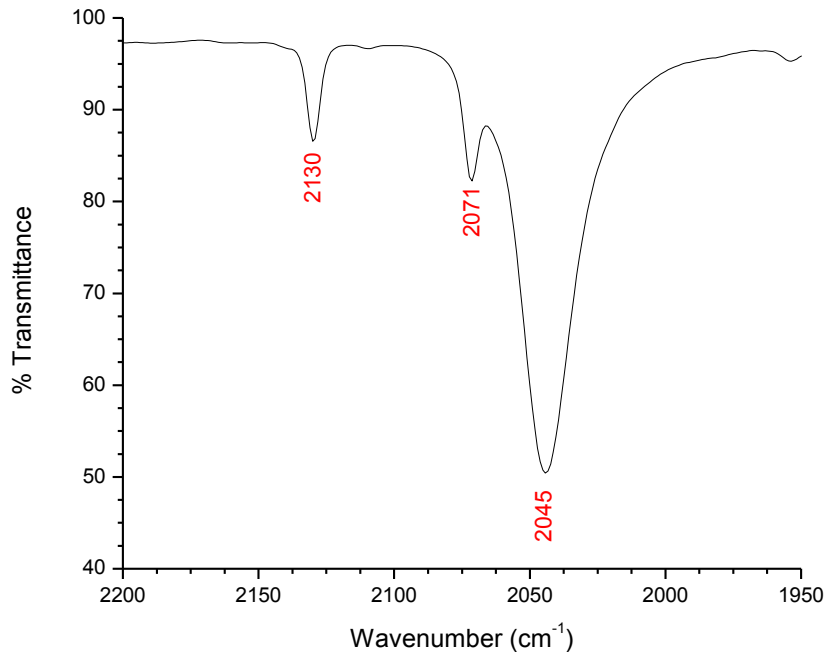
Figure 3.7. FTIR spectrum of **4** in pentane showing both N_2 bound complexes. IR was taken in a liquid cell with sodium bromide windows and a 0.1 mm path-length.

An isotopic study with $^{15}N_2$ gas confirmed the bound N_2 molecule on the Fe center by shifting the stretching frequency from 2045 cm^{-1} in **4(^{14}N$_2$)** to 1959 cm^{-1} in **4(^{15}N$_2$)** (**Figure 3.8**). Also, the ^{15}N{^{1}H} NMR spectrum of **4(^{15}N$_2$)** in solution with diethyl ether exhibited resonances at 113.5 and 104.7 ppm (**Figure 3.9**). These values fall within the range of previously reported reduced PDI dinitrogen complexes by Chirik and coworkers[46] and can be attributed to Nα and Nβ of the terminally bound $^{15}N_2$ ligand.

58
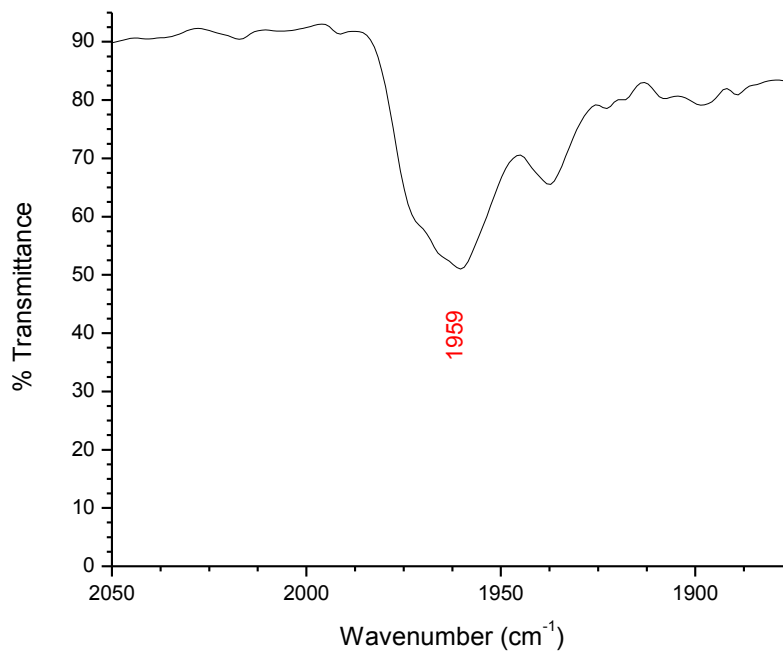
Figure 3.8. FTIR spectrum of **4(^{15}N)** in diethyl ether showing $^{15}N_2$ bound complexes. IR was taken in a liquid cell with sodium bromide windows and a 0.1 mm path-length.
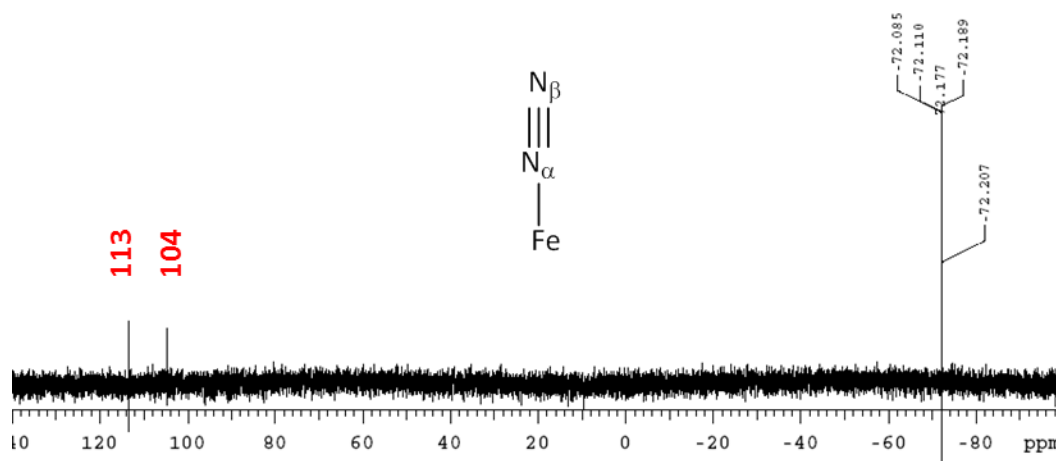
Figure 3.9. ^{15}N{^{1}H} NMR spectrum of **4($^{15}N_2$)**, 51 MHz, diethyl ether.

59

3.6 Characterization of [MeO]PDIFe Complex (Reduced Ligand or Metal)

Due to the unsuccessful isolation of **4**, another route was pursued in order to isolate the two electron reduced [MeO]PDIFe complex, particularly for the proper assignment the Fe center's oxidation state in [MeO]PDIFe, to prove the redox capability of the [MeO]PDI ligand when coupled with a metal. [MeO]PDIFe(CO)$_2$ (**5**) was synthesized and isolated to confirm the oxidation state of the Fe center. By exposing a solution of **4** in diethyl ether, to one atmosphere of CO, complex **5** was obtained (**eq. 9**). Note that the color of **5** is identical to that of **4,** and slow evaporation of diethyl ether in the solution yielded green crystals of **4**.

4		**5**
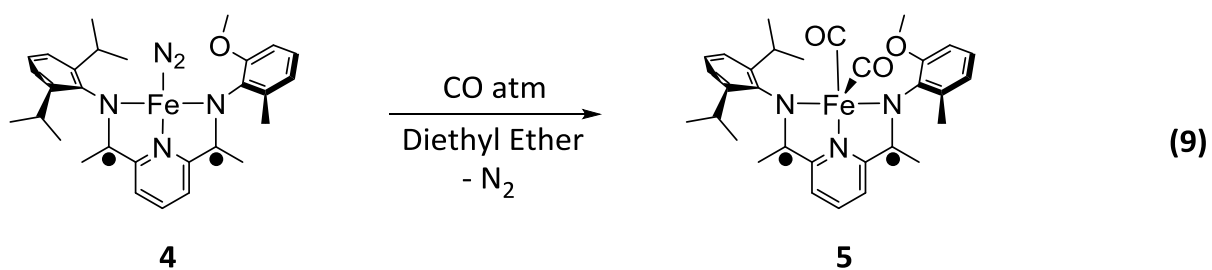
The solid IR of **5** confirmed two CO molecules bound to the Fe center, with stretching frequencies at 1947 and 1883 cm^{-1} (**Figure 3.10**). These values were identical with those of PDIFe(CO)$_2$ complexes from Chirik and coworkers, best described as having diradical dianionic ligands with an S equal to zero, Fe(II) center.[47]
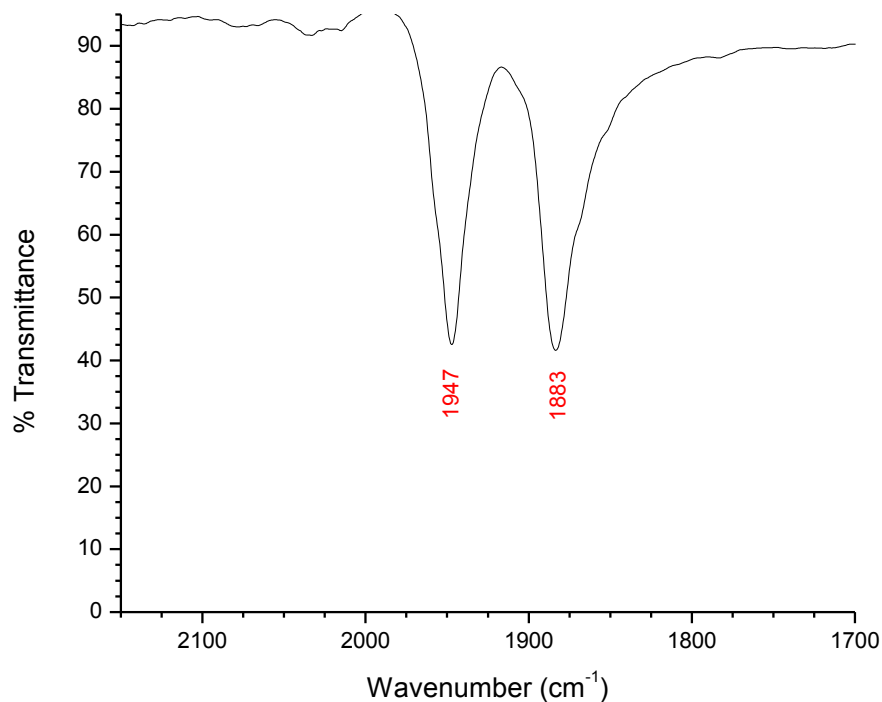
Figure 3.10. Solid FTIR of complex **5**.

Complex **5** is also diamagnetic, in both the solid state and in solution. Therefore, clean ^{1}H and ^{13}C{^{1}H} NMR spectra of **5** were obtained (**Figure 3.11 & 3.12**). The ^{13}C{^{1}H} NMR spectrum display the CO bound molecule at 216 ppm. The other CO bound molecule is not seen, due to the sensitivity of the ^{13}C NMR.

61
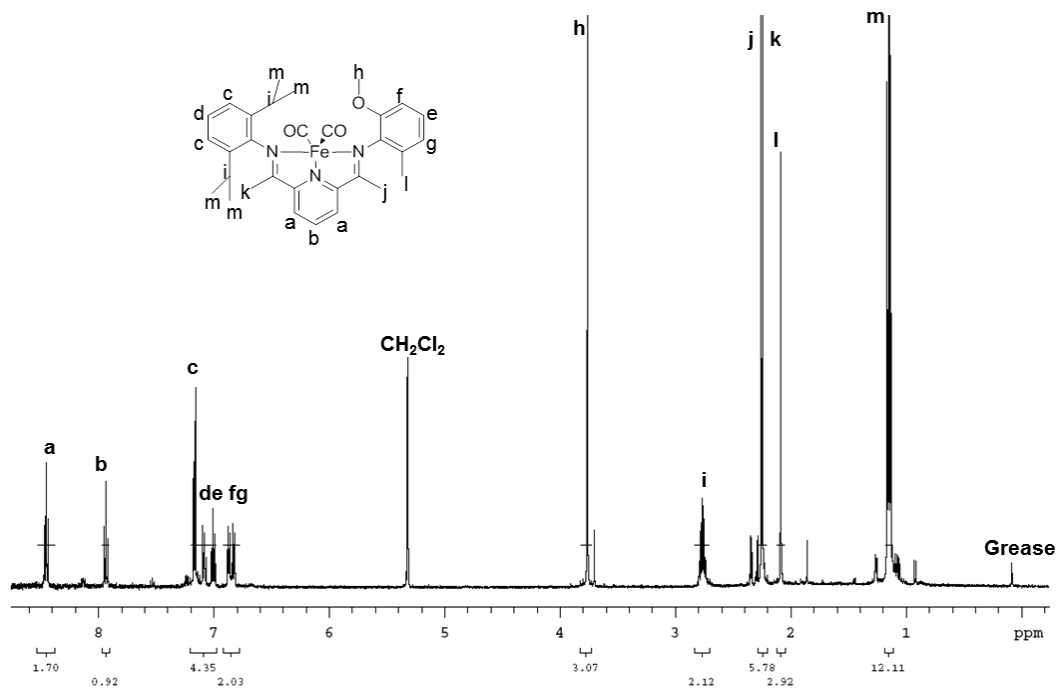
Figure 3.11. ^{1}H NMR spectrum of **5**, 500 MHz, CD$_2$Cl$_2$.
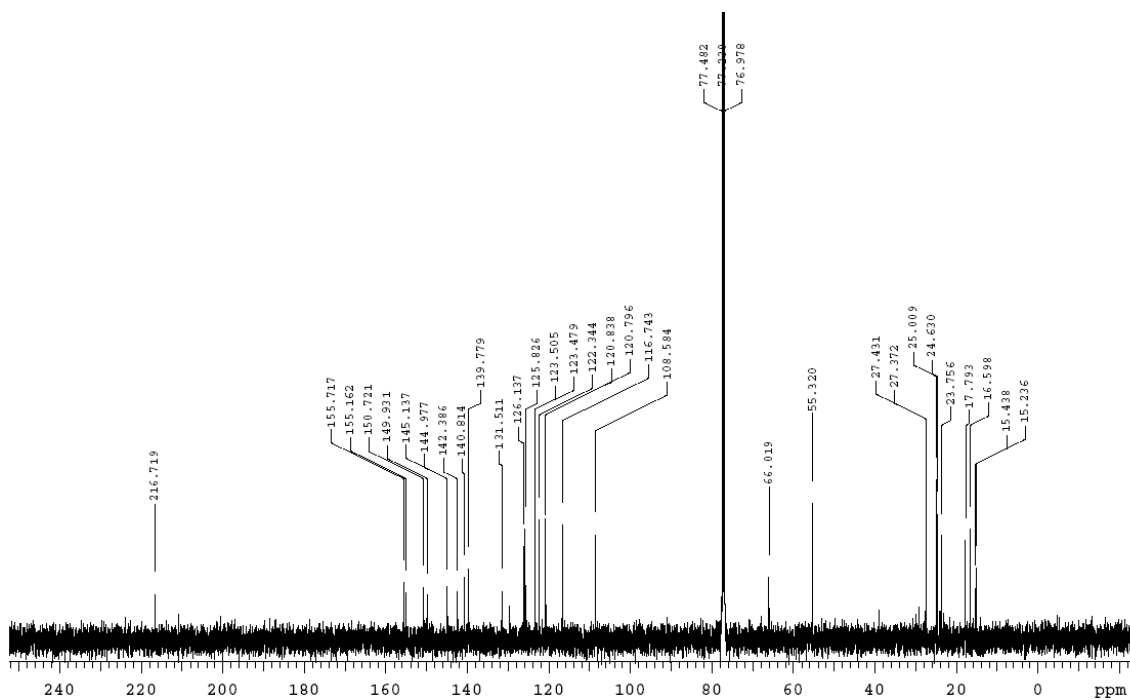
Figure 3.12. ^{13}C{^{1}H} NMR spectrum of **5**, 126 MHz, CDCl$_3$.

62

Recent computational studies of similar $(^{iPr}PDI)Fe(CO)_2$ have shown that an Fe(0) d^8 electronic description can also be an appropriate configuration, therefore, the electronic structure may in fact be a hybrid of the Fe(0) and Fe(II) resonance forms.[48] An Fe(II) with a diradical dianion ligand is a good description of complex **5** because of the crystallographic and Mössbauer data. A detailed ORTEP view of **5** (shown in **Figure 3.13**), depicts the Fe center having a five-coordinate, square-pyramidal geometry (τ = 0.06). Due to the electrons residing within the ^{MeO}PDI ligand, the bond order of the C=N bond is likely decreased and is displayed in the elongation of the C_{imine}–N_{imine} bonds from a value of 1.299(9) and 1.204(7) Å (average of both independent molecules) in **3** to 1.337(3) and 1.314(3) Å in **5**. The contraction of the C_{imine}–C_{ipso} (C from phenyl ring) bonds is also seen, from 1.467(9) and 1.489(9) Å in **3** to 1.412(3) and 1.427(3) Å in **5**. This data, taken in conjunction with the room temperature, zero-field Mössbauer parameters [(ΔEQ = 1.13(1); δ = −0.025(6) mm/s)], suggest that complex **5** is best described as an Fe(II) center with a doubly reduced ^{MeO}PDI ligand. This is surprising because the metal center is historically the electron acceptor in the presence of a reductant, not the organic scaffold surrounding it.[49]

Figure 3.13. Solid-state structure (30% probability) of **5** (left). H atoms have been omitted for clarity. Selected bond lengths (Å) and angles (deg): Fe(1)−C(1) 1.774(2), Fe(1)−C(2) 1.784(2), Fe(1)−N(1) 1.9458(16), Fe(1)−N(2) 1.8526(17), Fe(1)−N(3) 1.9482(17), C(4)−N(1) 1.337(3), C(10)−N(3) 1.314(3); C(1)−Fe(1)−C(2) 96.00(10), N(2)−Fe(1)−C(2) 156.29(9), N(1)−Fe(1)−N(3) 152.48(7). Zero-field Mössbauer spectrum of **5** (right).

3.7 Breakdown of CO_2 to CO on Reduced ^{MeO}PDI Fe(II) Complex

With evidence of the liable N_2 Fe complex **4**, CO_2 was introduced for the observation of the two electron reduction of CO_2-to-CO. Complex **4** was formed in situ in diethyl ether from two equivalents of $NaBHEt_3$. Once all of the hydride was consumed, the solution was filtered and charged with one atmosphere of CO_2, immediately turning brown and then back to green, with subsequent formation of a purple precipitate over six hours (**eq. 10**).

64

$$\text{4} \xrightarrow[\substack{\text{Diethyl Ether} \\ -\ N_2}]{\text{CO}_2\ \text{atm}} \text{5} + \text{Purple Solid} \qquad (10)$$
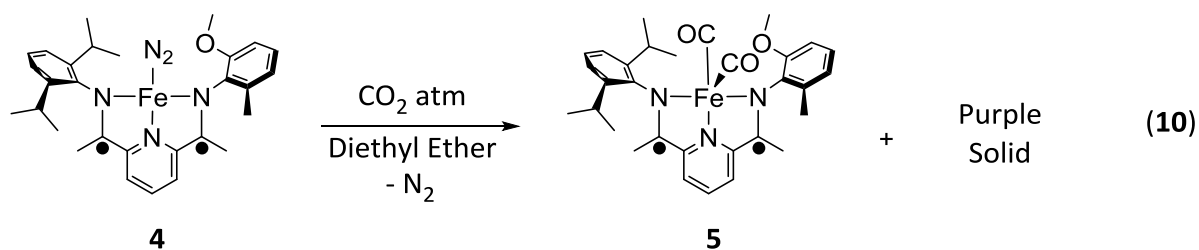
Spectroscopic analysis of the isolated green solution was revealed complex to be **5**. In order to determine if the CO molecules are derived from CO_2 and not adventitious CO gas in the N_2 filled glove box or the CO_2 gas tank, an isotopic study with $^{13}CO_2$ gas was employed. Complex **4** was once again formed in situ in diethyl ether from two equivalents of NaBHEt$_3$, and within half an hour, the solution was filtered into a J-Young NMR tube. The NMR tube was charged with $^{13}CO_2$ gas and a $^{13}C\{^1H\}$ NMR was taken. The $^{13}C\{^1H\}$ NMR spectrum revealed a resonance at 214 ppm, which is 2 ppm off of the isolated complex **5** from the CO reaction (**Figure 3.14**).
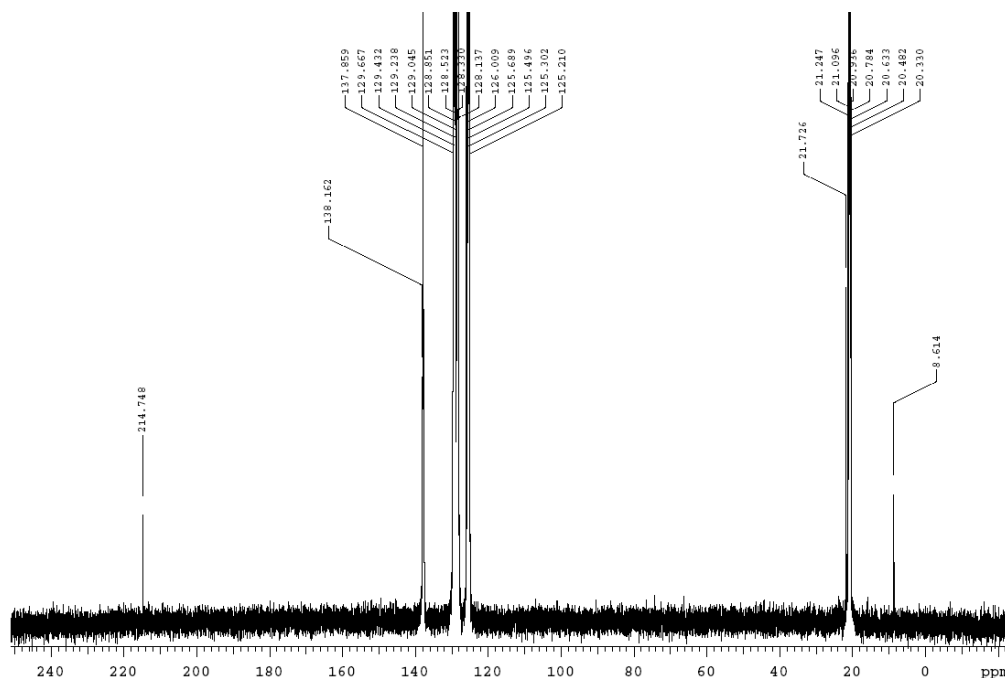
Figure 3.14. $^{13}C\{^1H\}$ NMR spectrum of a solution of **4** exposed to $^{13}CO_2$ gas to generate **5($^{13}CO)_2$**, 126 MHz, toluene-d_8.

The solution of **4** exposed to $^{13}CO_2$ gas in the J-Young NMR tube was then pipetted into a liquid IR cell. The liquid IR spectrum showed the shift in the two CO bound molecules from 1974 and 1914 cm^{-1} in **5($^{12}CO)_2$** to 1923 and 1868 cm^{-1} **5($^{13}CO)_2$** (**Figure 3.15**). The shifted values are within the calculated values of 1935 and 1876 cm^{-1} when exchanging ^{13}C for ^{12}C in the CO stretching frequency.

66
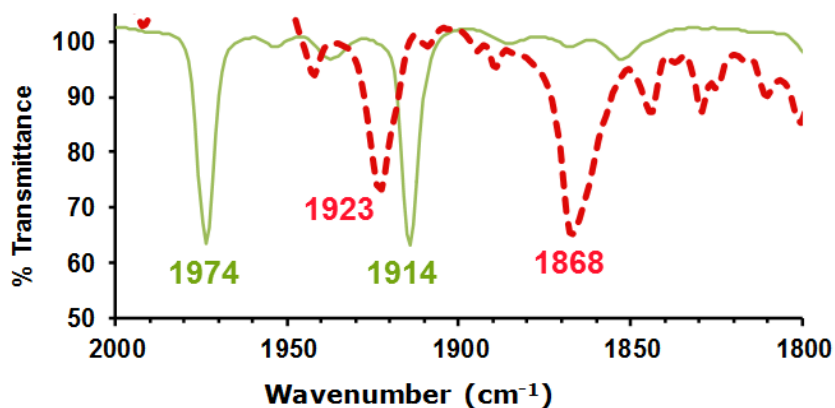
Figure 3.15. Overlay liquid IR spectra of **5(^{12}CO)$_2$** and **5(^{13}CO)$_2$**.

3.8 Oxygen Acceptors

With two CO molecules bound to the Fe center, there posed the question of the two remaining oxygen atoms from the two CO_2 reacted molecules. It was hypothesized that the two remaining oxygen atoms reside in the purple solid product. However, attempts to isolate the purple solid was unsuccessful, owing to the degradation of the purple solid within an hour standing in room temperature and up to four hours at -35 ^{o}C. Therefore, an oxygen atom acceptor such as bis-diethylphosinoethane (DEPE) and Trimethylsilyl chloride (TMSCl) was employed to trap the missing oxygen, in order to elucidate the stoichiometry.

A blue suspension of **4** in either diethyl ether or pentane was reacted with two equivalents of NaBEt$_3$H in a N$_2$ filled glove box for half an hour, followed by filtration

through a glass pipette plugged with glass wool and celite. Then, one equivalent of DEPE was added drop-wise, and a color change from green to red-brown was observed.[45] The reaction was allowed to stir for one hour, before filtering. A concentrated solution in a minimal amount of pentane (3 mL) was stored at -35 °C to furnish black crystals identified as ^{MeO}PDIFeDEPE (**6**).
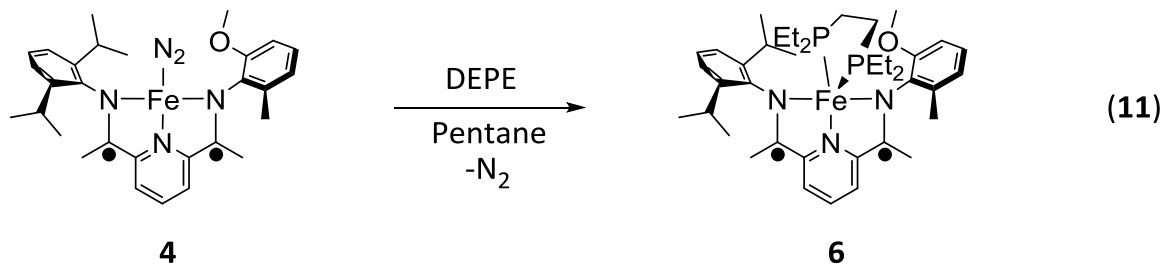
An ORTEP view of **6** is shown in **Figure 3.16**. The Fe center is a five-coordinate, semi-square-pyramidal/trigonal bypyrimidal geometry ($\tau = 0.45$). The C_{imine}–N_{imine} bonds are elongated from a value of 1.299(9) and 1.204(7) Å (average of both independent molecules) in **3** to 1.359(3) and 1.356(3) Å in **6**. The C_{imine}–C_{ipso} bonds are contracted from 1.467(9) and 1.489(9) Å in **3** to 1.408(3) and 1.407(3) Å in **6**.
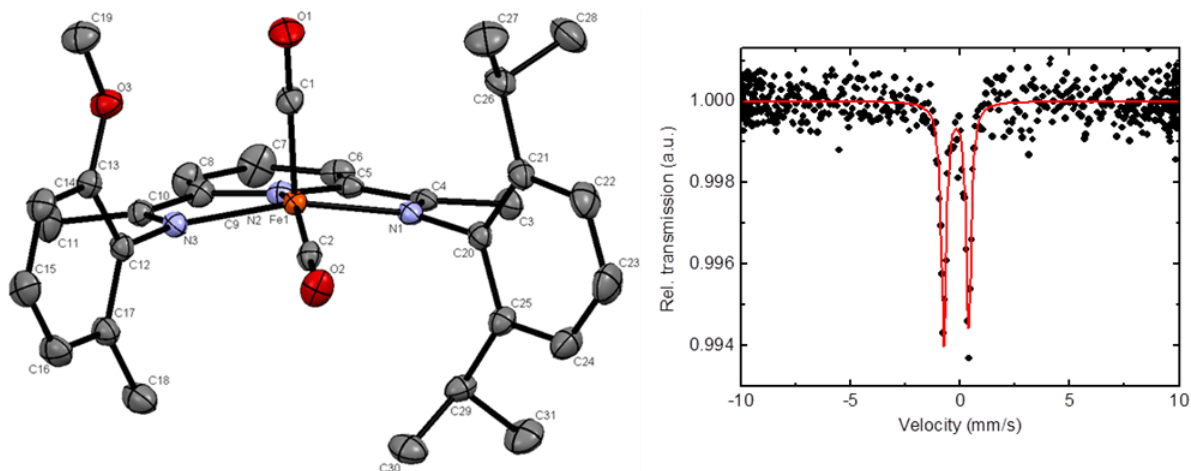
68
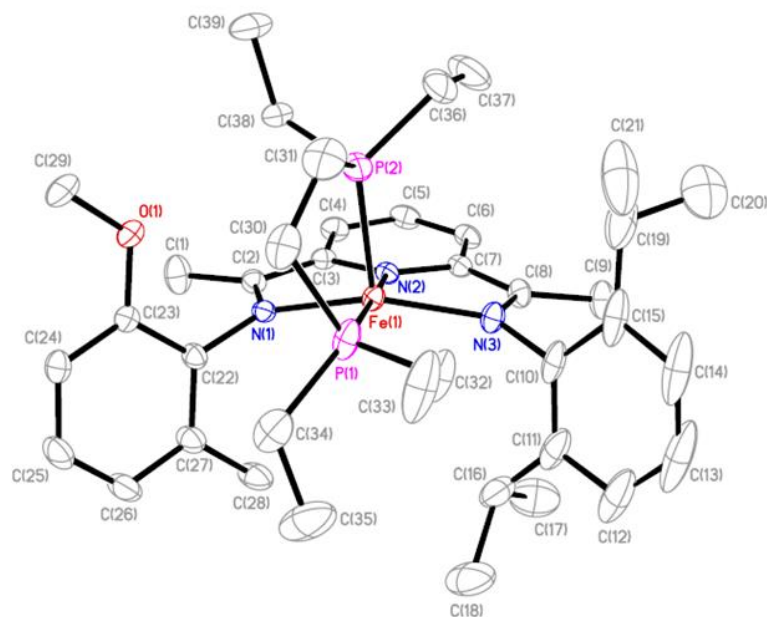
Figure 3.16. Solid-state structure (30% probability) of **6**. H atoms have been omitted for clarity. Selected bond lengths (Å) and angles (deg): Fe(1)–P(1) 2.249(2), Fe(1)–P(2) 2.224(5), Fe(1)–N(1) 1.952(8), Fe(1)–N(2) 1.860(6), Fe(1)–N(3) 1.992(2), C(2)–N(1) 1.359(3), C(8)–N(3) 1.356(3); P(1)–Fe(1)–P(2) 86.29(3), N(2)–Fe(1)–P(1) 175.58(6), N(1)–Fe(1)–N(3) 148.63(8).

Crystals of **6** were then dissolved in diethyl ether and pipetted into a pressurized tube to be charged with one atmosphere of CO_2. The color changed from black to brown within minutes and finally green after an hour, without any noticeable purple solid (**eq. 12**). The thought behind this experiment was to scrub out the oxygen atom from CO_2 with phosphine atoms in DEPE, which was originally presumed to bind to the Fe in ^{MeO}PDIFe to produce the purple solid. Through IR analysis, the green product matched previously to the characterized **5**, however, the oxidized DEPE product was not observed. Further attempts to produce more **5** to repeat the reaction with CO_2, for further spectroscopic analysis using NMR and liquid chromatography mass spectrometry (LCMS) were unsuccessful.

69

$$6 \xrightarrow[\text{Diethyl Ether}]{\text{CO}_2 \text{ atm}} 5 \;+\; \text{DEPE Oxide} \qquad (12)$$
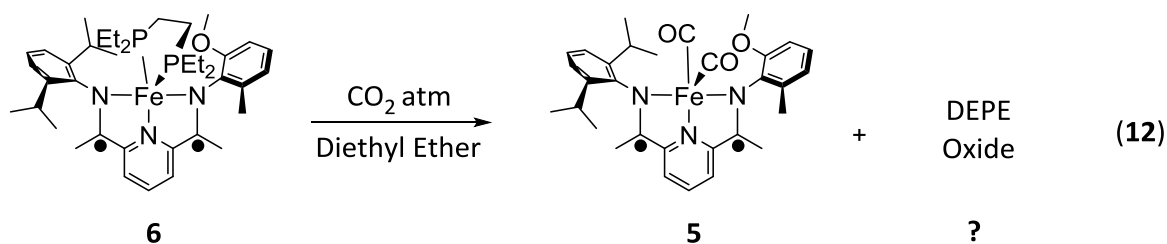
TMSCl, an external oxygen atom acceptor was then utilized. The complex **4** was formed in situ in diethyl ether from two equivalents of NaBHEt$_3$H. Once all of the hydride was consumed (indicated by ^{11}B{^{1}H} NMR spectrum (**Figure 3.17**)) the solution was filtered and four equivalents of TMSCl and tetramethylsilane (TMS, as an internal standard) were added to the solution. The solution was charged with one atmosphere of CO$_2$, immediately turning brown and then back to green, with subsequent formation of a blue precipitate over six hours (**eq. 13**).

$$4 \xrightarrow[\substack{\text{Diethyl Ether} \\ -\,2\,\text{TMS-O-TMS}}]{\substack{\text{CO}_2 \; 1\,\text{atm} \\ 4\,\text{TMSCl} \\ 4\,\text{TMS}}} 5 \;+\; 7 \qquad (13)$$
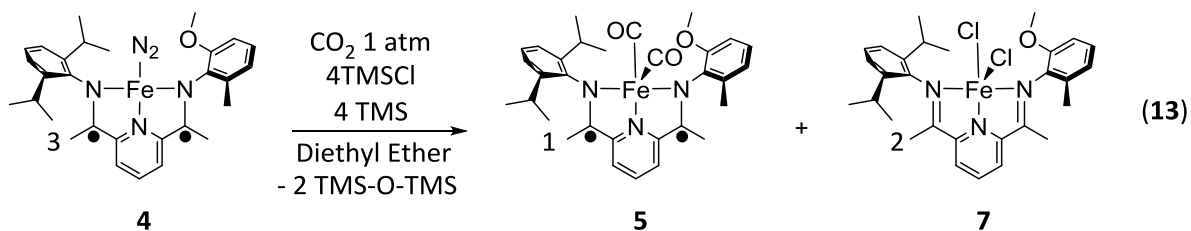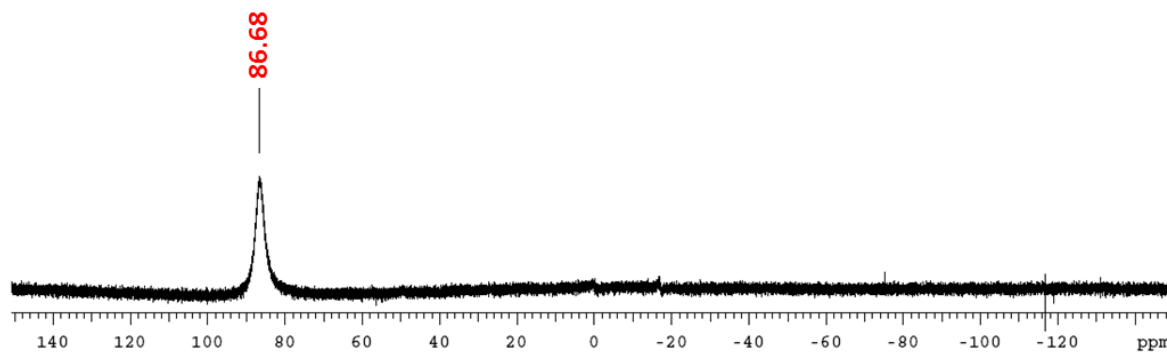
Figure 3.17. $^{11}B\{^1H\}$ NMR spectrum of **4** after filtration through a pipette plugged with glass wool and celite. 160 MHz, diethyl ether. The resonance at 86.68 ppm corresponds to BEt_3, which was derived from the complete reduction of **4** with two equivalents of $NaBHEt_3$.

Analysis of the paramagnetic blue precipitate revealed the (^{MeO}PDI)$FeCl_2$ complex **7**, which is the dichloride of the starting material (**3**). The IR and ^1H NMR spectra of **7** resembles that of complex **3**, with the C=N stretching frequency at 1581 cm^{-1} and resonances spanning 100 to - 50 ppm, respectively (**Figure 3.18 & 3.19**). Once again, the assignment of the ^1H NMR of **7** was compared to well characterized PDI $FeCl_2$ complex from Gibbon and coworkers.[42] Also, the prominent solvents displayed within the ^1H NMR spectrum are from adventitious solvents in the N_2 glove box.
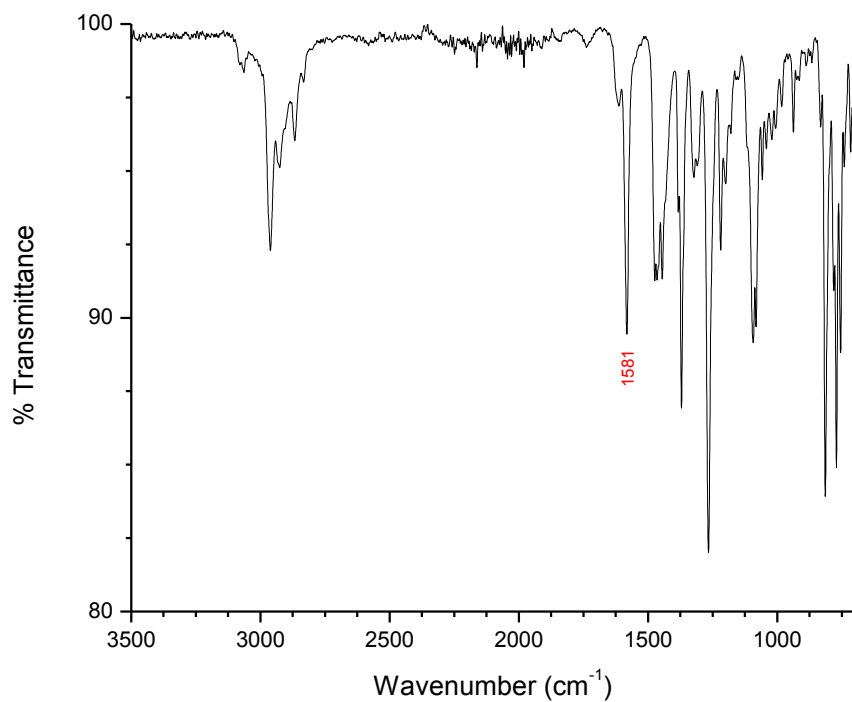
Figure 3.18. Solid FT-ATR infrared spectrum of **7.**
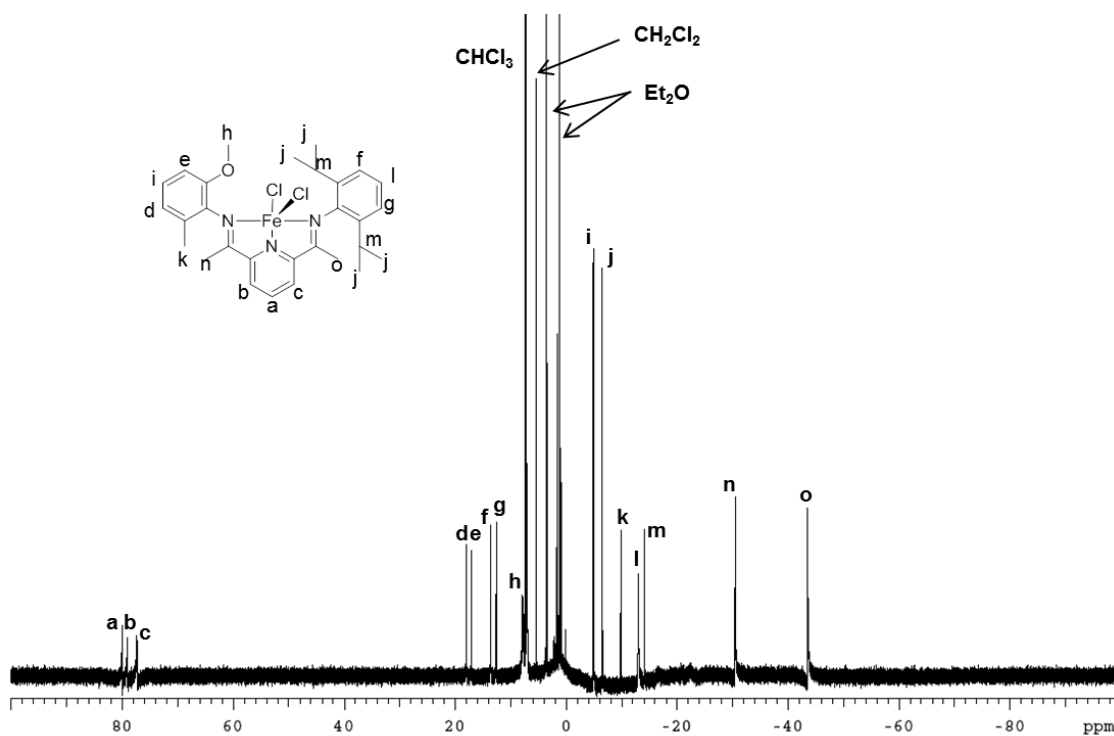
Figure 3.19. ^{1}H NMR spectrum of **7**, 500 MHz, CDCl$_3$.

72

Blue single crystals of **7** were acquired by layering diethyl ether into a solution of **7** in methanol. An ORTEP view of **7** is shown in **Figure 3.20**. The Fe center is a five-coordinate with square-pyramidal geometry (τ = 0.12). The bond lengths and angles are similar to **3**. The measured effective magnetic moment (μ_{eff}) of 5.58 (solid) and 4.94 μ_B (solution) are consistent with a high-spin (S = 2) Fe(II) center. At room temperature, the zero-field Mössbauer parameters were also similar to **3**, which is characterized as a high-spin Fe(II) center (ΔEQ = 0.88(2); δ = 0.677(9) mm/s) with a neutral ^{MeO}PDI ligand (**Figure 3.20**).
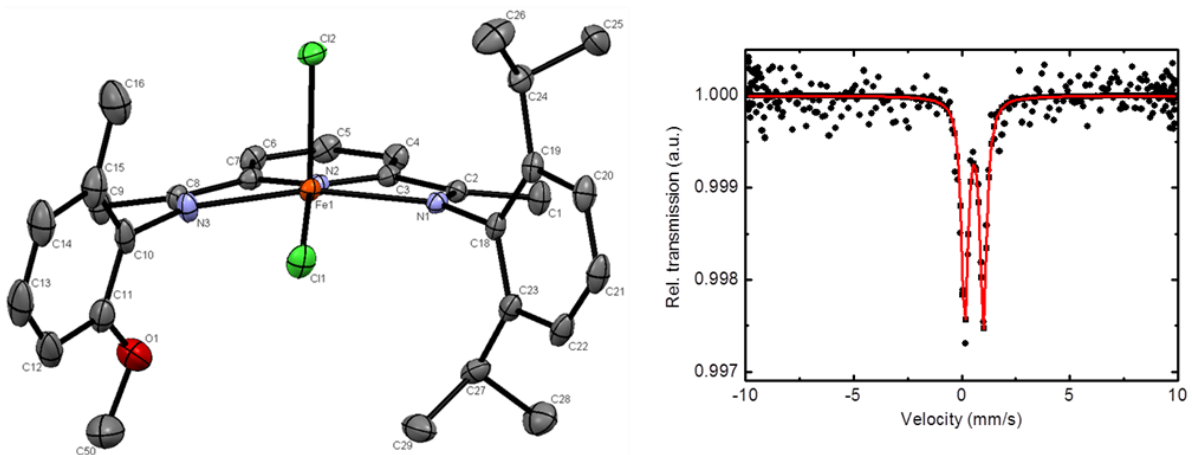
Figure 3.20. Solid-state structure (30% probability) of **7** (left). H atoms have been omitted for clarity. Selected bond lengths (Å) and angles (deg) for one independent molecule in the unit cell: Fe(1)–Cl(1) 2.270(2), Fe(1)–Cl(2) 2.332(3), Fe(1)–N(1) 2.207(2), Fe(1)– N(2) 2.104(2), Fe(1)–N(3) 2.215(2), C(2)–N(1) 1.284(3), C(8)–N(3) 1.284(4); Cl(1)–Fe(1)–Cl(2) 110.14(3), N(2)–Fe(1)–Cl(1) 150.53(6), N(1)–Fe(1)–N(3) 143.27(9). Zero-field Mössbauer spectrum of **7** (right).

^{29}Si{^{1}H} NMR analysis of the green solution revealed the remaining oxygen atoms from CO_2 in the molecule trimethylsilyl oxide (TMS-O-TMS) in a molar ratio of 1:2 (**Figure 3.21**). The ^{29}Si{^{1}H} NMR spectrum, prior to the introduction of CO_2 showed virtually all

73

TMSCl at 29.9 ppm, relative to an internal standard, TMS. After the addition of CO_2, the TMSCl resonance disappeared and a new resonance at 6.87 ppm appeared, relative to TMS, corresponding to bis-trimethylsilyl oxide (TMS-O-TMS).
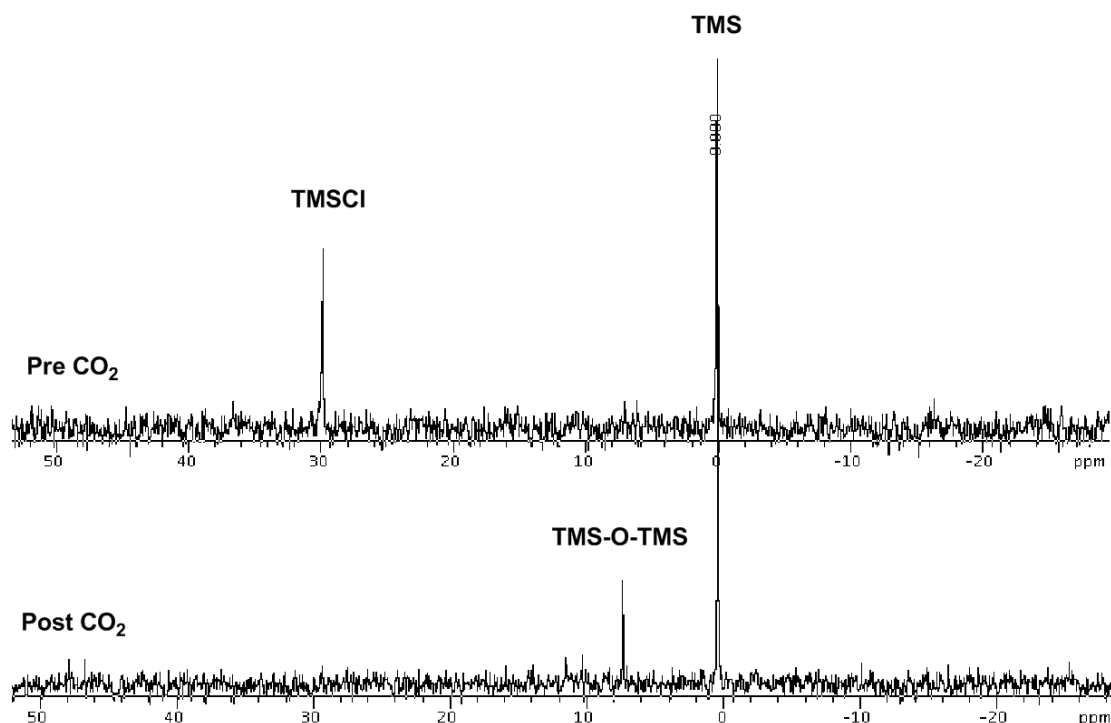
Figure 3.21. The $^{29}Si\{^{1}H\}$ NMR spectra of the before and after CO_2 reduction, where TMSCl is consumed and oxidized to form TMS-O-TMS.

It is important to note, the reduction of CO_2 to CO is done under room temperature. The ^{MeO}PDI ligand helped supply the electrons needed to reduce CO_2, while the Fe center binds the CO_2 molecule, in order for electrons to reduce CO_2. Throughout the reduction process, the ferrous state of the Fe center is conserved. Another example of the reductive cleavage of CO_2 to CO is realized on Fe(II), but this time, employing redox active ligands.[14]

74

3.9 Proposed Mechanism for the Binding and Breakdown of CO_2 to CO

The binding mode of CO_2 on the Fe center of the ^{MeO}PDIFe complex is under investigation, along with the mechanism. Several points can be proposed based off of the example of Chirik's developed mechanism of cycloaddition of dienes.[35] As shown in **Scheme 2.6**, the diene substrate binds end-on (through the π bond of the diene) to the Fe center of the ^{ipr}PDIFe(II) complex. The d-orbitals of the Fe overlap with the p-orbitals of the diene, long enough for electrons to transfer. CO_2 also has double bonds that can possibly bind to the Fe center of ^{MeO}PDIFe complex in the same fashion. Therefore, CO_2 is proposed to bind in an end-on mode, long enough for a two electron transfer to the CO_2 molecule to be reduced to CO. The CO molecule is released and ultimately reacts with complex **4** to produce complex **5**. The oxygen atom from CO_2, thought to be bound to the neutral ^{MeO}PDIFe complex, creates a proposed highly reactive bridging bis-μ^2-oxo Fe dimer (^{MeO}PDIFeO$_2$$^{4-}$Fe^{MeO}PDI). This proposed highly reactive ^{MeO}PDIFeO$_2$$^{4-}$Fe^{MeO}PDI complex can potentially be stabilized by the surrounding CO_2 molecules, to create a quasi-stable μ^2-dicarbonate Fe dimer, which may be the purple species. The addition of TMSCl produces the highly stable Si-O bond, which forms the TMS-O-TMS molecules. The Cl$^-$ ions can then bind to the neutral ^{MeO}PDIFe complex to form the dichloride of the starting material. However, this mechanism is purely speculative at this point and further experiments are currently underway.
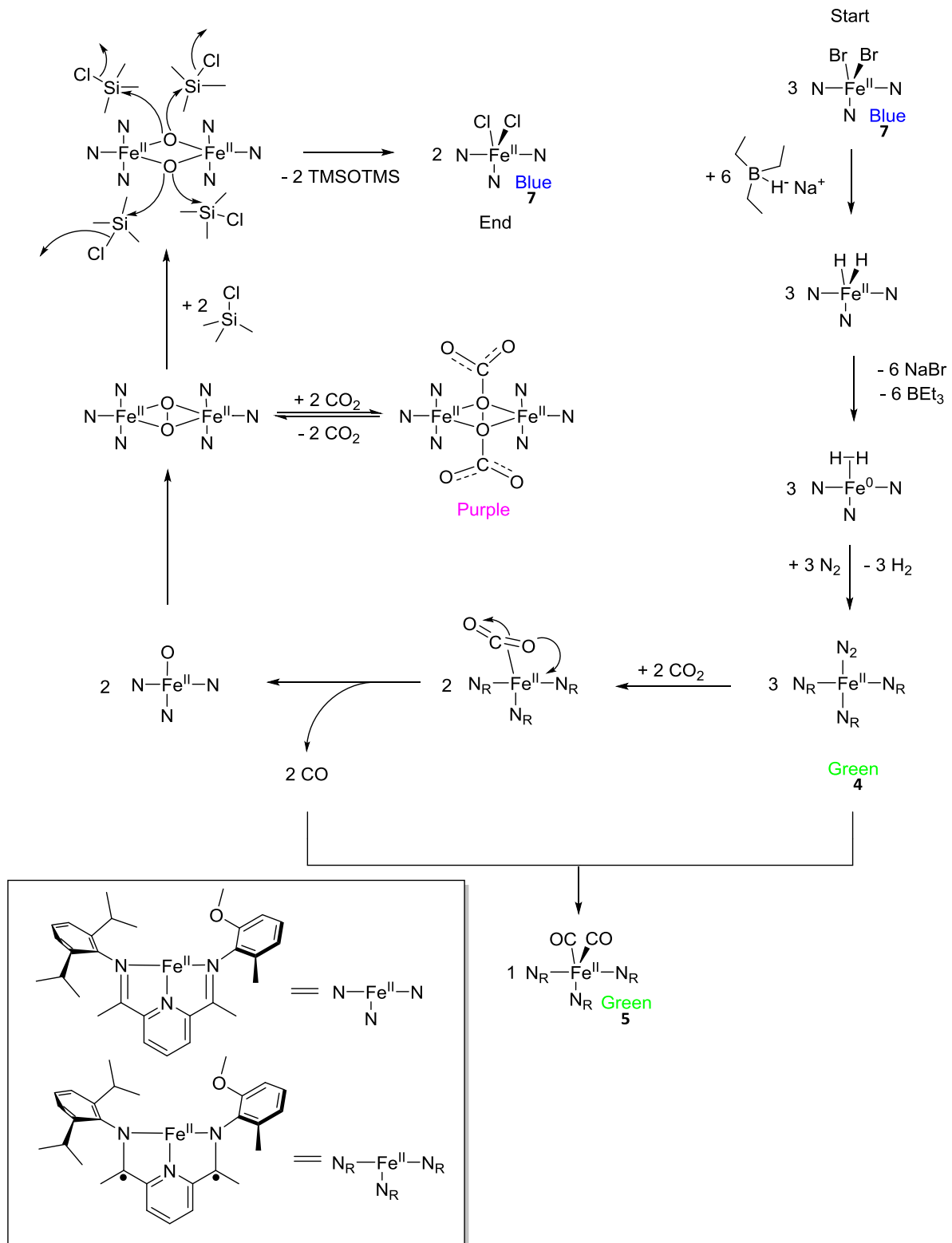
Figure 3.22. Proposed mechanism for the conversion of CO_2-to-CO on ^{MeO}PDIFe(II) complex.[35,36]

3.10 References

1. Aresta, M.; Nobile, C. F.; Albano, V. G.; Forni, E.; Manassero, M. *J. Chem. Soc., Chem. Commun.* **1975**, 15, 636.
2. Heats of formation taken from: CRC Handbook, 92nd ed.; http://www.hbcpnetbase.com/.
3. Meyer K.; Rodriguez C, I.; *J. Am. Chem. Soc*. **2005**, 127, 11242 – 11243.
4. Calabrese, J. C.; Herskovitz, T.; Kinney, J. B. *J. Am. Chem. Soc.* **1983**, 105, 18, 5914–5915.
5. Herskovitz, T. *J. Am. Chem. Soc*. **1977**, 99, 7, 2391–2392.
6. Aresta, M.; Nobile, C. F. J. *Chem. Soc. Dalton Trans.* **1977**, 7, 708–711.
7. Aresta, M.; Nobile, C. F. *Inorg. Chim. Act.* **1977**, 24, 2, L49–L50.
8. Komiya, S.; Akita, M.; Kasuga, N.; Hirano, M.; Fukuoka, A. *J. Chem. Soc. Chem. Commun*. **1994**, 9, 1115 – 1116.
9. Sakamoto, M.; Shimizu, L.; Yamamoto, A. *Organometallics*. **1994**, 13, 2, 407 – 409.
10. Tetrick, S. M.; Thom, F. S.; Cutler, A. R. *J. Am. Chem. Soc.* **1998**, 119, 26, 6193–6194.
11. Hanna, T. A.; Baranger, A. M.; Bergman, R. G. *J. Am. Chem. Soc*. **1995**, 117, 11, 3292–3293.
12. Audett, J. D.; Collins, T. J.; Santarsiero, B. D.; Spies, G. H. *J. Am. Chem. Soc.* **1982**, 104, 25, 7352 – 7353.
13. Kubiak, C. P.; Woodcock, C.; Eisenberg, R. *Inorg. Chem.* **1982**, 21, 6, 2119–2126.
14. Field, J. S.; Haines, R. J.; Sundermeyer, J.; Woollam, S. F. *J. Chem. Soc. Dalton Trans.* **1993**, 18, 2735 – 2748.
15. Tso, C. T.; Cutler, A. R. *J. Am. Chem. Soc.* **1986**, 108, 6069.
16. Vites, J. C.; Steffey, B. D.; Giuseppetti-Dery, M. E.; Cutler, A. R. *Organometallics.* **1991**, 10, 8, 2827–2834.
17. Senn, D. R.; Gladysz, J. A.; Emerson, K.; Larsen, R. D. *Inorg. Chem.* **1987**, 26, 17, 2737 – 2739.
18. Gibson, D. H.; Ye, M.; Sleadd, B. A.; Mehta, J. M.; Mbadike, O. P.; Richardson, J. F.; Mashuta, M. S. *Organometallics*. **1995**, 14, 3, 1242–1255.
19. Eady, C. R.; Guy, J. J.; Johnson, B. F. G.; Lewis, J.; Malatesta, M. C.; Sheldrick, G. M. *J. Chem. Soc. Chem. Commun.* **1976**, 602.
20. Balbach, B. K.; Helus, F.; Oberdorfer, F.; Ziegler, M. L. *Angew. Chem.* **1981**, 93, 5, 479 – 480.
21. Floriani, C.; Fachinetti, G. *J. Chem. Soc. Chem. Commun*. **1974**, 15, 615–16.
22. Gibson, D. H. *Coord. Chem. Rev.* **1999**, 185 – 186, 335 – 355.
23. Lundquist, E. G.; Huffman, J. C.; Folting, K.; Mann, B. E.; Caulton, K. G.; *Inorg. Chem.* **1990**, 29, 128 –134.
24. Ishida, H.; Tanaka, K.; Tanaka, T. *Organometallics*. **1987**, 6, 181.
25. DuBois, D. L.; Miedaner, A.; Haltiwanger, R. C. *J. Am. Chem. Soc.* **1991**, 113, 8753.
26. Raebiger, J. W.; Turner, J. W.; Noll, B. C.; Curtis, C. J.; Miedaner, A.; Cox, B.; DuBois, D. L. *Organometallics*, **2006**, 25, 3345.

27. Dubois, D. L.; *Comments Inorg. Chem*. **1997**, 19, 307.
28. Hammouche, M.; Lexa, D.; Momenteau, M.; Saveant, J. M. *J. Am. Chem. Soc.* **1991**, 113, 8455.
29. Grodkowski, J.; Neta, P.; Fujita, E.; Mahammed, A.; Simkhovich, L.; Gross, Z. J. *Phys. Chem.* **2002**, 106, 4772–4778.
30. Ruiz, J.; Guerchais, V.; Astruc, D. *J. Chem. Soc. Chem. Commun*. **1989**, 812 – 813.
31. Pun, S. N.; Chung, W. H.; Lam, K. M.; Guo, P.; Chan, P. H.; Wong, K. Y.; Che, C. M.; Chen, T. Y.; Peng, S. M. *J. Chem. Soc. Dalton Trans.* **2002**, 575 – 583.
32. Sadique, A. R.; Brennessel, W. W.; Holland, P. L. *Inorg. Chem*. **2008**, 47, 784 - 786.
33. Lu, C. C.; Saouma, C. T.; Day, M. W.; Peters, J. C. *J. Am. Chem. Soc*. **2007**, 129, 4 – 5.
34. Allen, O. R.; Dalgarno, S. J.; Field, L. D. *Organometallics*. **2008**, 27, 3328 – 3330.
35. Bouwkamp, M. W.; Bowman, A. C.; Lobkovsky, E.; Chirik, P. J. *J. Am. Chem. Soc.* **2006**, 128, 13340 – 13341.
36. Tondreau, A. M.; Milsmann, C.; Lobkovsky, E.; Chirik, P. J. *Inorg. Chem*. **2011**, 50, 9888 - 9895.
37. Britovsek, G. J. P.; Gibson, V. C.; Kimberley, B. S.; Maddox, P. J.; McTavish, S. J.; Solan, G. A.; White, A. J. P.; Williams, D. J. *Chem. Comm.* **1998**, 849.
38. Addison, A. W.; Rao, T. N.; Reedjik, J.; van Rijn, J.; Verschoor, G. C. *J. Chem. Soc. Dalton Trans.* **1984**, 1349 – 1356.
39. Small, B. L.; Brookhart, M.; Bennett, A. M. A. *J. Am. Chem. Soc.* **1998**, 120, 4049.
40. Strömberg, S. A.; White, A. J. P.; Williams, D. J. *J. Am. Chem. Soc*. **1999**, 121, 8728.
41. Bianchini, C.; Mantovani, G.; Meli, A.; Migliacci, F.; Zanobini, F.; Laschi, F.; Sommazzi, A. *Eur. J. Inorg. Chem*. **2003**, 1620.
42. Britovsek, G. J.; Clentsmith, G. K. B.; Gibson, V. C.; Goodgame, D. M. L.; McTavish, S. J.; Pankhurst, Q. A. *Catal. Commun*. **2002**, 3, 207–211.
43. Sur, S. K. *J. Mag. Res.* **1988**, *82*, 169 - 173.
44. Greenwood, N. N.; Gibb T. C. *Mössbauer Spectroscopy,* 1971, Chapman and Hall Ltd., London.
45. Bart, S. C.; Lobkovsky, E.; Bill, E.; Wieghardt, K.; Chirik, P.J. *Inorg. Chem*. **2007**, 46, 705 – 7063.
46. Russell, S. K.; Darmon, J. M.; Lobkovsky, E.; Chirik, P. J. *Inorg. Chem*. **2010**, 49, 2782 – 2792.
47. Stieber, S. C. E.; Milsmann, C.; Hoyt, J. M.; Turner, Z. R.; Finkelstein, K. D.; Wieghardt, K.; DeBeer, S.; Chirik, P. J. *Inorg. Chem*. **2012**, 51, 3770 – 3785.
48. Bart, S. C.; Chlopek, K.; Bill, E.; Bouwkamp, M. W.; Lobkovsky, E.; Neese, F.; Wieghardt, K.; Chirik, P. J. *J. Am. Chem. Soc*. **2006**, 128, 13901 – 13912.
49. Vlugt, J. I. *Eur. J. Inorg. Chem*. **2012**, 363 - 375

Chapter 4. CO Release

4.1 Fe-CO Bond

There are several notable examples of strong metal carbonyl bonds in inorganic chemistry and in nature; however, one of the most remarkable and physiologically significant examples can be found in the CO poisoning of our blood.[1] Our blood cells contain a metalloprotein called hemoglobin. This iron-containing oxygen-transporter carries the O_2 that is necessary for respiration from our lungs and deposits this O_2 to the tissues throughout our body.[2] Hemoglobin is composed of four polypeptide chains, each containing a heme group and one Fe ion (Protein Database #PDI1YVT) (**Figure 4.1**). Fe(II) is the site of O_2 binding, therefore, hemoglobin is capable of binding to a total of four O_2 molecules. When O_2 binds to one of the Fe centers, the Fe ion moves back towards the center of the plane of the porphyrin ring due to the oxidation to Fe(III), which induces a conformational change of the rest of the protein. This conformational change in the other heme sites can then allow binding of O_2 molecules in an easier and cooperative manner. In the presence of CO, however, the binding of O_2 to hemoglobin is hindered, due to hemoglobin's high binding affinity for CO (250 times greater than O_2).[3]

79
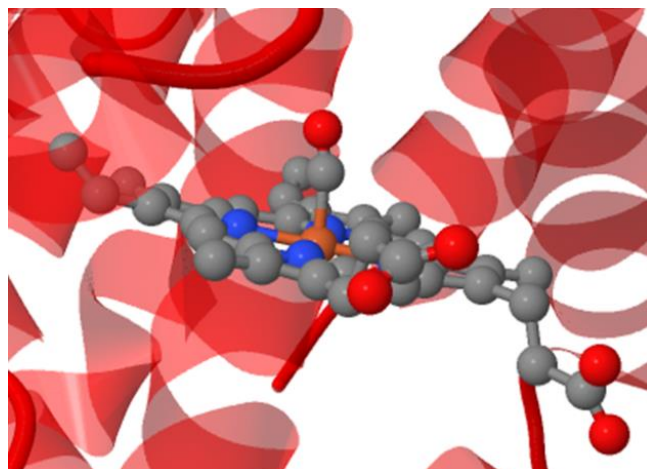
Figure 4.1. Crystal structure of CO bound hemoglobin (PDI1YVT).

The binding of CO to Fe in all complexes can be attributed to the surrounding ligand environment of the Fe center. In an Fe(II) center, the geometry and coordination number of the Fe complex play an important role in the binding/non-binding of CO molecules.[4] With respect to steric effects, the binding of CO can be seen in the four coordinate iron(II) diazadiene ((iPr-DAB)FeI$_2$) complex to form the octahedral CO bound Fe(II) species.[5] However, in an almost similar four coordinate iron(II) phosphine ((P^{t}Bu$_2$Me)FeCl$_2$) complex, the addition of CO was not observed. This difference is observed because the bulky tert-butyl group off of the phosphine hinders CO binding, despite the open coordination sites on Fe(II) (**Scheme 4.1**).[6] The overall field strength of the ligand also governs CO binding. Strong field ligands on Fe(II) will provide an easier binding mode for CO, while weak field ligands hinder the process.[4] The binding of CO onto Fe(II) with strong field ligands can be explained by the ligands stabilization of the low-spin (stable) complex.[4]

80
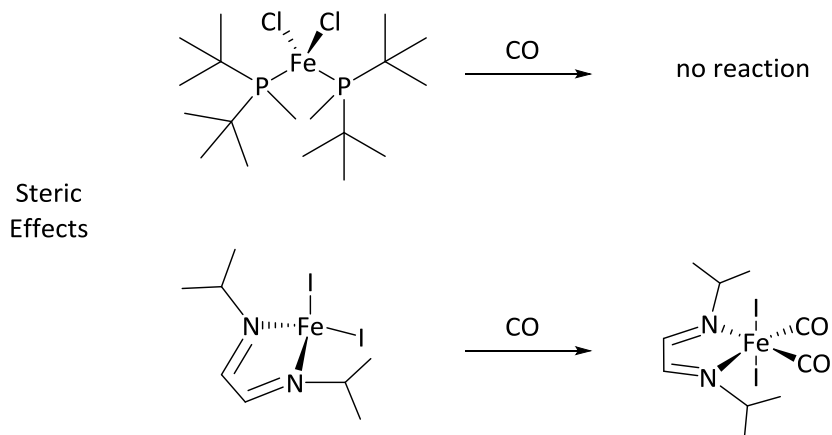
Scheme 4.1. Steric affects CO binding to the unsaturated Fe(II) complex.[5,6]

The ligand plays a big role in not only stabilizing the metal, but also in altering the d-orbital electron density of the metal when binding to CO.[4] CO can interact with metals such as Fe, through dative bonds. CO is considered a σ-donor ligand, therefore it has directional p-orbitals that overlap with the d_z^2-orbitals of Fe (**Figure 4.2**). Subsequently, another interaction occurs through a π-backbonding event in which orbitals overlap from the anti-bonding p-orbitals of CO and the bonding d-orbitals of Fe.
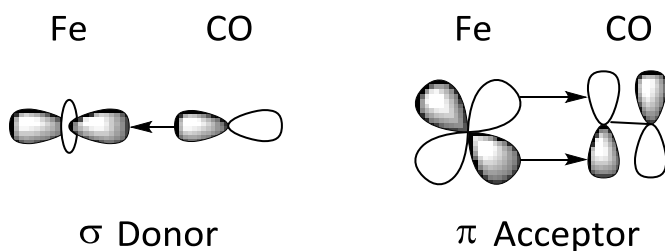
Figure 4.2. Orbital overlap in Fe-CO bonds.

4.2 Application of CO release

Due to the surprisingly beneficial effect of CO on our tissues and organs, particularly in response to oxidative stress, efforts have increased for the study of CO release from metals.[7] The development of solid storage forms for CO that are safe to handle and from which the CO can be released by specific trigger, is a rich subset of chemistry called CO releasing molecules (CORMs).[8-11] A number of metal-carbonyl complexes have been identified as CORMs that can trigger CO release by photo-activation (**Scheme 4.2**).[12,13] The most thoroughly studied CO releasing complex is the Rutheium(III) [(glycinate)Ru(CO)$_3$Cl] with three CO bound molecules.[14] However, the complex can only display a half life time of 3.6 minutes in human plasma which is not long enough to reach the specific targeted organ.[14] Therefore, more stable metal complexes must be explored if this field is likely to thrive in the fast growing competitive market. Solutions to bypass this problem include employing the use of a cheap Fe centered complex as well as altering the design of the ligand (for CO stabilization).
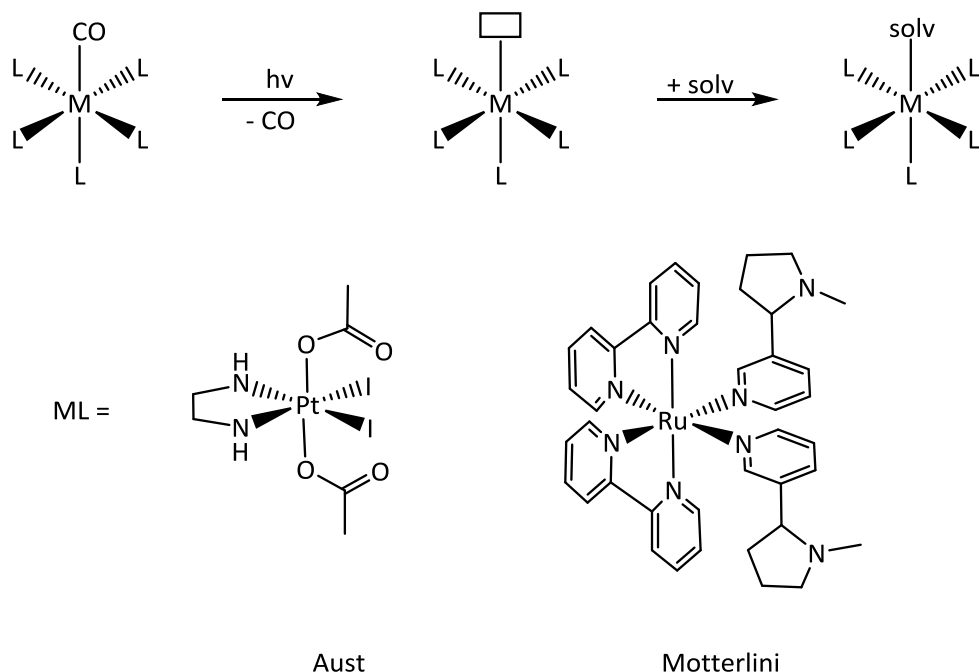
Scheme 4.2. Photo-activated CO release on Aust and Motterlini's metal complexes.[12,13]

4.3 Five-Coordinate CO bound Fe Complexes

Within this thesis, a tridentate ligand (PDI) Fe(II) complex with the bound CO molecules is reported as a product of the capture of CO gas (derived from CO_2). Examples of another five-coordinate carbonyl Fe complex were reported by Caulton and coworkers in 2008. They reported the reaction of a three-coordinate Fe(I) complex, [(PNP)Fe], with one atmosphere of CO, to yield a square-pyramidal dicarbonyl complex. One of the CO group in the apical position and the second one, trans to the central N atom of the PNP ligand (**Scheme 4.3**). However, CO coordination in this system proved to be irreversible and CO

could not be removed under vaccum.[15] Holland and coworkers also synthesized a five-coordinate Fe complex bearing a bulky bidentate β-diketiminate ligand that coordinated three CO molecules to form a square-pyramidal geometry (**Scheme 4.3**).[16] Once again, this system did not display reversible binding of CO on Fe.
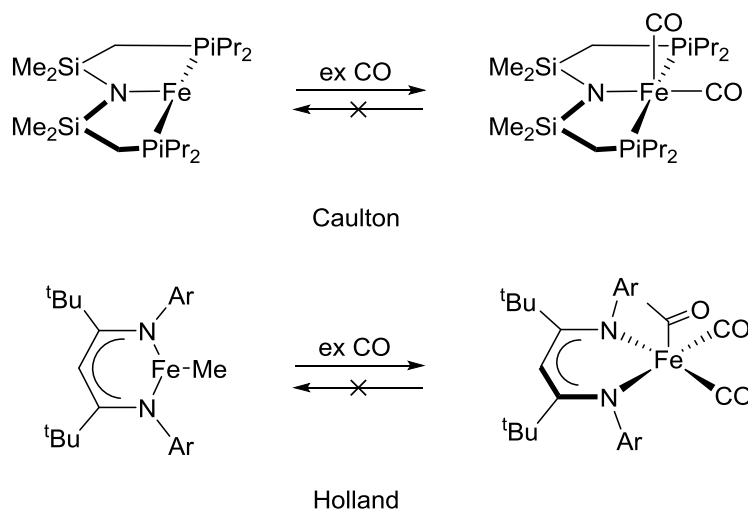
Scheme 4.3. Five coordinate CO bound Fe complexes that cannot reversibly bind CO molecules.

4.4 CO Binding Conditions (HOMO-LUMO Gap vs. Pairing Energy)

The ^{MeO}PDI ligand employed within this thesis also constrains the Fe center (in ^{MeO}PDIFe(CO)$_2$) to a square pyramidal geometry when two CO molecules are bound. As mentioned in chapter 3, the PDI ligand is redox active, and only in the reduced form, can CO

bind to the Fe center. This can be explained by the spin state (number of unpaired electrons, S) change of the PDIFe complex, when in the reduced form versus the neutral form. A spin allowed transition from high spin to low spin must occur for stable CO binding. The spin state of a complex is determined by comparing the energy difference (HOMO-LUMO gap, ΔE) and the pairing energy (energy of pairing two electrons, PE). The ΔE must be greater than PE, in order for stable CO binding, and the ΔE is affected by the ligand environment (**Figure 4.3**).[4] Chirik has written numerous reports on the spin state change of the PDI Fe complex (from S = 2 to S = 0) when CO binds.[17,35,38,39] Therefore, a switch can be envisioned, where the spin state change (due to the reduction of the ligand) can control the binding of CO molecules.
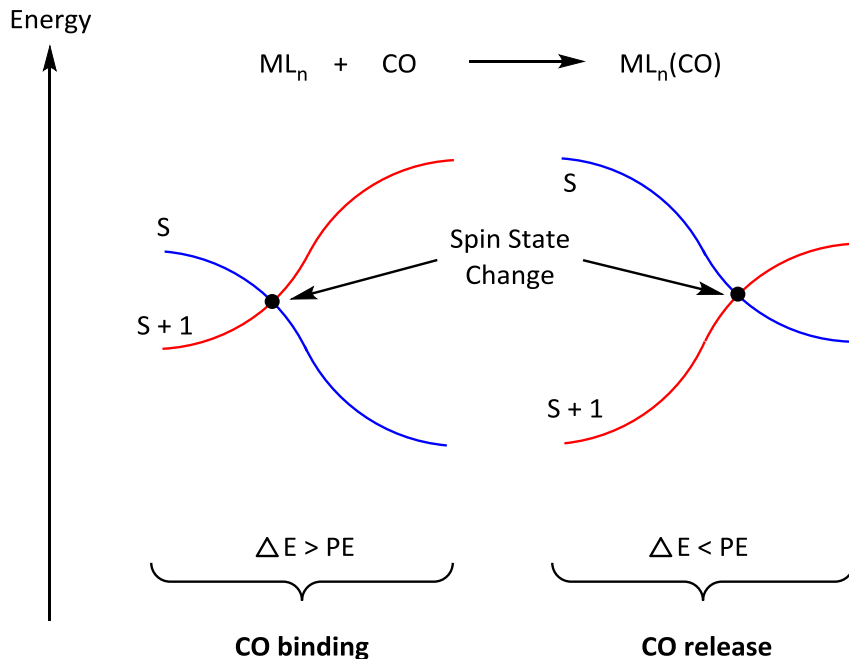
Figure 4.3. Energy profile of the binding and non-binding conditions of CO to unsaturated complex.[4]

4.5 Comparing other CO bound Fe complexes (derived from CO_2)

The CO release step, coupled with the CO_2 reduction from chapter 3, can ultimately produce CO gas for the FT process. Fe complexes that produced CO molecules from the reduction of CO_2 gas have been reported; however, the release of CO gas to complete the CO_2-to-CO cycle was not observed.

Holland has shown three different products from the reaction of CO_2 with a bridging dinitrogen Fe(I) complex, (LtBuFeNNFeLtBu), (L^{tBu} = 2,2,6,6-tetramethyl-3,5-bis[(2,6-diisopropylphenyl)imino]hept-4-yl). The dicarbonyl Fe complex was the major product (**Scheme 4.4**).[15] Meanwhile, Peters and coworkers have also shown that the tris(phosphine)borate Fe(I) complex, [PhBPCH$_2$Cy$_3$]FeH, can react with CO_2 to produce three products, with a bridging μ-oxo and μ-carbonyl Fe complex as the major product (**Scheme 4.4**).[18] However, both of these complexes utilized Fe(I) center for the CO_2 to CO reduction. Fe(II) complexes are more rare in literature for the reduction of CO_2 to CO due to the insufficient amount of electrons required for this process. The only known Fe(II) complex that can reduce CO_2-to-CO, prior to this work, was Field's Fe(dmpe)H$_2$ complex, (dmpe = 1,2-bis(dimethylphosphino)ethane). This complex produced a CO bound Fe complex, Fe(dmpe)(CO)H, and the bicarbonate counter anion (**Scheme 4.4**).[19] The three reactions summarized above can be found in greater detail in chapter 3 (**3.3. Breaking down CO_2 (Chemically)**). It is also important to note that the three reactions did not release the CO

www.manaraa.com

molecule that was derived from the reduction of CO_2, which sets the work presented herein noteworthy.
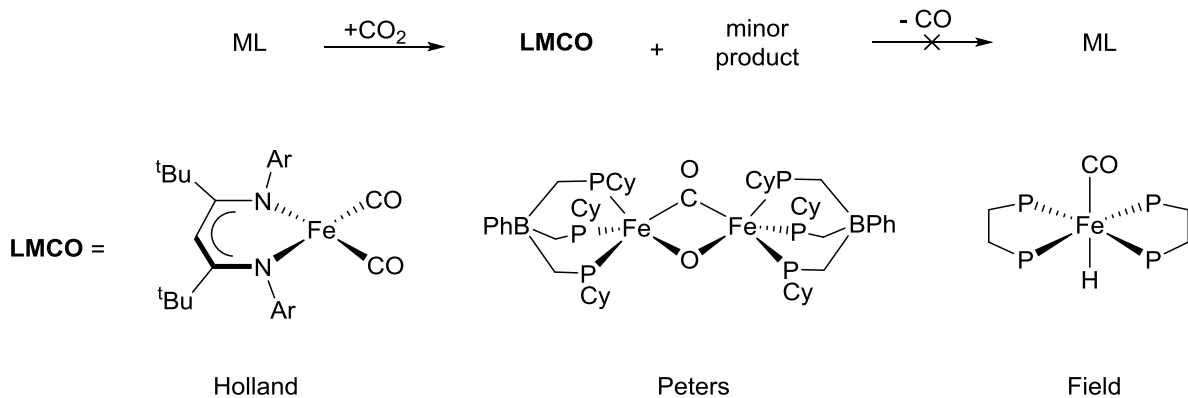
Scheme 4.4. Notable Fe(I) and Fe(II) complexes that can breakdown CO_2 to CO.[13,18,19]

Herein, the release of CO gas upon the oxidation of the reduced redox active [MeO]PDIFe complex is described. In addition, when an oxidant such as hydrochloric (HCl) is used, hydrogen gas (H_2) can also be produced. These two gases (CO and H_2) are important for the FT process, as described in chapter 1. This chapter will discuss the CO release step of [MeO]PDIFe(CO)$_2$ complex, chemically and electro-chemically, along with various acid/base substituted PDIFe(CO)$_2$ complexes that affect the redox potential of the CO release step.

4.6 CO Release (Chemical Oxidation)

When two equivalents of a chemical oxidant, such as HCl (1.0 M in diethyl ether), was added to the solution of **5**, product **7** precipitated out of solution (diethyl ether solution). CO and H_2 gas were also produced (**eq. 14**). Within two hours, the reaction noted as was complete as indicated by the formation of blue solid (**7**) surrounding the walls of the reaction vessel, and the absence of the green color of **5.**
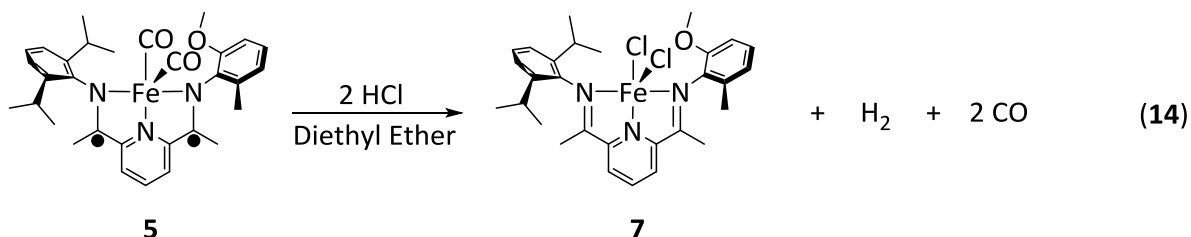
The CO and H_2 gases were verified by gas chromatography (GC). A set of standards were made from the introduction of known amounts of CO and H_2 gas (from a purified CO and H_2 gas tank) (**Figure 4.4**). Using the calibration curve, the amounts of CO and H_2 gas produced from the oxidation reaction were determined. However, due to the solubility of CO and H_2 gas within the diethyl ether solvent, a lower than expected value was obtained.[20] The CO and H_2 gas was measured in area counts, which were then converted to volume using the calibration curve. The gas law, $PV = nRT$, was then employed to calculate the moles of CO (0.0277 mmol) and H_2 (below quantification limits) gases within the headspace of the reaction vessel (**Figure 4.5**).
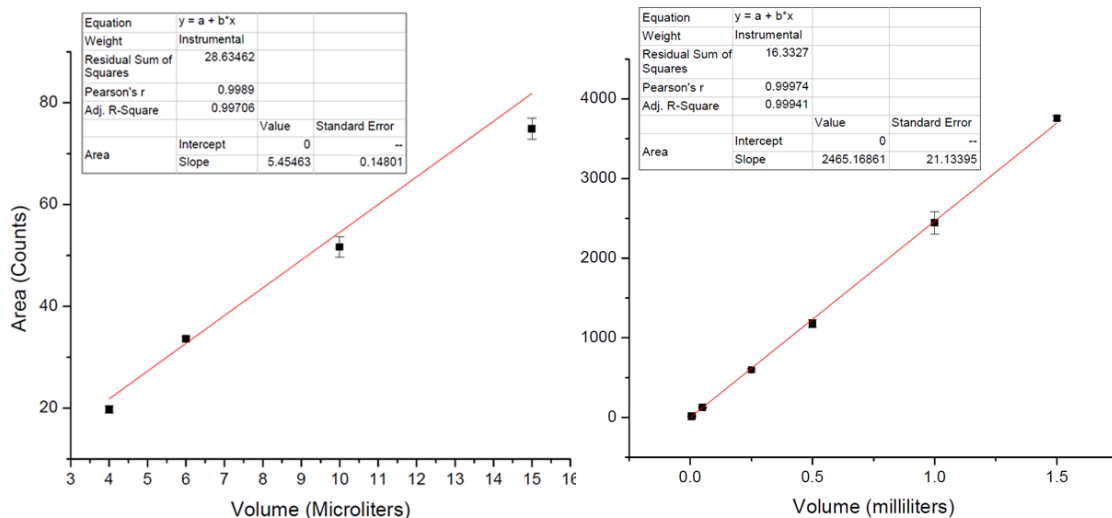
Figure 4.4. H$_2$ (left) and CO (right) gas calibration curve for the oxidation reaction of **5** with two equivalents of HCl.
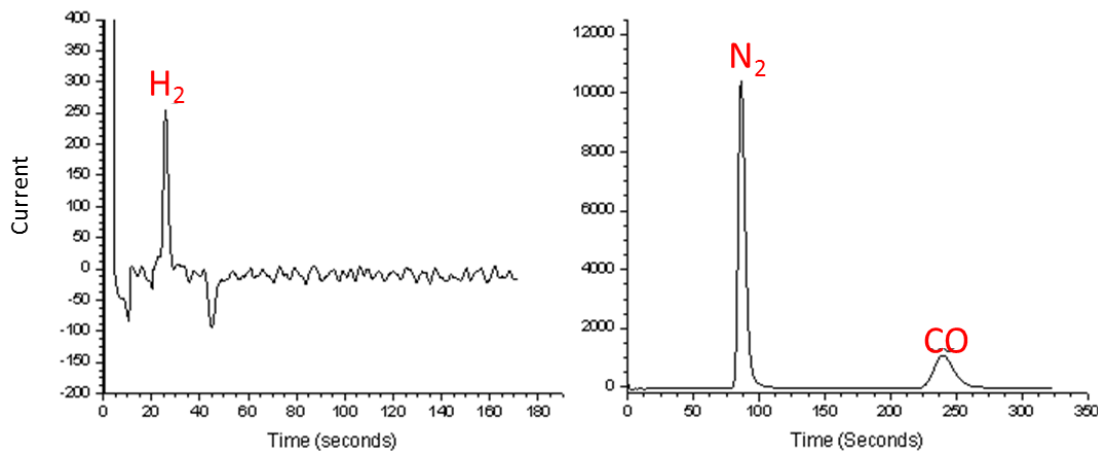
Figure 4.5. Gas Chromatographs of the headspace of the reaction vessel. The area of H$_2$ was calculated to be 5.9896 counts at a retention time of 1.38 sec from a 0.5 mL injection of a 10 mL headspace. The area of CO was calculated to be 20.0772 counts at a retention time of 240 sec from a 0.1 mL injection of a 10 mL headspace.

The GC data indicated a quarter of the CO gas was release, when compared to the theoretical value. This corresponded to 0.0579 mmol of CO molecules (with 0.152 mmol of reactant). The lower detected value can be attributed to the CO molecule dissolving in 10 mL of diethyl ether solvent as well as the incomplete oxidation reaction which produces the partially oxidized product (one electron reduced ^{MeO}PDI ligand with both CO still bound to the Fe center).[18] The partially oxidized product is bluish green and is detected by CO stretching frequencies, which are shifted from 1947 and 1883 cm^{-1} in **5** to 2075 and 2036 cm^{-1} (**Figure 4.6**). The partially oxidized product has an Fe(I) center with neutral a ^{MeO}PDI ligand, rather than an Fe(II) center in the previously observed ^{MeO}PDIFe complexes.[38] Therefore the Fe-CO bond is diminished and the stronger C-O stretching frequency observed.
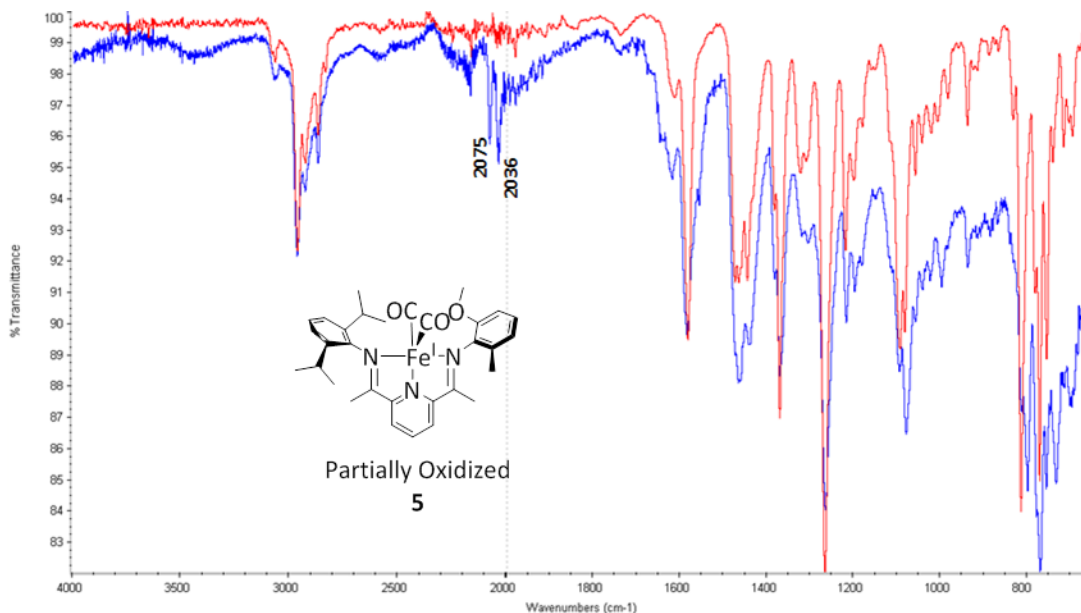
Figure 4.6. Overlay of infrared spectra of **7** and the partially oxidized product of **5**. The red line is the spectrum of independently synthesized **7** and the blue line is the product from the chemical oxidation of **5**.

5 must undergo a two electron oxidation in order to release the CO molecules. This can be explained by the spin state change that is required for CO to release. The complete oxidation of **5** (S = 0) produced the neutral form of the ^{MeO}PDIFe complex, with halide anions, corresponding to S = 2. The pairing energy in the neutral form of the ^{MeO}PDIFe complex is likely higher than ΔE, which does not meet the conditions for CO binding (**Figure 4.7**). These data prompted electrochemical oxidation studies in order to gain further insights into the reduction-oxidation (redox) potential of the ^{MeO}PDIFe complex, partially in respect to the release of CO molecules.
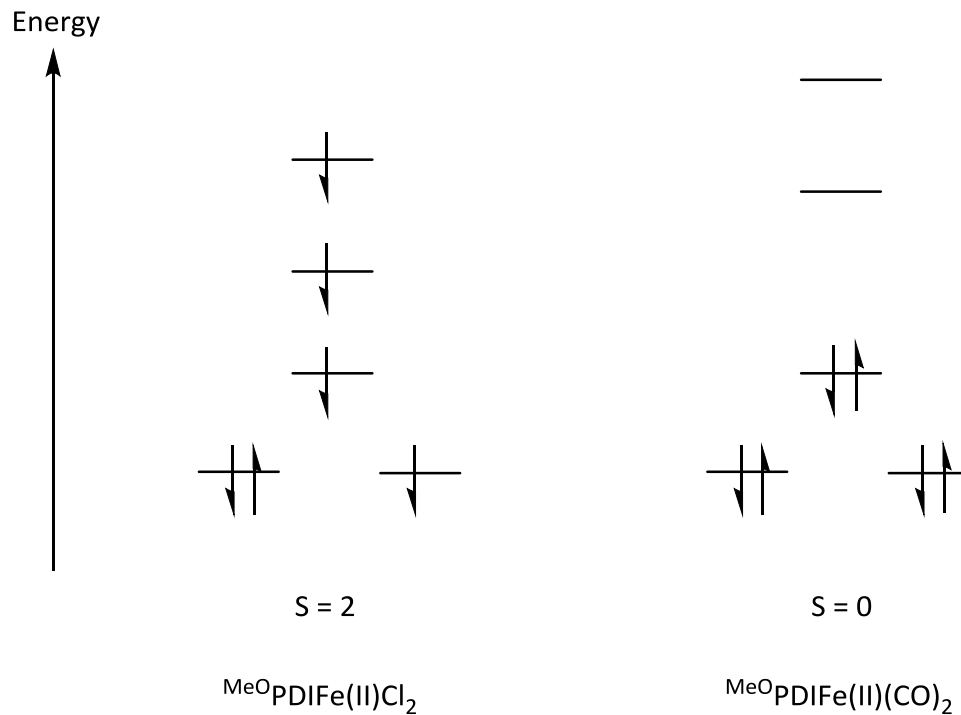
Figure 4.7. Molecular orbital diagram of the neutral (left) and reduced (right) form of the ^{MeO}PDIFe(II) complex. S corresponds to the number of unpaired electrons.[17]

4.7 CO Release (Electrochemical Oxidation)

In the N_2 filled glovebox, a solution of **5** (0.010 M), tetra(n-butyl)ammonium hexafluorophosphate (0.100 M) and dichloromethane (DCM) was prepared in a 50 mL three neck round bottom. To prevent the oxidation of Fe in the open atmosphere, the round bottom was sealed with three rubber septa before it was brought outside the glovebox. The cyclic voltammetry (CV) electrodes were then pierced through the rubber septa and quickly purged with argon gas, to remove all possible reactive species. After half an hour of purging,

92

the cyclic voltammogram of **5** revealed a quasi-reversible oxidation event at −0.524 V. This is believed to be the formation of the partially oxidized **5**, [^{MeO}PDIFe(I)(CO)$_2$]$^+$. Also, an irreversible oxidation event at 0.477 V was revealed. This is believed to be the complete oxidation to the neutral ^{MeO}PDIFe, with the concomitant irreversible release of CO (**Figure 4.8**).
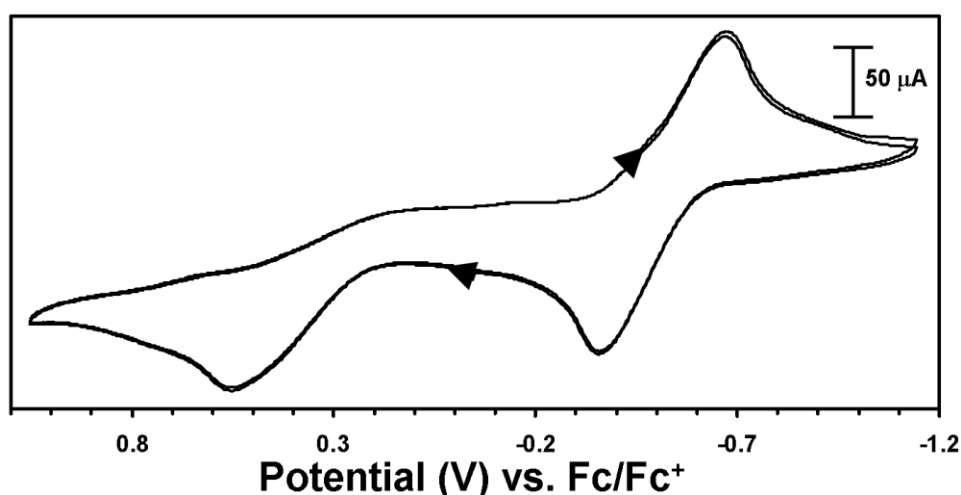
Figure 4.8. CV of 0.01 M 5, 0.1 M [(^{n}Bu)$_4$N][PF$_6$] in DCM, 200 mV/s scan rate, glassy carbon electrode (scan started at -1.15 V).[21]

4.8 Acid/Base PDIFe Complexes (Electrochemical Oxidation Studies)

The CO release study was further expanded by incorporating pendant Lewis basic sites and/or Lewis acidic in the secondary coordination sphere of the PDI scaffold (^{MeNH}PDIFe(CO)$_2$, ^{Me2N}PDIFe(CO)$_2$ and ^{Bpin}PDIFe(CO)$_2$). The secondary coordination sphere of a metal complex is the portion of the ligand that is not directly chelated to the metal.[22]

Recently, Savéant and coworkers have shown electro-catalytic increase in the reduction of CO_2 to CO on their tetraphenylporphyrin (TPP) Fe complexes by modifying all ortho position of the TPP phenyl groups to phenolic groups (**Figure 4.9**).[23] The substituted TPPFe complex with phenolic hydroxyls gave a faradaic yield above 90% through 50 million turnovers over four hours of electrolysis, with no observed degradation at a low over-potential (0.465 V). The basis for the enhanced activity is due to the high local concentrations of the protons associated with the phenolic hydroxyl substituents.

	E^0_{cat} (V vs. NHE)	-1.33
-1.69	η(V)	0.41-0.56
0.89-1.04	TOF (s^{-1})	15849
316		
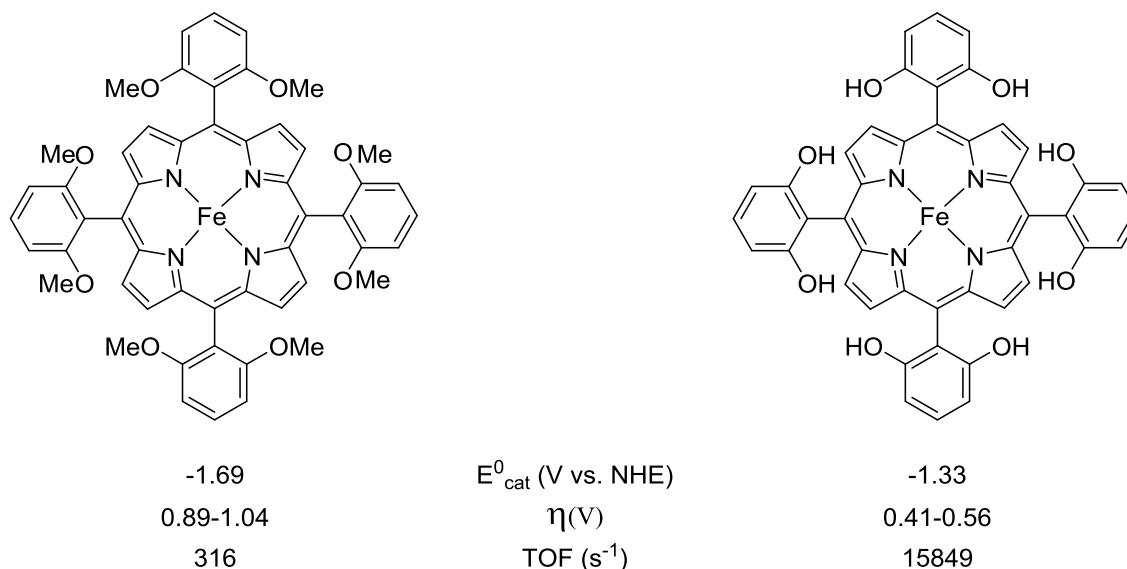
Figure 4.9. Savéant and coworkers' methoxy (left) and hydroxyl (right) substituted TPPFe complexes. Bottom numbers highlight lower redox (E^o_{cat}) and over potential (η) with high turnover frequency for the reduction of CO_2 to CO with the hydroxyl substituted TPPFe complex.[23]

Pendant boronic ester groups have also recently been shown to stabilize nitrogenase intermediates such as $N_2H_3^-$ in a Lewis triad system.[24] Previous group members and others have also developed complexes with Lewis basic sites in the secondary coordination sphere that have proven useful in stabilizing rare intermediates based on the protonation state of the amine (**Figure 4.10**).[25-27]
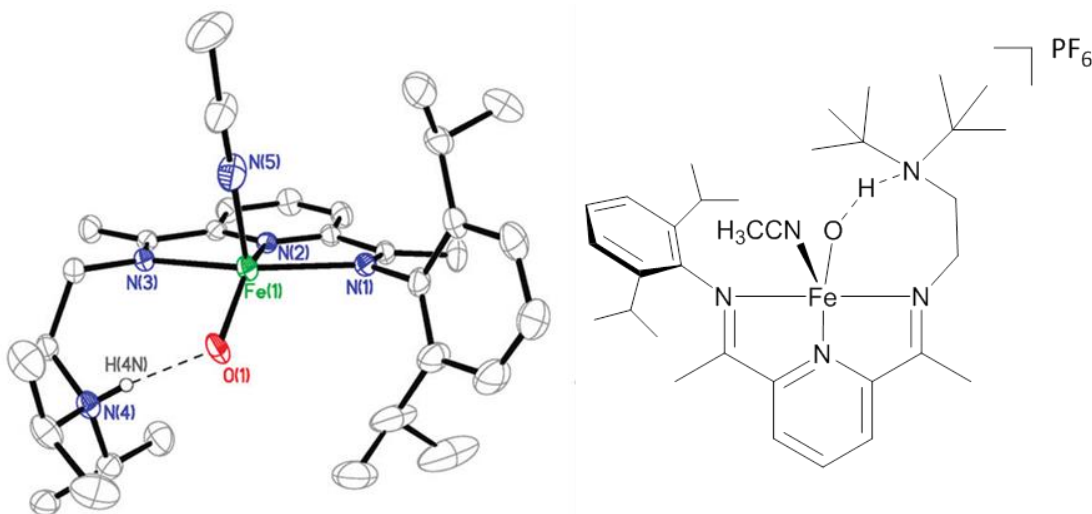
Figure 4.10. Ortep of [(Hdidpa)FeOH(NCC)][PF$_6$] that displays the use of a pendant amine for the intramolecular hydrogen bond stabilization of a rare Fe(II) hydroxo ligand.

4.9 Synthesis of Pendant Lewis Acid/Base PDIFeCl$_2$ Complexes

Three different aniline precursors were chosen for the electrochemical study of the CO release steps: *N*-methyl-1,2-phenylenediamine, *N*,*N*-dimethyl-1,2-phenylenediamine,[28] and 2-aminophenylboronic acid pinacol ester. These anilines were chosen to investigate the

effect on the reduction potential of the CO release step of varying the pendant groups from Lewis basic (2° and 3°amines) to Lewis acidic (boronic ester) sites.[29] The three PDIFe complexes were synthesized using the Schiff-base condensation method by mixing together an equal mole ratio of **1**, FeCl$_2$, and the aniline of choice (**Scheme 4.5**).[30]
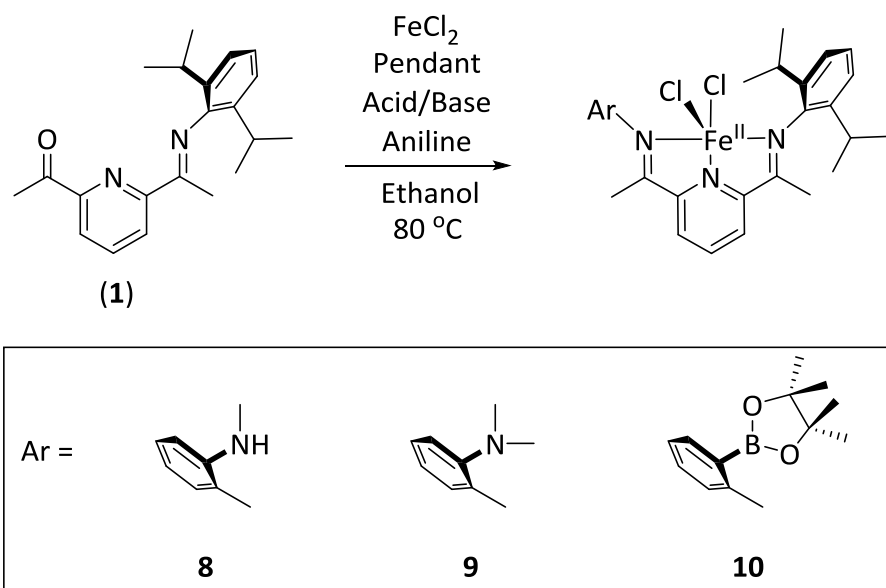
Scheme 4.5. Synthetic scheme for PDIFeCl$_2$ complexes containing pendant Lewis bases and Lewis acids

Within one hour, a distinct color change occurred from a purpled solution of **1** and FeCl$_2$ to a dark green solution of ^{MeNH}PDIFeCl$_2$ (**8**), light blue/green of ^{Me2N}PDIFeCl$_2$ (**9**), and bright blue of ^{Bpin}PDIFeCl$_2$ (**10**).

Green/black single crystals of **8** were furnished from a layered solution of **8** in DCM and diethyl ether, over a period of two days. The Fe center was determined by x-ray

crystallography to be five coordinate with a distorted square pyramidal geometry (average τ = 0.06) (**Figure 4.11, left**).[31] The N of the [MeNH]PDI ring and one Cl atom make up the basal plane, while the other Cl occupying the apical position. The bond lengths and angles are similar to the previously characterized PDIFe complexes, containing asymmetric PDI ligands.[21,32] The measured μ_{eff} yielded a value of 5.11 μ_B in the solid state and 4.93 µB in solution. This is consistent with a high spin (S = 2) square pyramidal Fe(II) center.[33] At room temperature, the zero-field Mössbauer parameters also confirmed the assignment of a high spin Fe(II) center (ΔEQ = 1.06(2), δ = 0.835(7) mm/s) (**Figure 4.11, right**).[34,35]
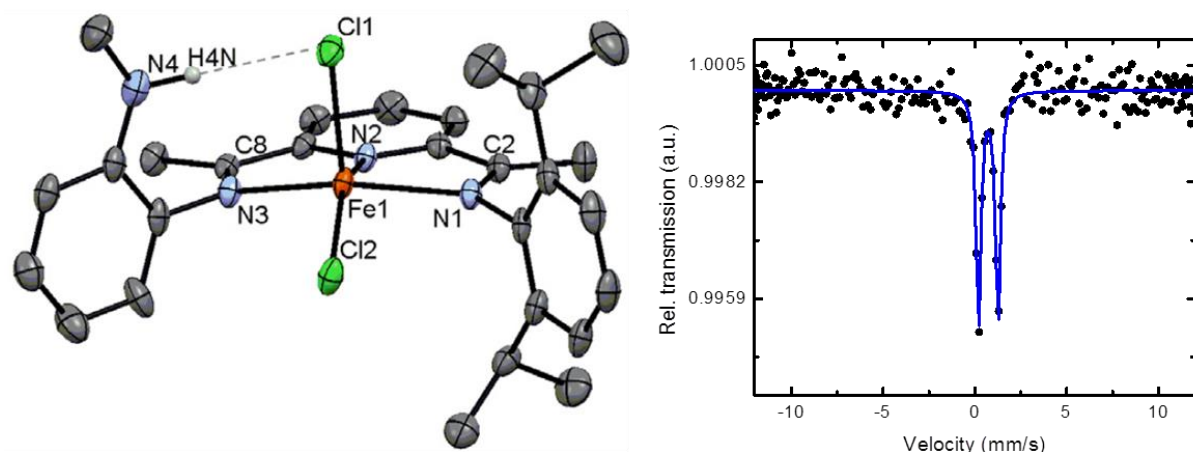
Figure 4.11. Solid-state structure (30% probability) of **8** (left). H atoms have been omitted for clarity. Selected bond lengths (Å) and angles (°): Fe(1)–Cl(1) 2.3284(8), Fe(1)–Cl(2) 2.2684(8), Fe(1)–N(1) 2.216(2), Fe(1)– N(2) 2.093(2), Fe(1)–N(3) 2.237(2), C(2)–N(1) 1.284(3), C(8)–N(3) 1.285(3); Cl(1)–Fe(1)–Cl(2) 112.68(3), N(2)–Fe(1)–Cl(2) 151.78(6), N(1)–Fe(1)–N(3) 140.41(8). Zero-field Mössbauer spectrum of **8** (right).

97

The solid state structure of **8** contains an intramolecular H-bond between the secondary amine group and the apical Cl atom. The hydrogen atom was located and refined, yielding a N(4)-H(4N)…Cl(1) distance of 2.41(8) Å, and a N(4)…Cl(1) distance of 3.378(5) Å; consistent with an intramolecular H-bond.[36] The N(4)H(4N) group is directed toward the Cl atom (the N-H…Cl angle is 163(6)^{o}) which is also indicative of intramolecular H-bonding.[37] The NH stretching frequency in the solid state IR spectrum is also observed at 3318 cm^{-1} (**Figure 4.12**).
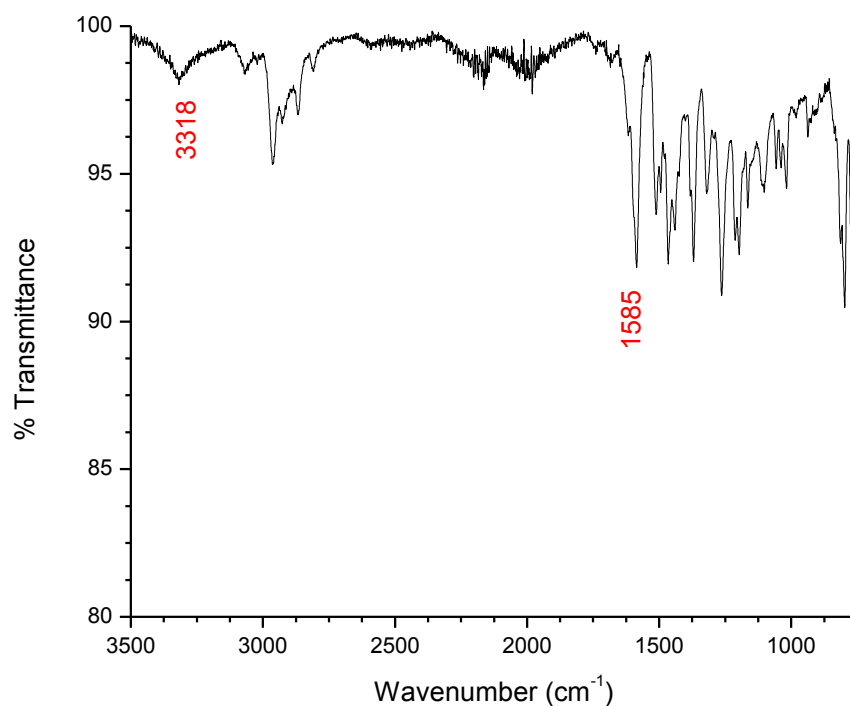
Figure 4.12. IR spectrum of **8**. The NH and C=N stretching frequencies are displayed at 3389 and 1585 cm^{-1}, respectively.

Bluish green crystals of **9** were afforded from the layering of diethyl ether into a solution of the product in DCM, over a period of two days. An ORTEP view of **9** is shown on the left in **Figure 4.13**. The Fe center was determined to be five coordinate with a distorted square pyramidal geometry (average τ = 0.19). As in the case of **8**, the bond lengths and angles of **9** are similar. The measured μ$_{eff}$ of the solid state and in solution were 5.01 and 4.99 μB, respectively, which is consistent with a high spin (S = 2) square pyramidal Fe(II) center. As shown on the right in **Figure 4.13**, the room temperature, zero-field Mössbauer spectrum of **9** which also confirmed the assignment of a high spin Fe(II) center, with a ΔEQ and δ of 1.215(4) and 0.840(2) mm/s, respectively.
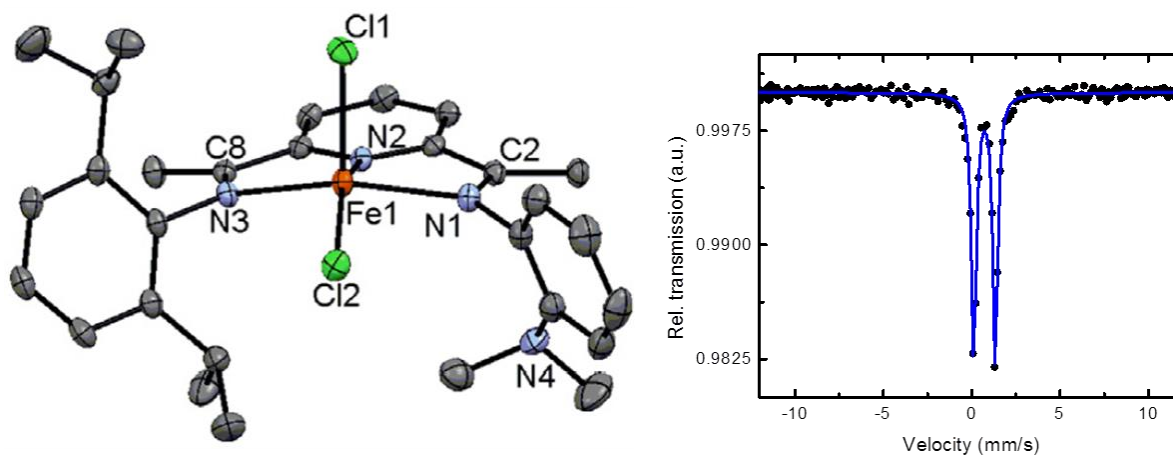
Figure 4.13. Solid-state structure (30% probability) of **9** (left). H atoms have been omitted for clarity. Selected bond lengths (Å) and angles (^{o}): Fe(1)–Cl(1) 2.3462(2), Fe(1)–Cl(2) 2.2417(2), Fe(1)–N(1) 2.195(4), Fe(1)– N(2) 2.068(4), Fe(1)–N(3) 2.185(4), C(2)–N(1) 1.280(6), C(8)–N(3) 1.274(6); Cl(1)–Fe(1)–Cl(2) 118.73(6), N(2)–Fe(1)–Cl(2) 147.33(1), N(1)–Fe(1)–N(3) 143.75(1). Zero-field Mössbauer spectrum of **9** (right).

99

Synthesis of **10** proved to be the most difficult due to a less prominent color change and also the absence of boron in the initial NMR spectroscopic analysis. It was found later that the ^{11}B NMR parameters must be tailored for the specific boron sample, and when running paramagnetic samples, longer scans are necessary to tease out the board boron resonance. After adjustments, the ^{11}B{^{1}H} NMR spectrum displayed a single resonance centered at 38.2 ppm, which is consistent with a trigonal planar B center (**Figure 4.14**).
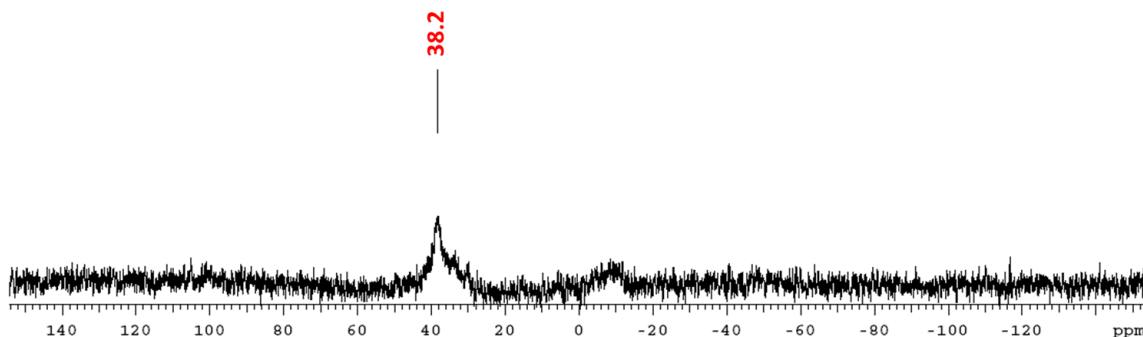
Figure 4.14. ^{11}B{^{1}H} NMR spectrum of **10**, 160 MHz, CDCl$_3$.

Weeks before the ^{11}B NMR detected the boron of the boronic pinacol ester group; crystals of **10** were furnished from the slow vapor diffusion of diethyl ether into a saturated acetonitrile solution of **10**. An ORTEP view of **10** is shown on the left in **Figure 4.15**. The Fe center was determined to be five coordinate with a distorted square pyramidal geometry (average τ = 0.05). The N of the PDI ring and one Cl atom make up the basal plane, while the other Cl occupy the apical position. As in the case of **8** and **9**, the bond lengths and angles are similar. The measured μ_{eff} in the solid state and in solution yielded values of 4.73 and

100

4.65 μ_B, respectively. This is consistent with a high spin (S = 2) square pyramidal Fe(II) center. As shown on the right in **Figure 4.15**, the room temperature, zero-field Mössbauer spectrum of **10** confirmed the assignment of a high spin Fe(II) center (ΔE_Q = 1.23(1), δ = 0.868(5) mm/s). Further inspection of the ORTEP of **10** shows very little B⋯Cl interaction between the boron in the boronic pinacol ester group and the basal Cl atom.[29] The B(1)⋯Cl(2) distance is 3.78(8) Å, which is outside of the Van der Waals radii.
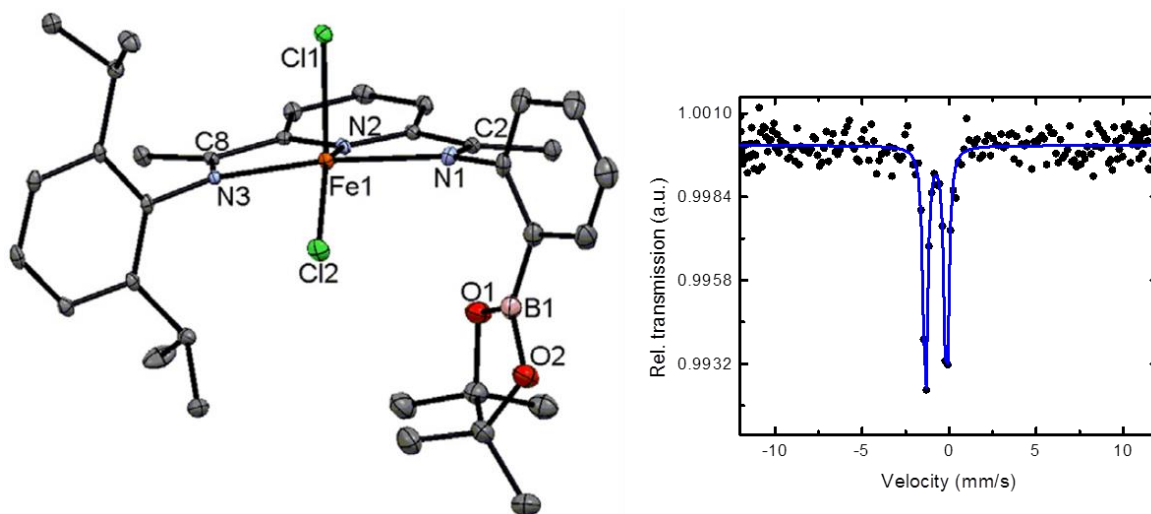
Figure 4.15. Solid-state structure (30% probability) of **10** (left). H atoms have been omitted for clarity. Selected bond lengths (Å) and angles (deg): Fe(1)−Cl(1) 2.3387(9), Fe(1)−Cl(2) 2.2622(9), Fe(1)−N(1) 2.220(3), Fe(1)−N(2) 2.101(2), Fe(1)−N(3) 2.251(2), C(2)−N(1) 1.283(4), C(8)−N(3) 1.286(4); Cl(1)−Fe(1)−Cl(2) 119.35(3), N(2)−Fe(1)−Cl(2) 141.98(7), N(1)−Fe(1)−N(3) 144.78(9). Zero-field Mössbauer spectrum of **10** (right).

4.10 Synthesis of Pendant Lewis Acid/Base PDIFe(CO)₂ Complexes

In order to investigate the CO release of these substituted Lewis acid and Lewis bases Fe complexes, the corresponding series of direduced dicarbonyl complexes were synthesized. The reduction of the Lewis acid and Lewis bases PDIFeCl₂ complexes was performed in 8 mL of DCM and five mole equivalents of NaHg amalgam, as illustrated in **Scheme 4.6**. This reaction was completed in a pressurized tube under one atmosphere of CO gas. After work up, slow evaporation of saturated diethyl ether solutions of either ^{MeNH}PDIFe(CO)₂ (**11**), ^{Me2NPDI}Fe(CO)₂ (**12**), or ^{Bpin}PDIFe(CO)₂ (**13**), yielded green, diamagnetic, crystalline solids.
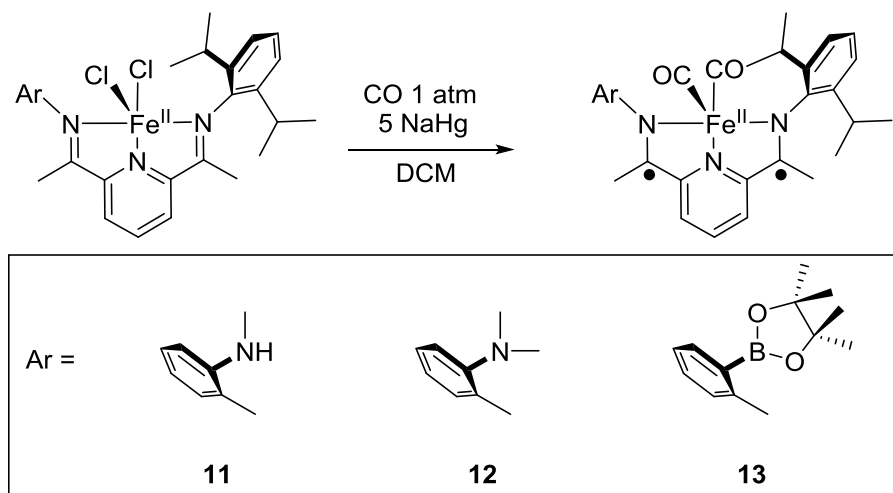
Scheme 4.6. Synthetic scheme for PDIFe(CO)₂ complexes containing pendant Lewis bases and Lewis acids.

An ORTEP view of **11** is shown on the left in **Figure 4.16**. The iron center was determined to be five coordinate with square pyramidal geometry (τ = 0.09). The N of the PDI ring and one CO ligand make up the basal plane, while the other CO occupies the apical position. Inspection of the bond lengths reveal that the C_{imine}-N_{imine} bond lengths are elongated from a value of 1.274(6) and 1.280(6) Å in **8** to 1.326(3) and 1.318(3) Å in **11**. Also, the C_{imine}-C_{ipso} bond lengths are contracted from 1.488(6) and 1.485(6) Å in **8** to 1.428(3) and 1.421(3) Å in **11**. This data, taken in conjunction with the room temperature zero-field Mössbauer parameters (ΔE_Q = 1.25(2), δ = - 0.076(9) mm/s), suggests that the complex is best described as a Fe(II) center with a doubly reduced ^{MeNH}PDI ligand.

Figure 4.16. Solid-state structure (30% probability) of **11** (left). H atoms have been omitted for clarity. Selected bond lengths (Å) and angles (^{o}): Fe(1)–C(1) 1.783(2), Fe(1)–C(2) 1.781(3), Fe(1)–N(1) 1.9451(2), Fe(1)–N(2) 1.8538(2), Fe(1)–N(3) 1.9522(2), C(4)–N(1) 1.328(3), C(10)–N(3) 1.333(3); C(1)–Fe(1)–C(2) 95.39(10), N(2)–Fe(1)–C(1) 156.53(9), N(1)–Fe(1)–N(3) 152.37(8). Zero-field Mössbauer spectrum of **11** (right).

Complex **11** is diamagnetic in the solid state and solution, yielding clean, diagnostic ^{1}H and ^{13}C{^{1}H} NMR spectra (**Figure 4.17 & 4.18**). The ^{13}C{^{1}H} NMR resonances due to the CO ligands appear at 217.6 and 210.6 ppm and the FTIR spectrum of **11** displays two CO stretching frequencies at 1950 and 1888 cm^{-1}, along with an NH stretching frequency at 3389 cm^{-1} (**Figure 4.19**). The CO stretching frequency shifts are identical to those seen in other characterized PDIFe(CO)$_2$ complexes that were best described as a diradical dianionic ligand with a low spin (S=0) Fe(II) center.[35] The NH group was designed to play a role in hindering the release of the CO molecule by hydrogen bond interaction of the H atom (in NH) to the O atom (in CO). Therefore, the electrochemical release of CO from complex **11** was expected to occur at a higher oxidation potential than ^{MeO}PDIFe(CO)$_2$ (0.477 V).
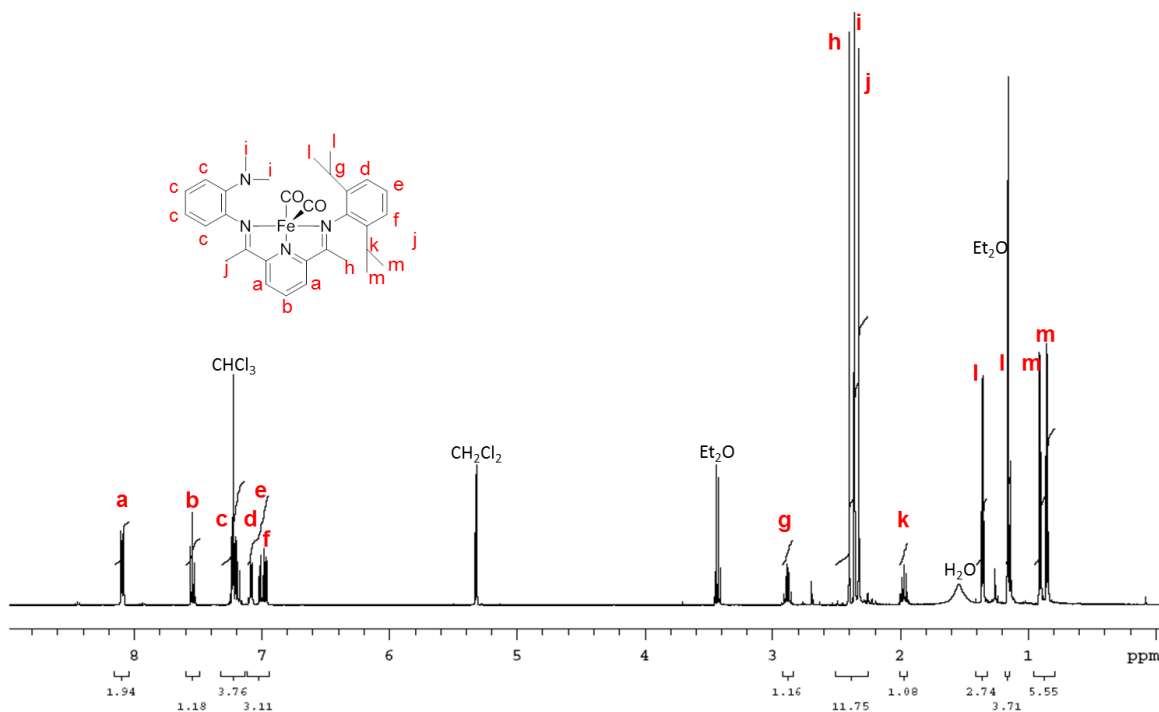
Figure 4.17. ^{1}H NMR spectrum of **11**, 500 MHz, CD$_2$Cl$_2$.
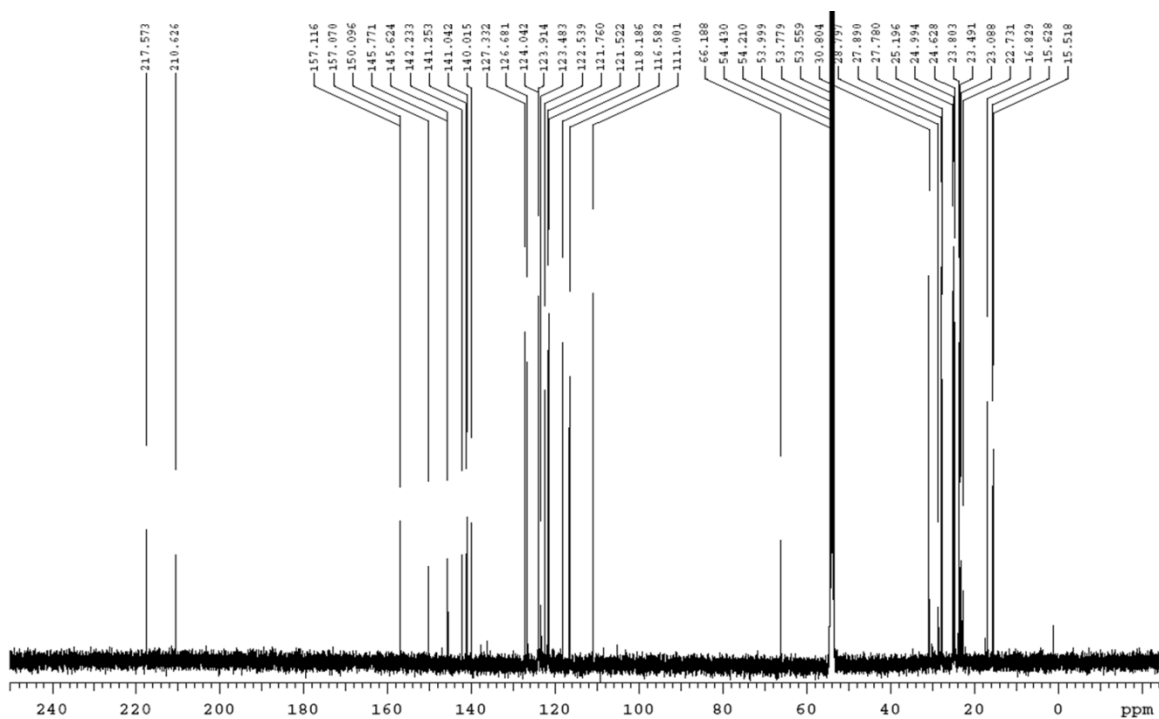
Figure 4.18. $^{13}C\{^1H\}$ NMR spectrum of **11**, 126 MHz, CD_2Cl_2.
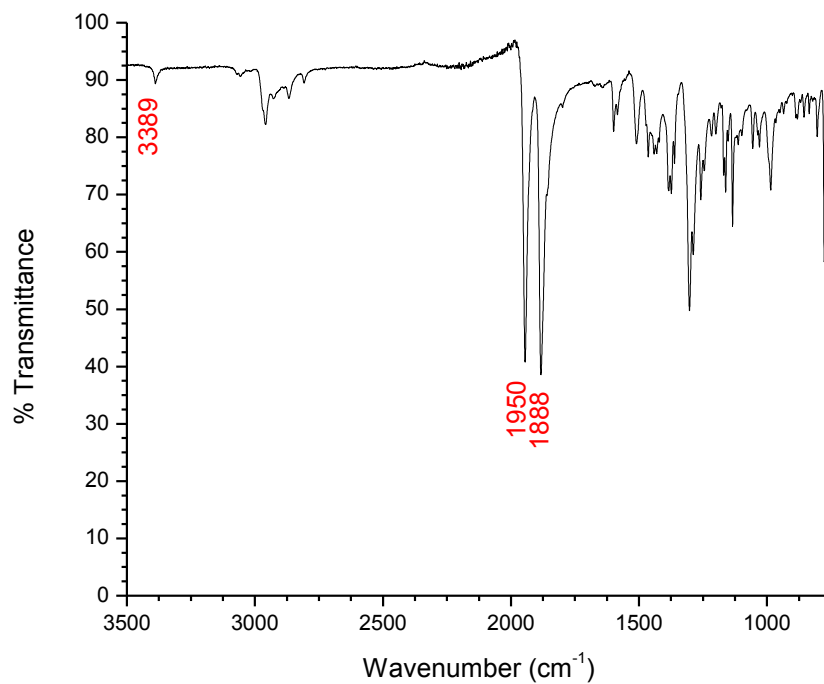
Figure 4.19. Solid FT-ATR infrared spectrum of **11**.

An ORTEP view of **12** is shown on the left in **Figure 4.20**. The iron center was determined to be five coordinate with square pyramidal geometry (τ = 0.07). Inspection of the bond lengths reveal that the C_{imine}-N_{imine} bond lengths are elongated from a value of 1.285(3) and 1.284(3) Å in **9** to 1.328(3) and 1.333(3) Å in **12**. Also, the C_{imine}-C_{ipso} bond lengths are contracted from 1.482(3) and 1.480(4) Å in **9** to 1.431(3) and 1.421(3) Å in **12**. This data, taken in conjunction with the room temperature zerofield Mössbauer parameters (ΔE_Q = 1.07(2), δ = -0.06(1) mm/s), suggests that the complex is best described as a Fe(II) center with a doubly reduced ^{Me2N}PDI ligand (**Figure 4.20, right**).

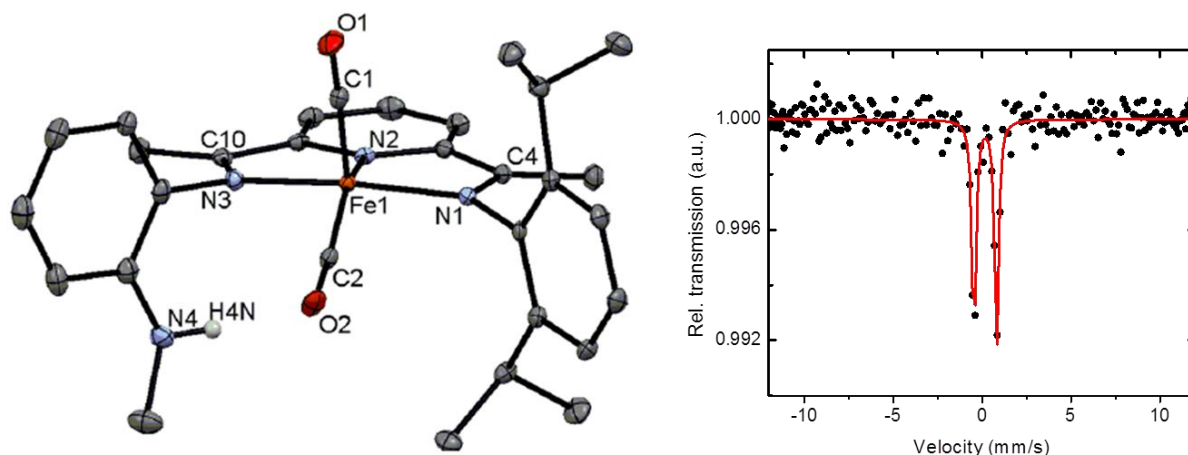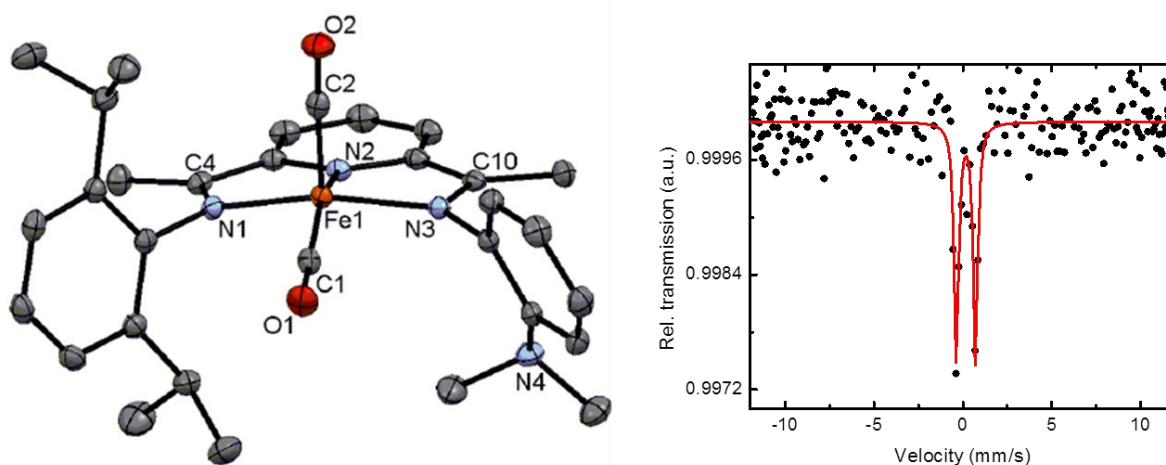**Figure 4.20**. Solid-state structure (30% probability) of **12** (left). H atoms have been omitted for clarity. Selected bond lengths (Å) and angles (^{o}): Fe(1)–C(1) 1.767(2), Fe(1)–C(2) 1.775(2), Fe(1)–N(1) 1.9486(2), Fe(1)–N(2) 1.8457(2), Fe(1)–N(3) 1.9486(2), C(4)–N(1) 1.326(3), C(10)–N(3) 1.318(3); C(1)–Fe(1)–C(2) 94.24(11), N(2)–Fe(1)–C(2) 150.49(9), N(1)–Fe(1)–N(3) 156.10(8). Zero-field Mössbauer spectrum of **12** (right).

Complex **12** is diamagnetic in both the solid state and solution, yielding clean, diagnostic ^{1}H and ^{13}C{^{1}H} NMR spectra (**Figure 4.21 & 4.22**). The ^{13}C{^{1}H} NMR resonances due to the CO ligands appear at 219.0 and 209.0 ppm and the FTIR spectrum of **12** displays two CO stretching frequencies at 1951 and 1892 cm^{-1} (**Figure 4.23**). These shifts are identical to those seen in other characterized PDIFe(CO)$_2$ complexes.[35]
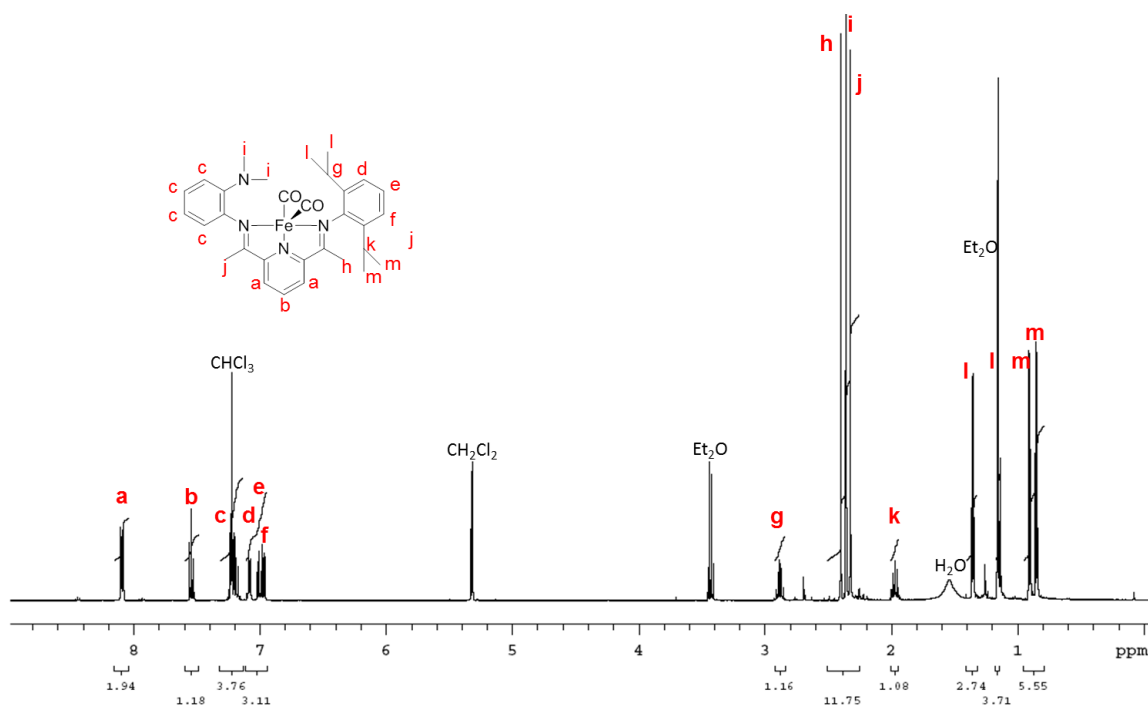
Figure 4.21. ^{1}H NMR spectrum of **12**, 500 MHz, CD$_2$Cl$_2$.
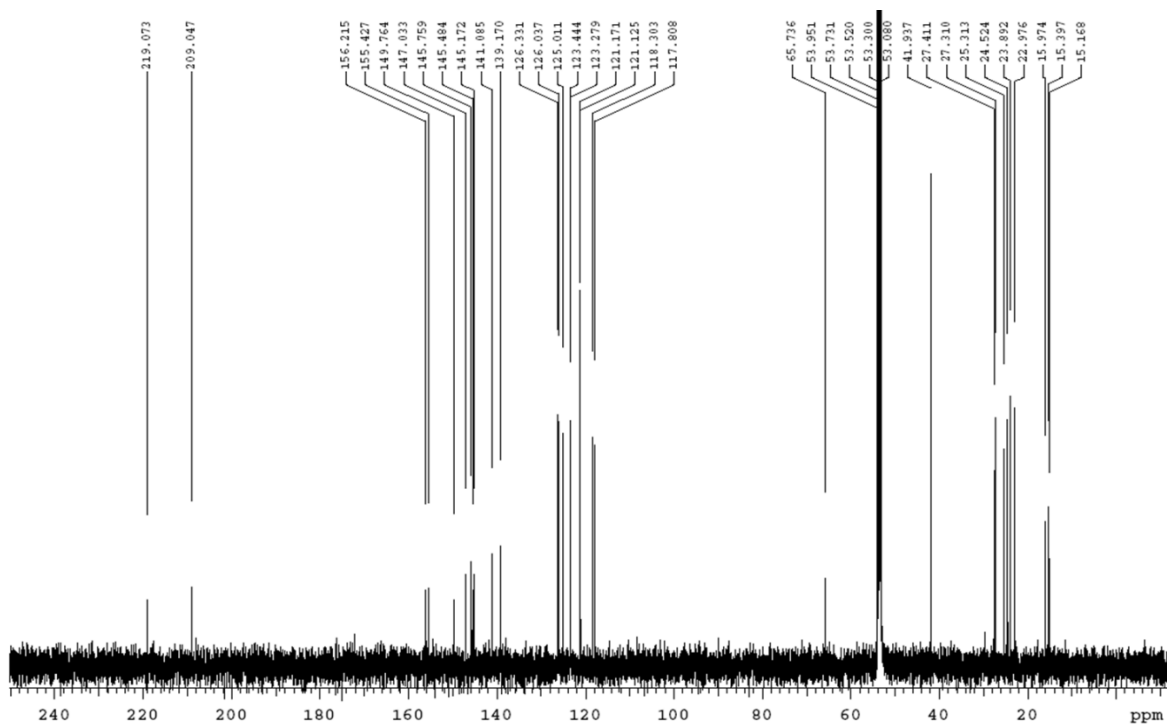
Figure 4.22. $^{13}C\{^{1}H\}$ NMR spectrum of **12**, 126 MHz, CD_2Cl_2.
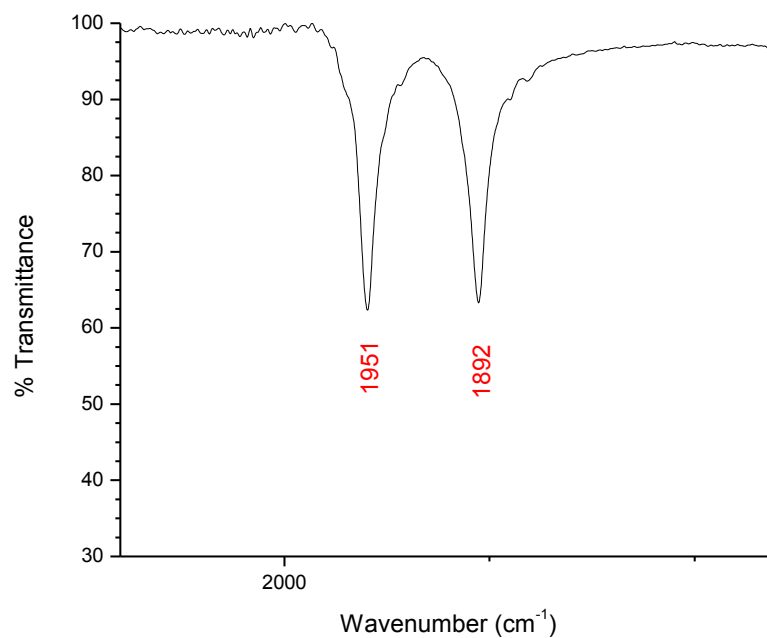
Figure 4.23. Solid FT-ATR infrared spectrum of **12**.

108

Lastly, an ORTEP view of **13** is shown on the left in **Figure 4.24**. The iron center was determined to be five coordinate with square pyramidal geometry (τ = 0.19). The N of the ^{Bpin}PDI and one CO ligand make up the basal plane, while the other CO ligand occupies the apical position. Inspection of the bond lengths reveal that the C_{imine}-N_{imine} bond lengths are elongated from a value of 1.286(4) and 1.283(4) Å in **10** to 1.331(5) and 1.327(5) Å in **13**. Also, the C_{imine}-C_{ipso} bond lengths are contracted from 1.489(4) and 1.482(4) Å in **10** to 1.425(6) and 1.423(6) Å in **13**. This data, taken in conjunction with the room temperature zero-field Mössbauer parameters (ΔE_Q = 1.510(8), δ = -0.061(4) mm/s), suggests that **13** is best described as a Fe(II) center with a doubly reduced ^{Bpin}PDI ligand (**Figure 4.24, right**).
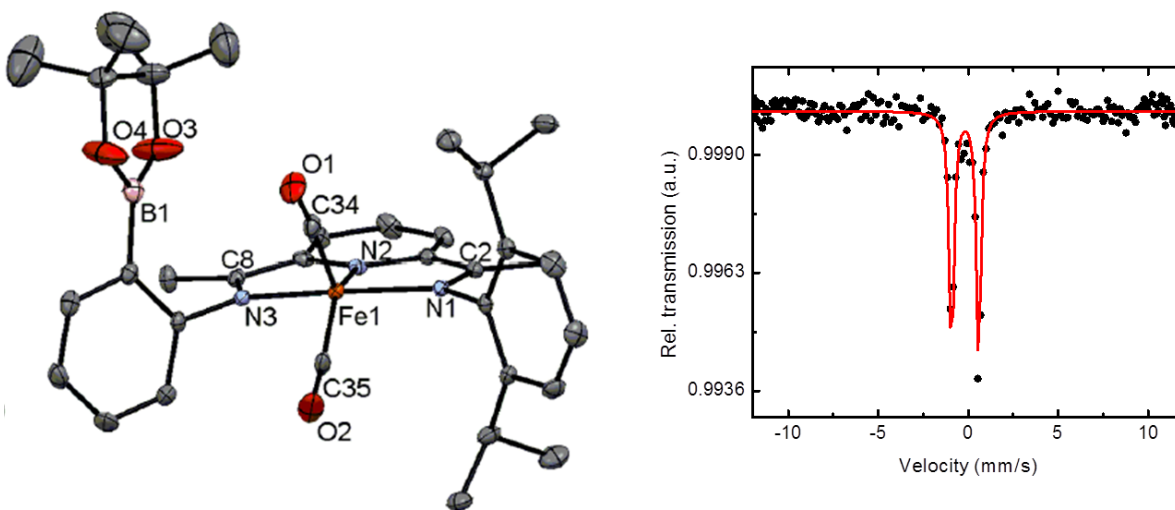
Figure 4.24. Solid-state structure (30% probability) of **13** (left). H atoms have been omitted for clarity. Selected bond lengths (Å) and angles ($^{\circ}$): Fe(1)–C(34) 1.785(5), Fe(1)–C(35) 1.786(5), Fe(1)–N(1) 1.966(3), Fe(1)–N(2) 1.853(3), Fe(1)–N(3) 1.952(3), C(2)–N(1) 1.331(5), C(8)–N(3) 1.327(5); C(34)–Fe(1)–C(35) 92.2(2), N(2)–Fe(1)–C(35) 145.58(19), N(1)–Fe(1)–N(3) 157.10(2). Zero-field Mössbauer spectrum of **13** (right).

Complex **13** is diamagnetic in the solid state and solution, yielding clean, diagnostic ^1H and ^13C{^1H} NMR spectra (**Figure 4.25 & 4.26**). The ^13C{^1H} NMR resonances due to the CO ligands appear at 216.3 and 213.1 ppm and the FTIR spectrum of **13** displays two CO stretching frequencies at 1950 and 1888 cm^-1 (**Figure 4.27**).
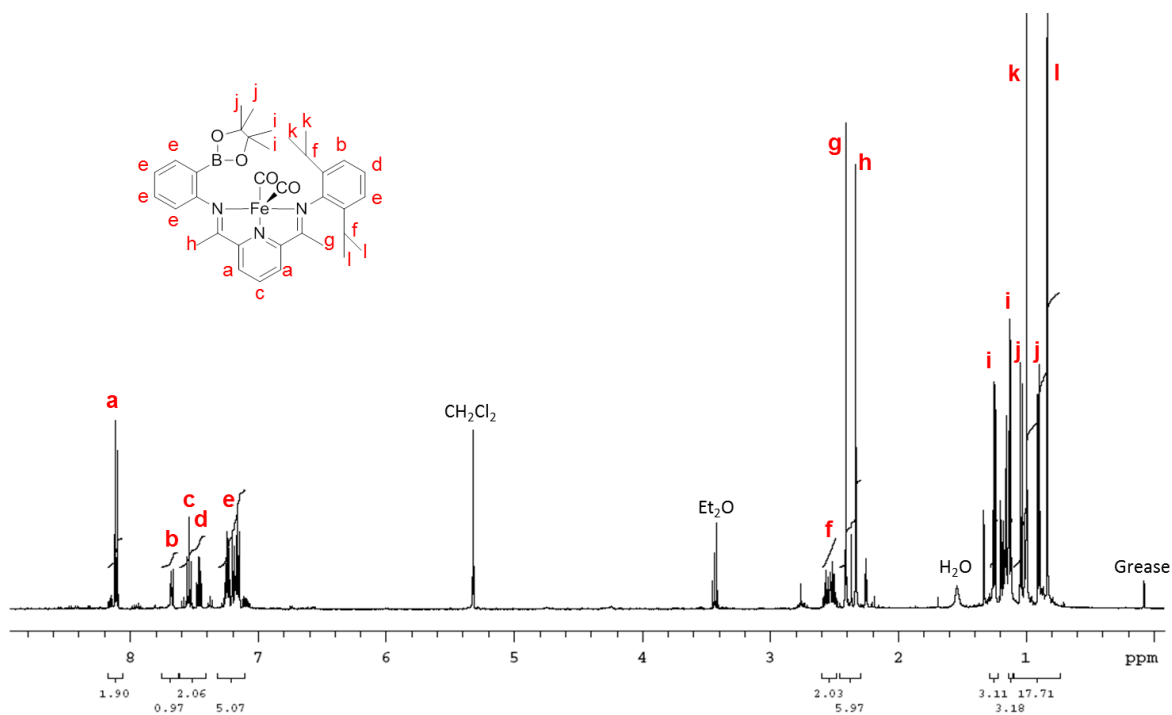
Figure 4.25. ^1H NMR spectrum of **13**, 500 MHz, CD$_2$Cl$_2$.
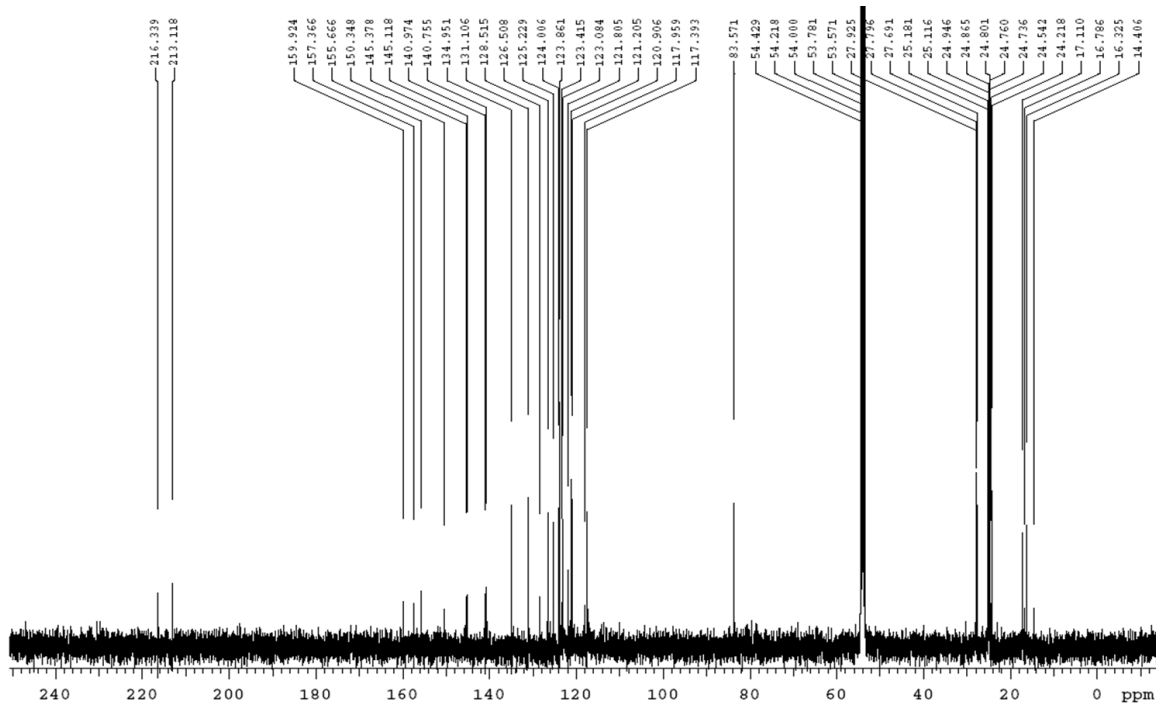
Figure 4.26. ^{13}C{^{1}H} NMR spectrum of **13**, 126 MHz, CD$_2$Cl$_2$.
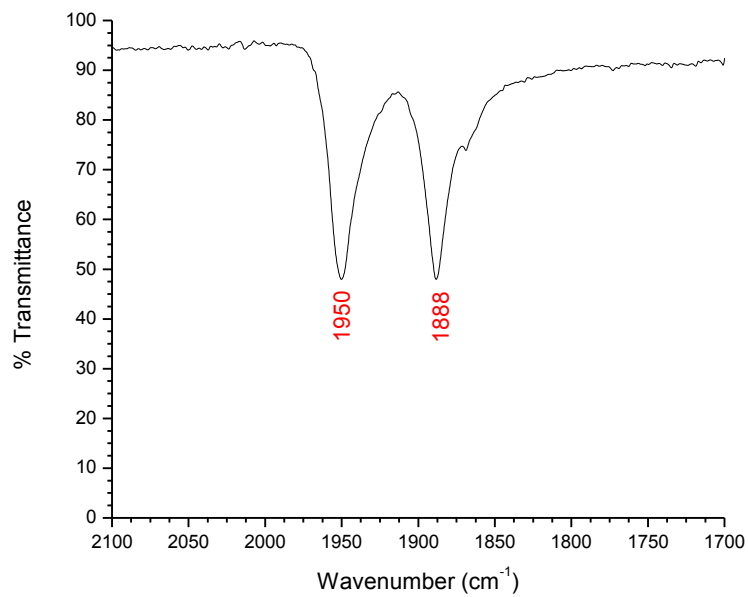
Figure 4.27. Solid FT-ATR infrared spectrum of **13**.

111

The design of the ^{Bpin}PDI ligand was thought to interact with the CO by creating a boron-oxygen interaction between the boron (in boronic pinacol ester) and the O atom (in CO). However, the ORTEP of **13**, in the solid state, showed no significant interaction between the B of the pinacol boronic ester group and the O atom in the apical CO ligand, in the solid state. The B(1)…O(1) distance is 3.415(8) Å, which is outside of the Van der Waals radii. The Fe-C-O bond angle in the Fe-COapical moiety is 175.0(4)°. The degree of pyramidalization at B(1) is ΣB_α = 359.9(4)° and the ^{11}B{1H} NMR spectrum displays a single resonance centered at 33.6 ppm. This resonance is slightly shifted from that observed in **10** (38.2 ppm), but consistent with a trigonal planar boron center (**Figure 4.28**).
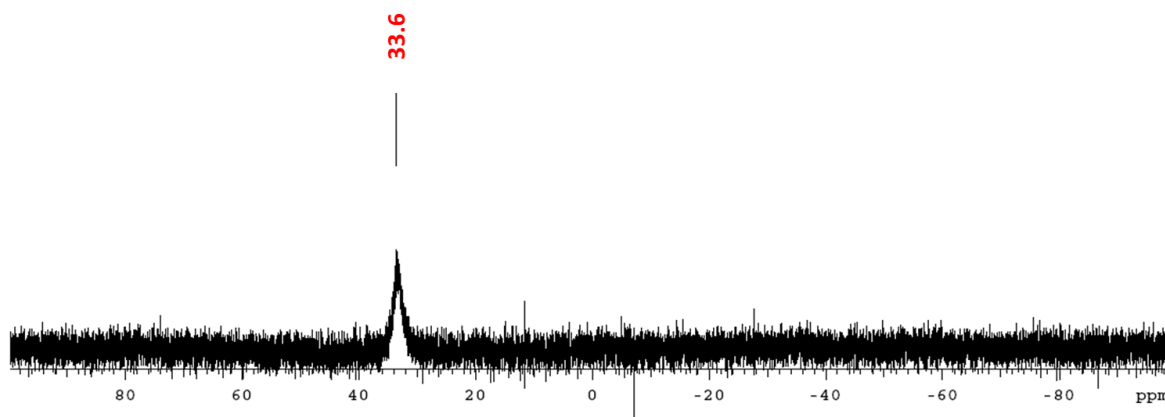
Figure 4.28. ^{11}B{^{1}H} NMR spectrum of **13**, 160 MHz, CD$_2$Cl$_2$.

4.11 Electrochemical Studies of Pendant Lewis Acid/Base PDIFe(CO)$_2$ Complexes

Electrochemical studies were carried out with the three synthesized substituted Lewis acid and Lewis bases PDIFe(CO)$_2$ complexes (**11-13**), in order to explore the CO release step (**Scheme 4.7**). As previously established in chapter 3, the direduced dicarbonyl ligand scaffold in **5** displays two oxidation events in the cyclic voltammogram. The first is a quasireversible one electron event due to the formation of the one electron oxidized product, [PDIFe(CO)$_2$]$^+$.[38,39] The second is an irreversible event at a more positive potential due to the oxidation to the neutral PDI ligand, with subsequent irreversible release of CO.
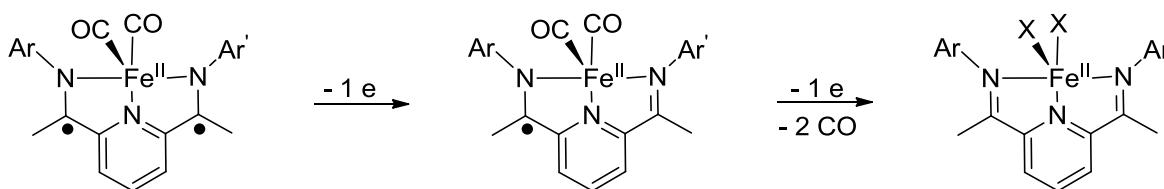
Scheme 4.7. Electrochemical oxidation of the direduced dicarbonyl PDIFe(CO)$_2$ complexes with concomitant CO release.

All three Lewis acid and Lewis base PDIFe(CO)$_2$ complexes display the same characteristic CV, yet the pendant group has an effect on the reduction potential of each complex (**Figure 4.29**). The CV of **11** reveal the quasi-reversible oxidation event at -0.395 V from the formation of the one electron oxidized product, [(^{MeNH}PDI)Fe(CO)$_2$]$^+$. Additionally, the CV reveals the irreversible oxidation event at 0.535 V from the oxidation to the neutral ^{MeNH}PDI, with concomitant irreversible release of CO. The same quasi-reversible event due

113

to the one electron oxidation was observed for **12** and **13** at -0.511 and -0.489 V, respectively. Complex **12** displayed the irreversible oxidation event at 0.431 V due to oxidation to the neutral ^{Me2N}PDI, with concomitant irreversible release of CO. A second irreversible event at 0.767 V is likely due to oxidation of the tertiary amine group. Complex **13** also displayed the irreversible oxidation at 0.647 V to the neutral ^{Bpin}PDI, with concomitant irreversible release of CO.
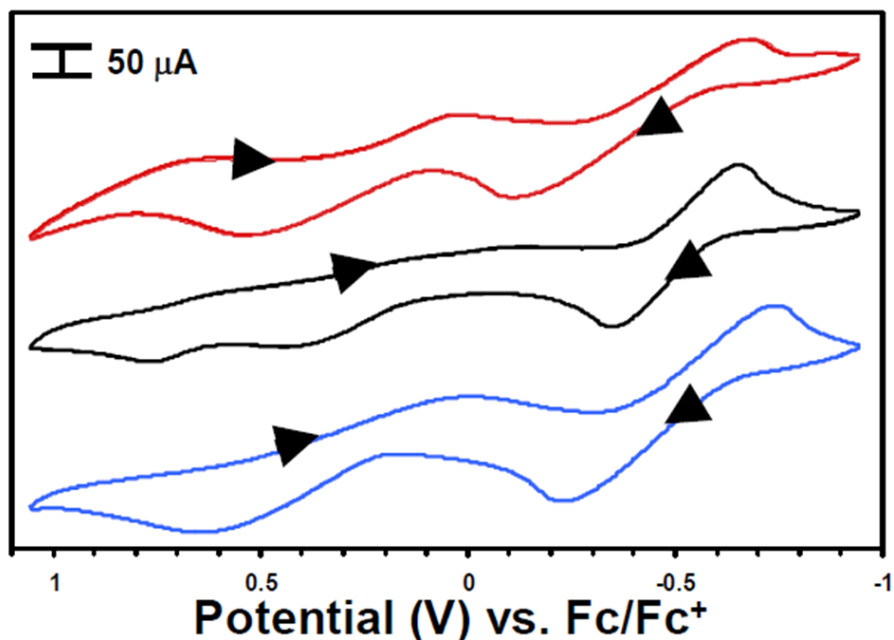
Figure 4.29. CV scans of **11** (top, red), **12** (middle, black), and **13** (bottom, blue). Two repeat scans are shown for each molecule and the scans were initiated at -0.95 V. Each solution had a concentration of 0.1 M of the PDIFe(CO)$_2$ complex and 0.1M [(^{n}Bu)$_4$N][PF$_6$], in DCM, 100 mV/s scan rate, glassy carbon electrode (scan started at -1.15 V).

It appears that the irreversible CO release step (as well as the quasi-reversible one electron oxidation) is affected by the placement of the Lewis acid or Lewis base in the secondary coordination sphere. This is likely due to electronic effects that change the redox potential of the PDIFe(CO)$_2$ complex. In the case of the pendant Lewis base complexes **10** and **11**, the irreversible CO release is observed at lower potentials (0.535 V and 0.431 V) than the pendant Lewis acid complex, **12**, displaying the CO release at 0.647 V. Therefore, by altering the electronics of the pendant arm, the CO release can be tuned by over 200 mV.

4.12 References

1. Prockop, L. D.; Chichkova, R. I. *J. Neuro. Sci*. **2007**, 262, 1-2, 122–130.
2. Anthea, M; Hopkins, J.; McLaughlin, C. W.; Johnson, S.; Quon. M.; LaHart, D.; Wright, J. D. *Human Biology and Health*. 1993, Englewood Cliffs, New Jersey, Prentice Hall.
3. Thompson, D. W.; Kretzer, R. M.; Lebeau, E. L.; Scaltrito, D. V.; Ghilardi, R. A.; Lam, K. C.; Rheingold, R. A.; Karlin, K. D.; Meyer, G. J. *Inorg. Chem.* **2003**, 42, 5211;
4. Garagorri-Benito, D.; Lagoja, I.; Velros, L. F.; Kirchner, K. A. *Dalton Trans*, **2011**, 40, 4778 - 4792.
5. Breuer, J. Fruhauf, H.; Smeets, W. J. J; Spek, A. L. *Inorg. Chim. Acta*. **1999**, 291, 438.
6. Renkema, K. B.; Ogasawara, M.; Streib, W. E.; Huffman, J. C. Caulton, K. G. *Inorg. Chim*. **1999**, 291, 226.
7. Motterlini, R.; Otterbein, L. E. *Nat. Rev. Drug Discovery.* **2010**, 9, 728.
8. Johnson, T. R.; Mann. B. E.; Clark, J. E.; Foresti, R.; Green, C. J.; Motterlini, R. *Angew. Chem., Int. Ed.* **2003**, 42, 3722.
9. Motterlini, R.; Mann, B. E.; Johnson, T. R.; Clark, J. E.; Foresti, R.; Green, C. J. *Curr. Pharm. Des.* **2003**, 9, 2525.
10. Mann, B. E.; Motterlini, R. *Chem. Commun.* **2007**, 4197.
11. Motterlini, R.; Mann, B. E.; Foresti, R. *Expert Opin. Invest. Drugs*. **2005**, 14, 1305.
12. Farrer, N. J.; Sadler, P. J.; Aust. A. *J. Chem.* **2008**, 61, 669.
13. Szacilowski, K.; Macyk, W.; Drzewiecka-Matuszek, A.; Brindell, M.; Stochel, G. *Chem. Rev.* **2005**, 105, 2647.
14. Johnson, T. R.; Mann, B. E.; Teasdale, I. P.; Adams, H.; Foresti, R.; Green, C. J.; Motterlini, R. *Dalton Trans*. **2007**, 1500.
15. Smith, J. M.; Lachicotte, R. J.; Holland, P. L. *Organometallics*, **2002**, 21, 4808.
16. Ingleson, M. J.; Fullmer, B. C.; Buschhorn, D. T.; Fan, H.; Pink, M.; Huffman, J. C.; Caulton, K. G. *Inorg. Chem.* **2008**, 47, 407.
17. Bowman, A.C.; Milsmann, C.; Bill, E.; Turner, Z.R.; Lobkovsky, E.; DeBeer, S.; Wieghardt, K.; Chirik, P.J. *J. Am. Chem. Soc.* **2011**, 133, 43, 17353-17369.
18. Lu, C. C.; Saouma, T.; Day, M. W.; Peters, J. C. *J. Am. Chem. Soc*. **2007**, 129, 4-5.
19. Allen, O. R.; Dalgarno, S. J.; Field, L. D. *Organometallics*. **2008**, 27, 3328–3330.
20. Prausnitz, A. *Molecular Thermodynamics of Fluid Phase Equilibria, 3rd ed*. 1999, Prentice Hall, pp. 586.
21. Thammavongsy, Z.; Seda, T.; Zakharov, L. N.; Kaminsky, W.; Gilbertson, J. D. *Inorg. Chem*. **2012**, 51, 17, 9168-9170.
22. Borovik, A. S. *Acc. Chem. Res.* **2005**, *38*, 54-61
23. Costentin, C.; Drouet, S.; Robert, M.; Saveant, J.M. *Science*. **2012**, 338, 90-94.
24. Tutusaus, O.; Ni, C.; Szymczak, N. K. *J. Am. Chem. Soc.* **2013**, *135*, 3403–3406.
25. Kendall, A. J.; Zakharov, L. N.; Gilbertson, J. D. *Inorg. Chem.* **2010**, *49*, 8656–8658
26. DuBois, M. R.; DuBois, D. L. *Acc. Chem. Res.* **2009**, *42*, 1974–1982.
27. Reid, S. D.; Wilson, C.; Blake, A. J.; Love, J. B. *Dalton Trans.* **2010**, *39*, 418-425.

116

28. Ren, P.; Vechorkin, O.; Csok, Z.; Salihu, I.; Scopelliti, R.; Hu, X. *Dalton Trans*. **2011**, 40, 35, 8906-8911.
29. Ionkin, A. S.; Marshall, W. J.; Adelman, D. J.; Bobik Fones, B.; Fish, B. D.; Schiffhauer, M. F. *Organometallics*, **2008**, 27, 1902–1911.
30. Jiang, Y.; Widger, R. L.; Kasper, G. D.; Siegler, M. A.; Goldberg, D. P. *J. Am. Chem. Soc.* **2010**, *132*, 12214-12215.31.
31. Addison, A. W.; Rao, T. N.; Reedjik, J.; van Rijn, J.; Verschoor, G. C. *J. Chem. Soc. Dalton Trans.* **1984**, 1349-1356.
32. Kendall, A. J.; Zakharov, L. N.; Gilbertson, J. D. *Inorg. Chem.* **2010**, *49*, 8656–8658.
33. Small, B. L.; Brookhart, M.; Bennett, A. M. A. *J. Am. Chem. Soc.* **1998**, *120*, 4049.
34. Britovsek, G. J.; Clentsmith, G. K. B.; Gibson, V. C.; Goodgame, D. M. L.; McTavish, S. J.; Pankhurst, S. A. *Catal. Commun.* **2002**, *3*, 207-211.
35. Bart, S. C.; Chlopek, K.; Bill, E.; Bouwkamp, M. W.; Lobkovsky, E.; Neese, F.; Wieghardt,   K.; Chirik, J. P. *J. Am. Chem. Soc.* **2006**, 128, 13901-13912.
36. Brammer, L.; Bruton, E. A.; Sherwood, P. *Cryst. Growth Des*. **2001**, 1, 277-290.
37. Luck, W. A. P.; Schuster, P.; Zundel, G.; Sandorfy, C. *In The Hydrogen Bond: Recent Developments in Theory and Experiments* 1st *Eds.*; 1976, North-Holland: New York; pp.   527-562.
38. Tondreau, A. M.; Milsmann, C.; Lobkovsky, E.; Chirik, P. J. *Inorg. Chem.* **2011**, *50*, 9888 - 9895.
39. Darmon, J. D.; Turner, Z. R.; Lobkovsky, E.; Chirik, P. J. *Organometallics*, **2012**, *31*, 2275 - 2285.

117

Chapter 5. Conclusion

The two electrons required to reduce CO_2 to CO came from the redox active PDI ligand, rather than a Fe(0) source. This is the second known example of the reduction of CO_2 to CO occurring on a Fe(II) complex. Furthermore, the release of the two CO molecules from the oxidation of the ^{MeO}PDIFe(CO)$_2$ complex completed the CO_2-to-CO cycle, demonstrating the first known example of this cycle on an Fe(II) center. When a chemical oxidant such as HCl was used, the production of H_2 gas (along with the release of CO gas) was detected. These two gases combined are known as synthesis gas (syngas) and are the starting material for the Fischer-Trospch process for the production of diesel fuel.
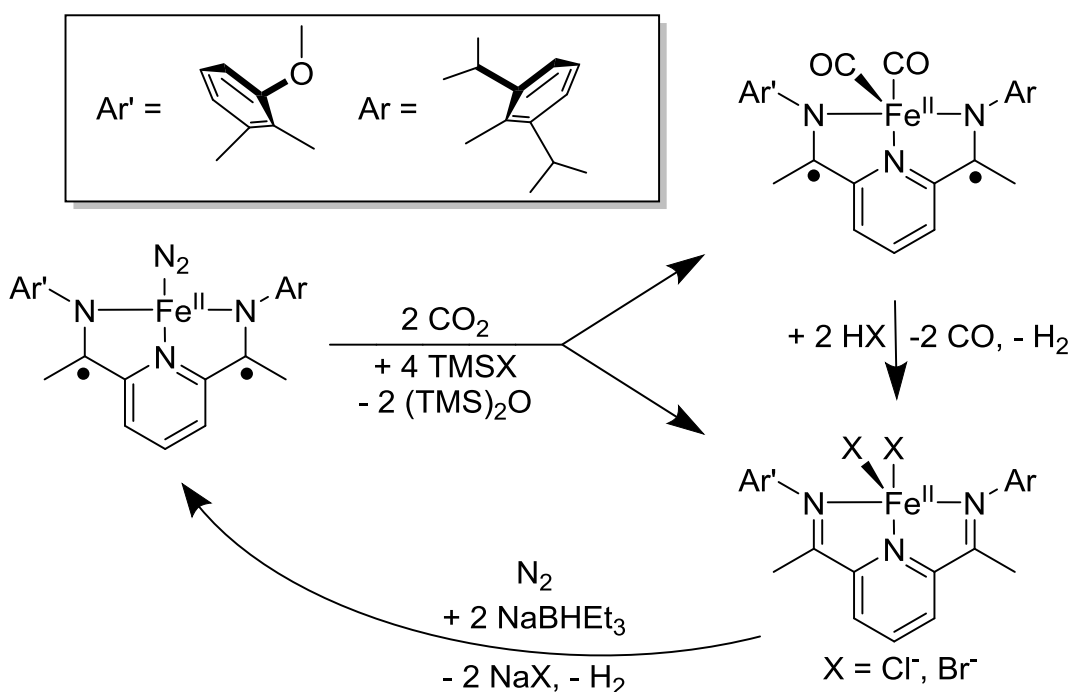
Scheme 5.1. CO_2-to-CO cycle on ^{MeO}PDIFe(II) complex.

118

Incorporation of various Lewis acid and bases within the secondary coordination sphere of the PDIFe(II) complex demonstrated electronic effects on the reduction-potential of the PDIFe(CO)$_2$ complex. The reduction-potential of the PDIFe(CO)$_2$ complexes can vary by up to 200 mV, by tuning the secondary coordination sphere of the PDIFe(CO)$_2$ with Lewis acids or bases. Therefore, the CO release step of these complexes can occur at much lower potentials.

Chapter 6. Experimental

6.1 General Considerations

All reactions were carried out using standard schlenk technique, Fisher-Porter pressure tubes, or in an MBraun inert atmosphere glovebox (N_2) equipped with a cold well. Carbon dioxide (99.9%) and carbon monoxide (99.0%) gas were purchased from Praxair Distribution, Inc. All solvents were dried and deoxygenated with a PureSolv solvent purification system (CuO and alumina columns) unless otherwise noted. Diethyl ether and tetrahydrofuran were distilled over sodium metal. Deuterated methylene chloride-d_2 (D, 99.9%), chloroform-d_1 (D, 99.9%), and toluene-d_8 (D, 99.9%) were purchased from Cambridge Isotope Laboratories, Inc. and were degassed bythree cycles of freeze-pump-thaw and stored in an N_2-filled glove box. Sodium triethylborohydride (1.0 M solution in toluene), hydrochloric acid (2.0 M solution in diethyl ether), trimethylsilyl chloride (99%), bis(pinacolato)diboron (99%), tetramethylsilane (99%), nitromethane (95%), 2,6-diisopropylaniline (90%), 2,6-diacetylpyridine (99%), 2-methoxy-6-methylaniline (98%), 1,2-bis(diethylphosphino)ethane (97%), N-methyl-1,2-phenylenediamine (97%) and 2-aminophenylboronic acid pinacol ester (98%) were purchased from Sigma-Aldrich and used as received except for the 2,6-diisopropylaniline (90%), which was distilled prior to use. Iron(II) dichloride anhydrous (98%), Iron(II) dibromide anhydrous (98%) and sodium-mercury amalgam, 5% Na (99.9%) were purchased from Strem Chemicals Inc and used as

120

received. The asymmetric PDI ligand [(ArN=C(CH$_3$))C$_2$H$_3$N((CH$_3$)C=O] (Ar= 2,6-$^{\text{i}}$Pr-C$_6$H$_3$) and 2-amino-N,N-dimethylaniline was synthesized according to a published producer.[1,2]

Fourier transform infrared spectra were recorded on a Thermo Scientific Nicolet iS10 FT-IR spectrometer equipped with an ATR accessory. ^{1}H spectra were recorded on a Unity Inova FT-NMR spectrometer operating at 499.75 MHz. All ^{1}H chemical shifts were reported relative to SiMe$_4$ using residual chemical shifts of the solvent as a secondary standard. ^{13}C{^{1}H} spectra were recorded on a Unity Inova FT-NMR spectrometer operating at 125.66 MHz. All ^{13}C chemical shifts were reported relative to SiMe$_4$ using residual chemical shifts of the solvent as a secondary standard. ^{11}B{^{1}H} spectra were recorded in either a teflon insert or a quartz J-Young tube on a Unity Inova FT-NMR spectrometer operating at 160.34 MHz. All ^{11}B chemical shifts were reported relative to BF$_3$ by referencing to an external solution of bis(pinacolato)diboron in diethyl ether. The parameters for collecting ^{11}B{^{1}H} for CO$_2$ reactivity (**4 – 7**) were as follows: pw = 7.850 µs @tpwr = 51, d1 = 1 s, nt = 512, sw = 64102.6 Hz , and tof = 4816.1 Hz. The parameters for collecting ^{11}B{^{1}H} for **10** and **13** were as follows: pw = 13.124 µs @tpwr = 51, d1 = 5 s, nt = 5000, sw = 96153.8 Hz , and tof = 4824.1 Hz. ^{15}N{^{1}H} spectra were recorded on a Unity Inova FT-NMR spectrometer operating at 50.66 MHz. All ^{15}N chemical shifts were referenced to external neat nitromethane. The 90° pulse was calibrated to 11.25 µs @tpwr = 60 prior to use. The remaining parameters utilized for collecting ^{15}N{^{1}H} spectra were as follows: d1 = 5 s, nt = 4096, sw = 40588.5 Hz, and tof = 14289.8 Hz. ^{29}Si{^{1}H} NMR spectra were recorded on a 500 MHz Unity Inova FT-

NMR spectrometer operating at 99.29 MHz utilizing standard borosilicate NMR tubes. All ^{29}Si chemical shifts were internally referenced to $SiMe_4$. The 90° pulse was calibrated to 20.25 μs @tpwr = 51 and the relaxation time of 5T1 was found to correspond to a d1 of 40 s prior to use. The remaining parameters utilized for collecting $^{29}Si\{^1H\}$ were as follows: nt = 4096 sw = 8912.7 Hz, and tof = 1600.7 Hz.

GC mass spectrometry was recorded on a Varian CP3800 GC with Saturn 2000 ion trap (70 eV). Solution magnetic susceptibilities were calculated from Evan's method NMR measurements.[3] Solid-phase magnetic susceptibilities were recorded on a Johnson Matthey MSB-1 magnetic susceptibility balance that was calibrated with $HgCo(SCN)_4$. Diamagnetic correction factors were calculated from Pascal's constants.[4] Elemental analyses were performed by ALS (formerly Columbia Analytical Services) in Tuscon, AZ.

Mössbauer spectra were recorded at room temperature with a constant-acceleration spectrometer (Wissel GMBH, Germany) in a horizontal transmission mode using a 50 mCi ^{57}Co source. Approximately 0.080 g of sample was crushed in a Mössbauer sample holder and a drop of paratone was used to cover the sample to prevent oxidation. Data acquisition varied from 2 days to 7 days to get a statistically reasonable spectrum for each sample to analyze. The velocity scale was normalized with respect to metallic iron at room temperature; hence all isomer shifts were recorded relative to metallic iron. The Mössbauer spectra were fitted by assuming Lorentzian line shapes using the NORMOS

(Wissel GMBH) least-square fitting program. The isomer shifts and quadrupole splitting parameters were determined from the fitted spectra.

Cyclic voltammetry was carried out using a Parstat 2273 potentiostat employing a standard three-electrode electrochemical cell consisting of a glassy carbon working electrode and a platinum auxiliary electrode. All potentials are reported relative to a Ag/Ag$^+$ reference electrode which was calibrated to the ferrocene redox couple. Experiments were carried out under an argon atmosphere at room temperature using methylene chloride solutions of the analyte at 0.010 M and with 0.100 M tetra(n-butyl)ammonium hexafluorophosphate as the supporting electrolyte.

X-ray diffraction experiments for **5** and **7** were carried out on a Bruker Smart Apex diffractometer at 173(2) K using MoKα radiation (λ=0.71070 Å). Absorption corrections were applied by SADABS.[5] The structures were solved using direct methods and refined with full-matrix least-squares methods based on F^2. All non-hydrogen atoms were refined with anisotropic thermal parameters. H atoms in **5** were found on the difference F-map and refined with isotropic thermal parameters. H atoms in **5** were refined in calculated positions in a rigid group model. Highly disordered solvent molecules, CH3OH, in **5** were treated by SQUEEZE.[6] Correction of the X-ray data by SQUEEZE is 13 electrons/cell; the required value is 18 electrons/cell. All calculations were performed using the SHELXTL (v. 6.10) package.[7] X-ray diffraction experiment for **3** was collected at -133°C on a Bruker APEX II single crystal X-

ray diffractometer, Mo-radiation. A brown plate, measuring 0.35 x 0.17 x 0.07 mm^3 was mounted on a loop with oil. Crystal-to-detector distance was 40 mm and exposure time was 10 seconds per frame for all sets. The scan width was 0.5^o. Data collection was 99% complete to 25° in ϑ. A total of 53475 reflections were collected covering the indices, h = -71 to 71, k = -10 to 10, l = -31 to 31. 11794 reflections were symmetry independent and the Rint = 0.0973 indicated that the data was of slightly less than average quality (0.07). Indexing and unit cell refinement indicated a C – centered monoclinic lattice. The space group was found to be C 2/c (No.15). The data was integrated and scaled using SAINT, SADABS within the APEX2 software package by Bruker.[8] Solution by direct methods (SHELXS, SIR97[9]) produced a complete heavy atom phasing model consistent with the proposed structure of **3**. The structure of **3** was completed by difference Fourier synthesis with SHELXL97.[10,11] Scattering factors are from Waasmair and Kirfel.[12] Hydrogen atoms were placed in geometrically idealized positions and constrained to ride on their parent atoms with C---H distances in the range 0.95-1.00 Angstrom. Isotropic thermal parameters U_{eq} were fixed such that they were 1.2U_{eq} of their parent atom U_{eq} for CH's and 1.5U_{eq} of their parent atom U_{eq} in case of methyl groups. All non-hydrogen atoms were refined anisotropically by full-matrix least-squares. Extensive disorder of pentane and ethyl alcohol impose disorder in one of the two independent molecules of the asymmetric unit. A high R1 value and unusually large second weighting parameter indicate that some amount of twinning is present which could not be resolved. X-ray diffraction intensities were collected at 173(2) K (**8**, **9** and **13**) and 193 K (**12**) on a Bruker Apex CCD diffractometer and at 100 K

124

(**11** and **10**) on a Bruker Apex2 diffractometer using MoKσ radiation λ= 0.71073 Å. Space group was determined based on systematic absences and intensity statistics (**12**). Absorption corrections were applied by SADABS. Structures were solved by direct methods and Fourier techniques and refined on F^2 using full matrix leastsquares procedures. All non-H atoms were refined with anisotropic thermal parameters. H atoms in **12** and **13** were found from the residual density maps and refined with isotropic thermal parameters except those in terminal Me groups in **13** which were treated in calculated positions. The H atom at the N atom in **8** involved in H-bonds was found from the residual density map and refined, other H atoms in these structures and all H atoms in **9** and **10** were treated in calculated positions in a rigid group model. All calculations were performed by the Bruker SHELXTL (v. 6.10) package.

Gas Chromatography was performed on a SRI 8610c GC using a 6 foot 13x molecular sieve column and a TCD detector. Calibration curves and analyses were performed through on-column injection by use of gastight syringes from Hamilton. Varying volumes of pure carbon monoxide and hydrogen were injected to construct calibration curves. For headspace samples, a volume of nitrogen equivalent to the sample volume was first injected into headspace. The syringe was then purged thoroughly, after which the sample was drawn up and then injected into the GC.

Preparation of [(2,6-^{i}PrC$_6$H$_3$N=CMe)(O=CMe)C$_5$H$_3$N] (1)
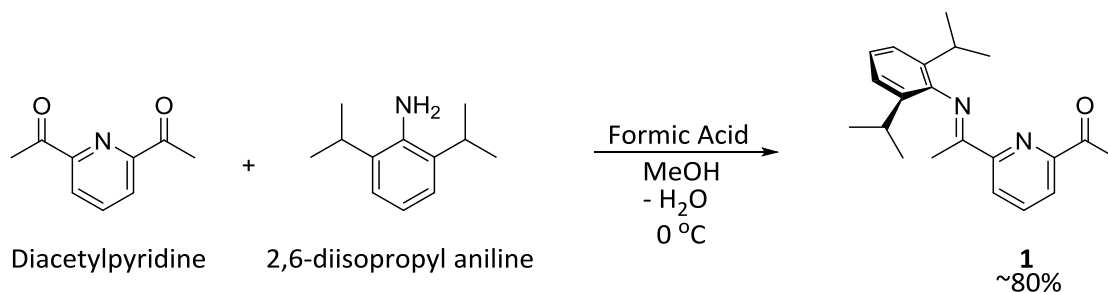
In a 250 mL round bottom flask, 2,6-diacetylpyridine (4.51g, 27.6mmol) and a stir bar was added. Using a graduated pipette, 2,6-diisoproylaniline (5.22mL, 27.6mmol) was then added to the 250mL round bottom flask. The round bottom flask was capped with a rubber septum. Dry methanol (~40mL) was then added to the solution via syringe while the solution was stirring. The solution stirred until all reactants were dissolved. The round bottom was placed under an ice bath while still stirring. About 10 drops of 99% formic acid (.25mL) was carefully added to the solution via a syringe. The round bottom was allowed to stir in the ice bath for 1 hour. The round bottom was then placed in a refrigerator at 0°C for 48 hours. After 1 hour, the round bottom was moved to the freezer (-30°C) for 24 hours. The resulting yellow solid was vacuum filtered through a Buchner funnel, with a No. 2 filter paper, while also being washed with dry methanol. The dry yellow solid was dried through the schlenk line and identified as **1** (85.5%).

FTIR (ATR): ν(C=N) 1647 and 1698 (C=O) cm^{-1}.

^{1}H NMR (CDCl$_3$): δ = 8.55 (d, J = 7.8 Hz, 1 H, m-pyr), 8.12 (d, J = 7.8 Hz, 1 H, m-pyr), 7.94 (t, J = 7.8 Hz, 1 H, p-pyr), 7.15 (d, J = 7.3 Hz, 2 H, m-^{iPr}Ar), 7.09 (t, J = 7.3 Hz, 1 H, m-^{iPr}Ar), 2.77 (s, 3 H, (CH$_3$)C=O), 2.69 (septet, J = 6.8 Hz, 2 H, CH(CH$_3$)$_2$), 2.49 (s, 3 H, (CH$_3$)C=N), 1.14 (d, J = 1.5 Hz, 6 H, (CH$_3$)$_2$CH)), 1.12 (d, J = 1.5 Hz, 6 H, (CH$_3$)$_2$CH)).

Preparation of [(2,6-^{i}Pr-C$_6$H$_3$)N=CMe)(2-MeO-6-Me-C$_6$H$_3$)N=CMe)C$_5$H$_3$N] (2)

1

2-methyl-6-methoxy
aniline

2
~60%
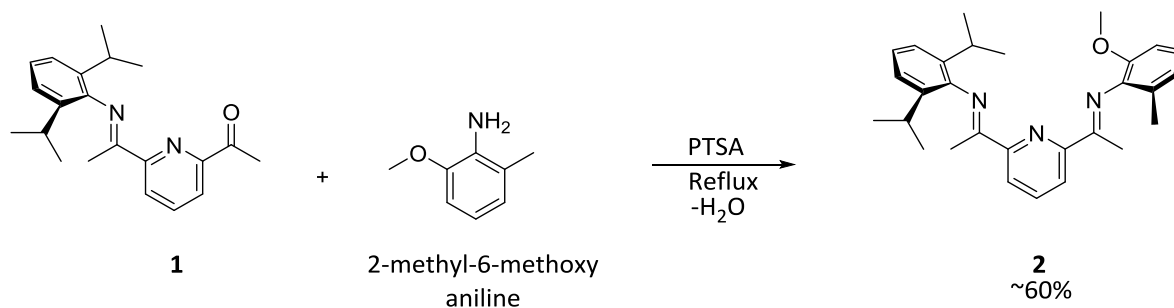
In an oven-dried 500 mL round bottom flask, equipped with a Dean-Stark apparatus [(ArN=C(CH$_3$))C$_2$H$_3$N((CH$_3$)C=O] (Ar= 2,6-^{i}Pr-C$_6$H$_3$) (2.00 g, 6.20 mmol) was added with a slight excess of 2-methoxy-6-methylaniline (0.852 g, 6.21 mmol) and catalytic amount of p-toluenesulfonic acid monohydrate (0.0352 g, 0.185 mmol). The mixture was dissolved with dry toluene (200 mL). The solution was stirred and refluxed at 120 °C for 12 h followed by concentration under vacuum. Acetonitrile (100 mL) was added to precipitate out a yellow solid. The mixture was filtered through a Büchner funnel and washed with dry acetonitrile yielding a pale yellow solid identified as ^{MeO}PDI (2) (63%).

FTIR (ATR): ν(C=N) 1643 cm^{-1}.

^{1}H NMR (CD$_2$Cl$_2$): δ = 8.47 (d, J = 7.8 Hz, 1 H, m-pyr), 8.45 (d, J = 7.8 Hz, 1 H, m-pyr), 7.93 (t, J = 7.8 Hz, 1 H, p-pyr), 7.17 (d, J = 7.3 Hz, 2 H, m-^{iPr}Ar), 7.09 (t, J = 7.3 Hz, 1 H, p-^{iPr}Ar), 7.01 (t, J = 7.8 Hz, 1 H, p-^{MeO}Ar), 6.87 (d, J = 7.3 Hz, 1 H, m-^{MeO}Ar), 6.83 (d, J = 8.3 Hz, 1 H, m-^{MeO}Ar), 3.76 (s, 3 H, O-CH$_3$), 2.77 (septet, J = 6.8 Hz, 2 H, C$\underline{H}$(CH$_3$)$_2$), 2.27 (s, 3 H, (CH$_3$)C=N), 2.25 (s, 3 H, (CH$_3$)C=N), 2.09 (s, 3 H, CH$_3$(o-^{MeO}Ar)), 1.16 (d, J = 1.5 Hz, 6 H, (C$\underline{H}_3$)CH)), 1.15 (d, J = 1.5 Hz, 6 H, (C$\underline{H}_3$)$_2$CH)).

^{13}C{^{1}H} NMR (CD$_2$Cl$_2$): δ = 168.9 (C=N(^{MeO}Ar)), 167.6 (C=N(^{iPr}Ar)), 155.9, 155.7, 148.4, 147.1, 139.3, 137.4, 136.3, 128.7, 124.1, 124.0, 123.5, 122.9, 122.8, 122.6, 109.4, 56.1, 28.8, 23.5, 23.1, 18.0, 17.5, 15.9, 1.34.

GCMS (M$^+$): Calculated for C$_{29}$H$_{35}$N$_3$O: 441.3 Found: 441.4.
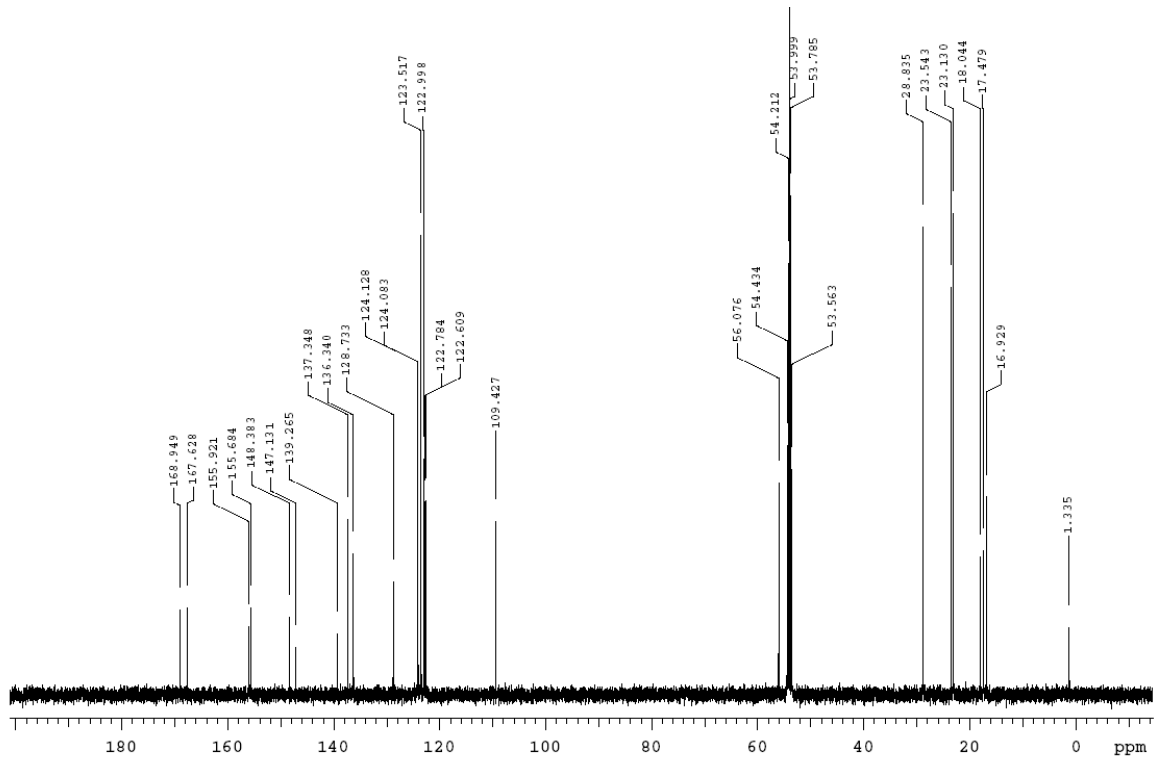
Figure 6.1. ^{13}C{^{1}H} NMR spectrum of **2**, 126 MHz, CD$_2$Cl$_2$.

128

Preparation of ^{MeO}PDIFeBr₂ (3)

Preparation of ^{MeO}PDIFeBr$_2$ (3)
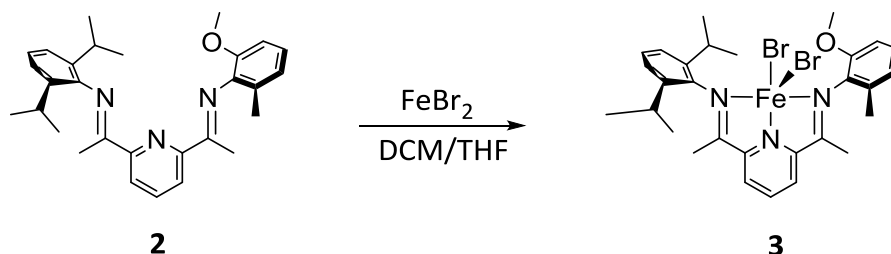
In an oven-dried 50 mL Erylenmeyer flask, ^{MeO}PDI (0.200 g, 0.452 mmol) was dissolved in methylene chloride (10 mL) producing a faint yellow solution. While stirring, a suspension of FeBr$_2$ (0.0977 g, 0.452 mmol) in THF (3 mL) was added, instantly producing a blue colored solution. The solution was allowed to stir overnight. The solution was filtered through a pipette packed with glass wool and celite and layered with pentane (40 mL) forming blue crystals identified as ^{MeO}PDIFeBr$_2$ **(3)** (71%).

^{1}H NMR (CDCl$_3$): δ = 82.4 (s, 1 H, *p*-pyr), 74.2 (s, 1 H, *o*-pyr), 73.2 (s, 1 H, *o*-pyr), 18.6 (s, 1 H, *o*-^{MeO}Ar), 17.6 (s, 1 H, *o*-^{MeO}Ar), 13.5 (s, 1 H, *o*-^{iPr}Ar), 12.9 (s, 1 H, *o*-^{iPr}Ar), 9.49 (s, 3 H, O-CH$_3$), -4.37 (s, 1 H, *p*-^{MeO}Ar), -5.16 (s, 12 H, (C$\underline{H}_3$)$_2$CH), -9.81 (s, 3 H, CH$_3$(*m*-^{MeO}Ar)), -12.1 (s, 1 H, *p*-^{iPr}Ar), -14.8 (s, 2 H, C$\underline{H}$(CH$_3$)$_2$), -25.8 (s, 3 H, (CH$_3$)C=N-^{MeO}Ar), -35.2 (s, 3 H, (CH$_3$)C=N-^{iPr}Ar).

Evan's Method: μ$_{eff}$ = 4.89 μ$_B$ (solution), 5.49 μ$_B$ (solid).

Elemental: C$_{29}$H$_{35}$Br$_2$FeN$_3$O: C, 52.99; H, 5.37; N, 6.39. Found: C, 53.46; H, 5.36; N, 6.18.

Generation of ^{MeO}PDIFeN₂ (4)
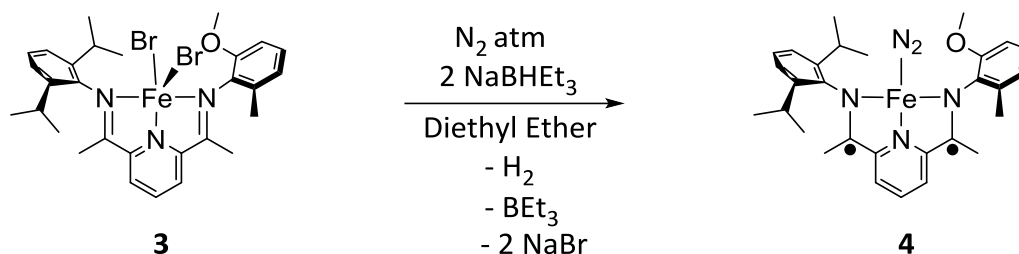
In an oven-dried 20 mL scintillation vial fitted with a #33 Suba Seal septum and a stirbar, **3** (0.100 g, 0.152 mmol) was added with anhydrous diethyl ether (5 mL). This suspension was stored at -30 °C in the glovebox freezer for 1 h prior to reduction. The suspension was removed from the freezer and NaBHEt₃ (-30 °C, 0.304 mL, 0.304 mmol) was syringed into the solution drop-wise resulting in an immediate color change to a deep green colored solution that was allowed to warm to room temperature with stirring. This solution was identified as **^{MeO}PDIFeCl₂ (4)**.

FTIR (Pentane): v(N₂) 2045 cm⁻¹, v((N₂)₂) 2130 and 2071 cm⁻¹.

Generation of ^{MeO}PDIFe¹⁵N₂ (4(¹⁵N₂))
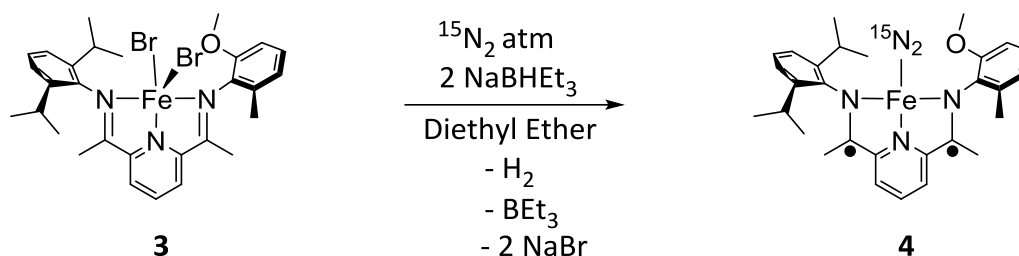
The green solution produced above (from **3** and two equivalents of NaBHEt₃) was allowed to stir for 30 min before filtration through a pipette packed with glass wool and celite. In a J-Young NMR tube fitted with a pressure lid, the green solution (0.500 mL) was added and frozen in a cold well. Once frozen, the headspace was evacuated and refilled with $^{15}N_2$ gas. The tube was allowed to come to room temperature, shaken for 10 min, and immediately placed into the spectrometer.

^{15}N{^{1}H} NMR (Et₂O): δ = 113.5 and 104.7. IR (pentane): ν(N₂) 1959 cm^{-1}.

Generation of ^{MeO}PDIFe(CO)$_2$ (5)
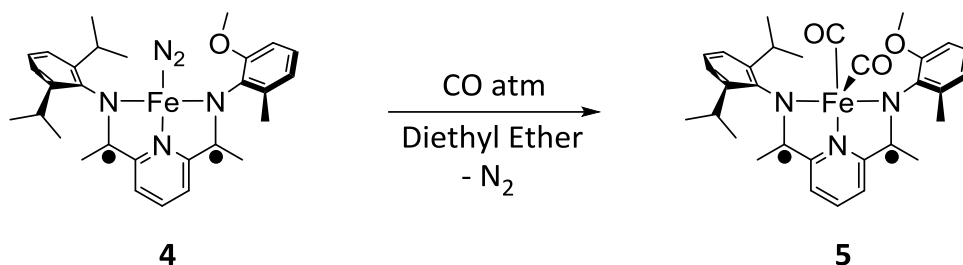
Inside the glove box, an 88 mL pressure tube fitted with a pressure gauge, an inlet needle valve, and an outlet needle valve, was charged with a freshly prepared solution of **4** (0.152 mmol in 10 mL diethyl ether). The pressure tube was sealed and brought outside the glove box to be pressurized with CO gas (1 atm). The solution was allowed to stir overnight. The solvent was removed in vacuo and brought back into the glove box for filtration through a pipette packed with glass wool and celite. Slow evaporation of the diethyl ether yielded green crystals identified as ^{MeO}PDIFe(CO)$_2$, **5** (60%).

^{1}H NMR (CD$_2$Cl$_2$): δ = 8.46 (d, J = 7.7 Hz, 1 H, o-pyr), 8.45 (d, J = 7.7 Hz, 1 H, o-pyr), 7.94 (t, J = 7.7 Hz, 1 H, p-pyr), 7.17 (d, J = 7.7 Hz, 2 H, o-^{iPr}Ar), 7.08 (t, J = 7.7 Hz, 1 H, p-^{iPr}Ar), 7.00 (t, J = 7.7 Hz, 1 H, p-^{MeO}Ar), 6.87 (d, J = 7.4 Hz, 1 H, o-^{MeO}Ar), 6.83 (d, J = 8.0 Hz, 1 H, o-^{MeO}Ar), 3.76 (s, 3 H, O-CH$_3$), 2.77 (septet, J = 6.7 Hz, 2 H, C$\underline{H}$(CH$_3$)$_2$), 2.26 (s, 3 H, (CH$_3$)C=N), 2.24 (s, 3 H, (CH$_3$)C=N), 2.09 (s, 3 H, CH$_3$(m-^{MeO}Ar)), 1.16 (d, J = 7.1 Hz, 6 H, (C$\underline{H}_3$)$_2$CH), 1.14 (d, J = 7.1 Hz, 6 H, (C$\underline{H}_3$)$_2$CH).

^{13}C{^{1}H} NMR (CD$_2$Cl$_2$): δ = 216.7 (FeCO), 155.7, 155.2, 150.7, 149.9, 145.1, 144.9, 142.4, 140.8, 139.78, 131.51, 126.14, 125.83, 123.51, 123.51, 123.48, 122.34, 120.84, 120.80, 116.74, 108.48, 66.02, 55.32, 27.43, 27.37, 25.01, 24.63, 23.76, 17.79, 16.60, 15.44, 15.24.

FTIR (ATR): ν(CO) 1947 and 1883 cm^{-1}. Anal calcd for C$_{30}$H$_{35}$FeN$_3$O$_3$: C, 60.01; H, 6.55; N, 7.00. Found: C, 60.52; H, 6.20; N, 6.95.
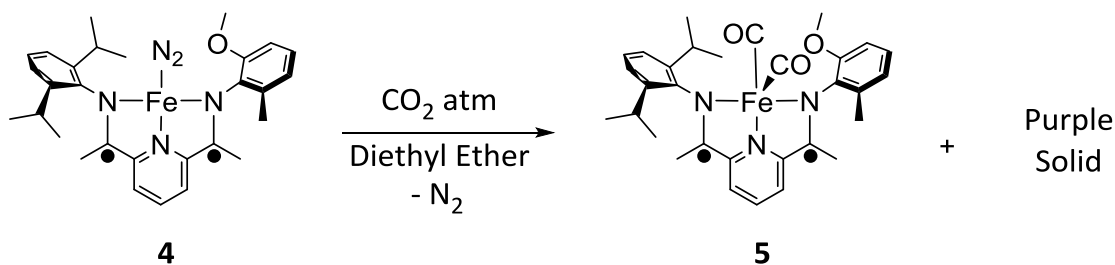
Reactivity of 4 with CO₂ gas to form 5 and Purple Solid

Inside the glove box, an 88 mL pressure tube fitted with a pressure gauge, an inlet needle valve, and an outlet needle valve, was charged with **4** (0.152 mmol) and anhydrous diethyl ether (10 mL). The pressure tube was sealed, and pressurized inside the glove box with CO_2 gas (1 atm). The solution was allowed to stir overnight, during which time the solution changed color from dark green to brown and then finally back to green. Purple precipitate was present at the bottom of tube. The tube was degassed in vacuo and the contents re-dissolved in diethyl ether. The solution was filtered through a pipette packed with glass wool and celite into a scintillation vial, stoppered with a rubber septum. The vial was removed from the glove box in order to dry the sample at 80 °C, which resulted in a green solid identified as **5**(43 %). The purple solid on the celite was dissolved in DCM and filtered through a pipette packed with glass wool and celite. The purple solution degraded to yellow slush within an hour at room temperature.

Reactivity of 4 with $^{13}CO_2$ gas to form ($5(^{13}CO)_2$)

4   **5**
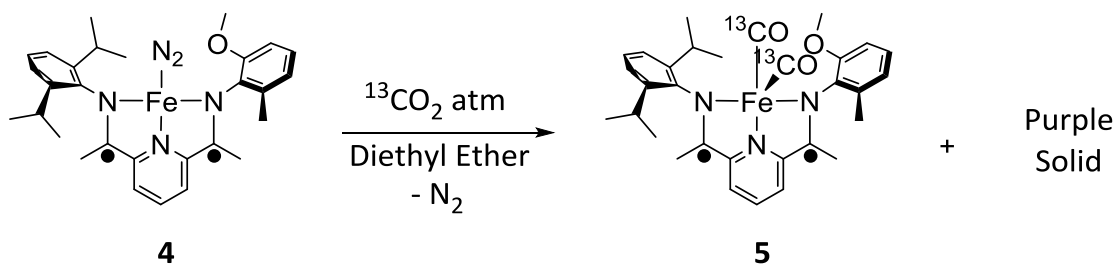
In an oven-dried 20 mL scintillation vial, **3** (0.040 g, 0.061 mmol) was dissolved in toluene-d_8 (2 mL). This suspension was stored at -30 °C in the glovebox freezer for 1 h prior to reduction. The suspension was removed from the freezer and sodium triethylborohydride (-30 °C, 0.122 mL, 0.122 mmol) was syringed into the solution drop-wise resulting in an immediate color change to a deep green solution of **4**. The green solution of **4** was allowed to stir for 30 min before filtered through a pipette packed with glass wool and celite into a J-Young NMR tube. The tube was placed in a liquid nitrogen cold well, the solution was frozen, and the headspace was removed. The tube was removed from the cold well and the headspace was backfilled with $^{13}CO_2$, allowed to warm to room temperature, and shaken for 10 min before being placed immediately in the NMR spectrometer.

FTIR (pentane): $v(^{13}CO)$ 1923 and 1867 cm^{-1}.

$^{13}C\{^1H\}$ NMR (toluene-d_8): δ = 214.8 Fe^{13}CO.

Preparation of ^{MeO}PDIFeDEPE (6)
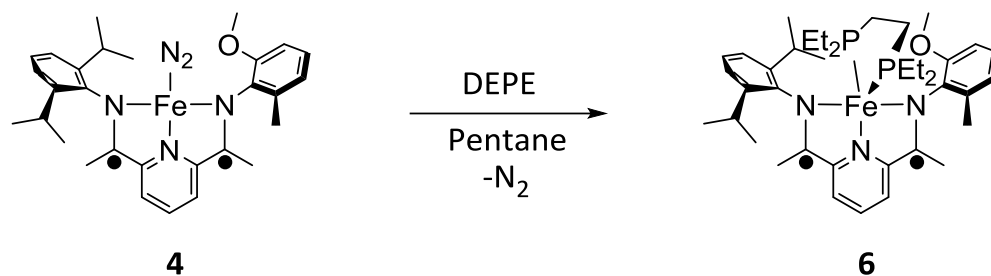
The green solution of **4** was prepared from **3** (63.7 mg, 0.097 mmol), $NaBHEt_3$ (0.193 mL, 0.194 mmol) and 10 mL of diethyl ether. After 30 min of stirring, DEPE (0.022 mL, 0.0943 mmol) was slowly added, to see a slow color change from dark green to red-brown. The solution was allowed to stir over night before vacuuming off the solvent. The mixture was re-dissolved in pentane and filtered through a pipette packed with glass wool and celite. After one day of sitting in the pentane solution at - 35 ^{0}C, black crystals were furnished and identified as ^{MeO}PDIFeDEPE (6).

Reactivity of 6 with CO₂ gas to form (5)
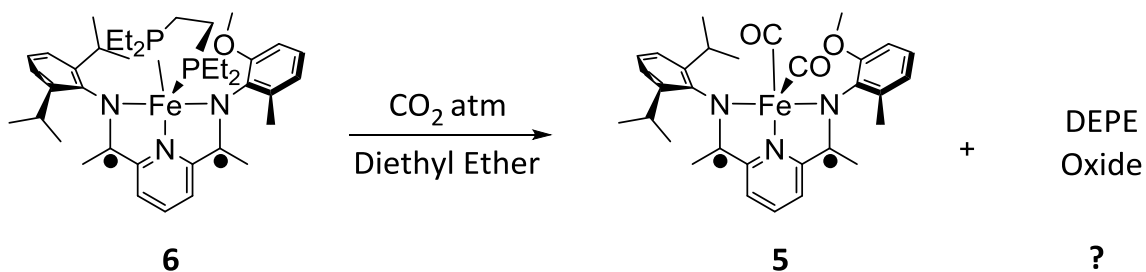
Inside the glove box, an 88 mL Fisher-Porter tube fitted with a pressure gauge, an inlet needle valve, and an outlet needle valve, was charged with **6** (20.0 mg, 0.028 mmol), and anhydrous diethyl ether (10 mL). The Fisher-Porter tube was sealed, and pressurized inside the glove box with CO_2 gas (1 atm). The solution was allowed to stir for two hours, during which time the solution changed color from black to brown and then finally to green. The tube was degassed in vacuo and filtered through a pipette packed with glass wool and celite into a scintillation vial, stoppered with a rubber septum. The green solid was identified as **5.** Analysis of the solution for the oxidized DEPE products was inconclusive.

Reactivity of 4 with CO_2 gas and TMSCl to form (5) and $^{MeO}PDIFeCl_2$ (7)
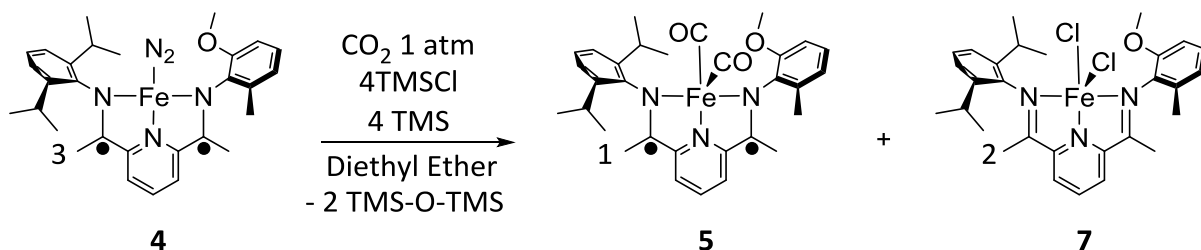
Inside the glove box, an 88 mL Fisher-Porter tube fitted with a pressure gauge, an inlet needle valve, and an outlet needle valve, was charged with **4** (0.152 mmol), trimethylsilyl chloride (0.039 mL, 0.304 mmol) and anhydrous diethyl ether (10 mL). The Fisher-Porter tube was sealed, and pressurized inside the glove box with CO_2 gas (1 atm). The solution was allowed to stir overnight, during which time the solution changed color from dark green to brown and then finally back to green. Blue precipitate was present at the bottom of tube and on the stir bar at the end of the reaction. The tube was degassed in vacuo and filtered through a pipette packed with glass wool and celite into a scintillation vial, stoppered with a rubber septum. The vial was removed from the glove box in order to dry the sample at 80 °C, which resulted in a green solid identified as **5** (35.5%). The blue solid on the celite was dissolved in methanol and layered with diethyl ether to furnish blue crystals identified as $^{MeO}PDIFeCl_2$ **(7)** (66.9%).

^1H NMR (CDCl$_3$): δ = 79.9 (s, *p*-pyr), 79.1 (s, 1 H, *o*-pyr), 77.4 (s, 1 H, *o*-pyr), 17.9 (s, 1 H, *o*-^{MeO}Ar), 17.0 (s, 1 H, *o*-^{MeO}Ar), 13.5 (s, 1 H, *o*-^{iPr}Ar), 12.5 (s, 1 H, *o*-^{iPr}Ar), 7.78 (s, 3 H, O-CH$_3$), -4.98 (s, 1 H, *p*-^{MeO}Ar), -6.55 (s, 12 H, (C$\underline{H}_3$)$_2$CH), -9.88 (s, 3 H, CH$_3$(*m*-^{MeO}Ar)), -13.1 (s, 1 H, *p*-^{iPr}Ar), -14.1 (s, 2H, C$\underline{H}$(CH$_3$)$_2$), -30.5 (s, 3 H, (CH$_3$)C=N-^{MeO}Ar), -43.6 (s, 3 H, (CH$_3$)C=N-^{iPr}Ar).

Evan's Method: μ$_{eff}$ = 4.94 μ$_B$ (solution), 5.58 μ$_B$ (solid).

Elemental: $C_{30}H_{39}Cl_2FeN_3O_2 \cdot C_2H_5O$ (0.5 etherate): C, 66.22; H, 6.74; N, 7.02. Found: C, 66.20; H, 6.41; N, 7.18.
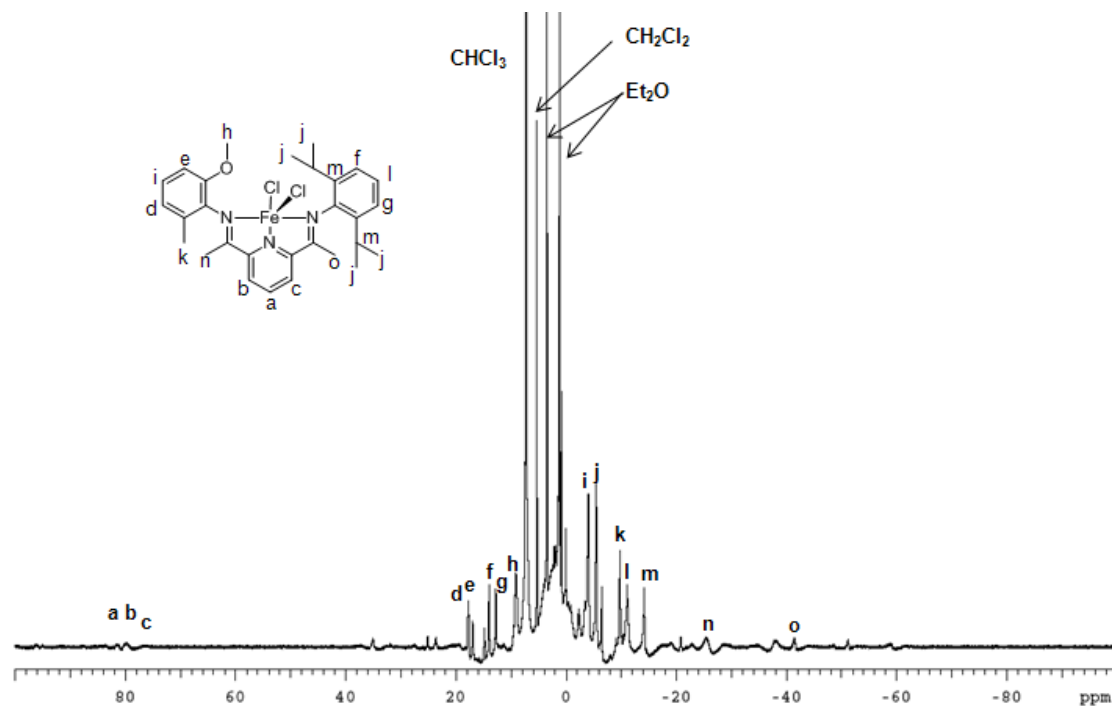

Figure 6.2. ^{1}H NMR spectrum of **7** from the HCl/Et$_2$O reaction with **5**, 500 MHz, CDCl$_3$. Although there are resonances from a small amount of likely [^{MeO}**PDIFe(CO)$_2$**]$^+$, the majority of relevant resonances from **7** are present.

Reactivity of 3 with an HCl/Et₂O solution
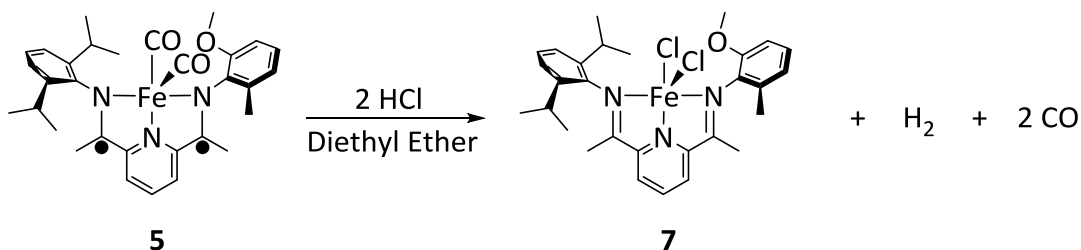
5 (0.035 mg, 0.063 mmol) was placed in an oven-dried 20 mL scintillation vial fitted with a #33 Suba Seal septum and a stirbar. The solid was dissolved in anhydrous diethyl ether (10 mL), and stored in the glovebox freezer at -30 °C for 30 min. The solution was removed and while stirring, HCl/Et₂O (0.063 mL of 2M HCl/Et₂O, 0.126 mmol) was syringed into the solution. The reaction was allowed to warm to room temp and stir for 3 h, during which time formation of precipitates was observed. After GC analysis of the headspace, the diethyl ether was removed under vacuum, resulting in a mixture of blue and green solids. The green solid was redissolved in diethyl ether, filtered through a pipette packed with glass wool and celite, and concentrated in vacuo to yield a blue solid identified as **5** (29%)**.** The remaining solid left on the celite filter and on the scintillation vial was recovered with methylene chloride and concentrated in vacuo to yield a blue solid identified as **7** (47%)**.**

Quantitation of hexamethyldisiloxane by $^{29}Si\{^1H\}$ NMR.

In a glove box, an 88 mL Fisher-Porter tube fitted with a pressure gauge, an inlet needle valve, and an outlet needle valve, was charged with a freshly prepared solution of **2** (0.152 mmol), trimethylsilyl choride (0.039 mL, 0.304 mmol), tetramethylsilane (0.040 mL, 0.304 mmol) and anhydrous diethyl ether (10 mL). The Fisher-Porter tube was sealed and pressurized inside the glove box with CO_2 gas (1 atm). The solution was allowed to stir overnight, during which time the solution changed color from dark green to brown and then finally back to green. The solution (0.500 mL) was transferred into an NMR tube and an inverse gated ^1H decoupled ^{29}Si NMR spectrum was obtained. The integrated value of hexamethyldisiloxane (0.78) was used relative to the internal reference, tetramethylsilane (1.00) to calculate the amount of moles of hexamethyldisiloxane produced.[13]
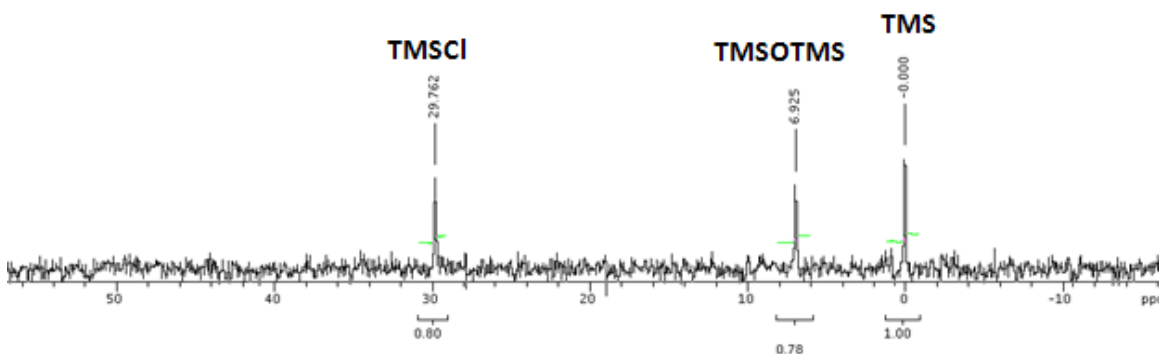

Figure 6.3. $^{29}Si\{^1H\}$ NMR spectrum (99 MHz, Et$_2$O) of the reaction mixture of 0.152 mmol **4** and an excess of TMSCl in diethyl ether post exposure (12 hours) to 1 atm CO_2. The resonance at 30 ppm is attributed to unreacted trimethylsilyl chloride. TMS (0.304 mmol) was present as an internal standard.

140

Observation of triethylborane pre/post reaction with CO_2.

In an oven-dried 20 mL scintillation vial fitted with a #33 Suba Seal septum and a stirbar, **1** (0.100 g, 0.152 mmol) was added with anhydrous diethyl ether (5 mL). This suspension was stored at -30 °C in the glovebox freezer for 1 h prior to reduction. The suspension was removed from the freezer and sodium triethylborohydride (-30 °C, 0.304 mL, 0.304 mmol) was syringed into the solution drop-wise resulting in an immediate color change to a deep green colored solution identified as **2** that was allowed to warm to room temperature with stirring. The solution (0.500 mL) was transferred into a quartz J-Young NMR tube and a $^{11}B\{^1H\}$ NMR spectrum was obtained, showing a resonance at 86.7 ppm, corresponding to triethylborane with no other boron containing species. The J-Young NMR tube was then degassed by repeated cycles of freeze-pump-thaw and then backfilled with CO_2 gas. Another ^{11}B NMR spectrum was obtained over the course of 5 h, showing a major resonance at 86.7 ppm.

141

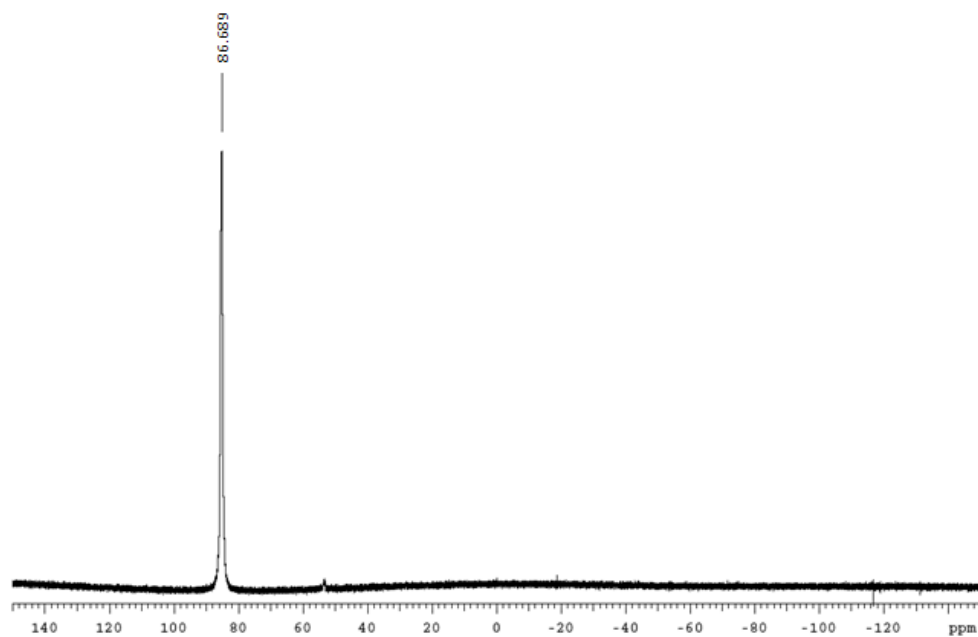**Figure 6.4.** $^{11}B\{^{1}H\}$ NMR spectrum of the post-CO_2 reaction, 160 MHz, Et_2O. The majority of the boron exist as BEt_3 (86.69 ppm).
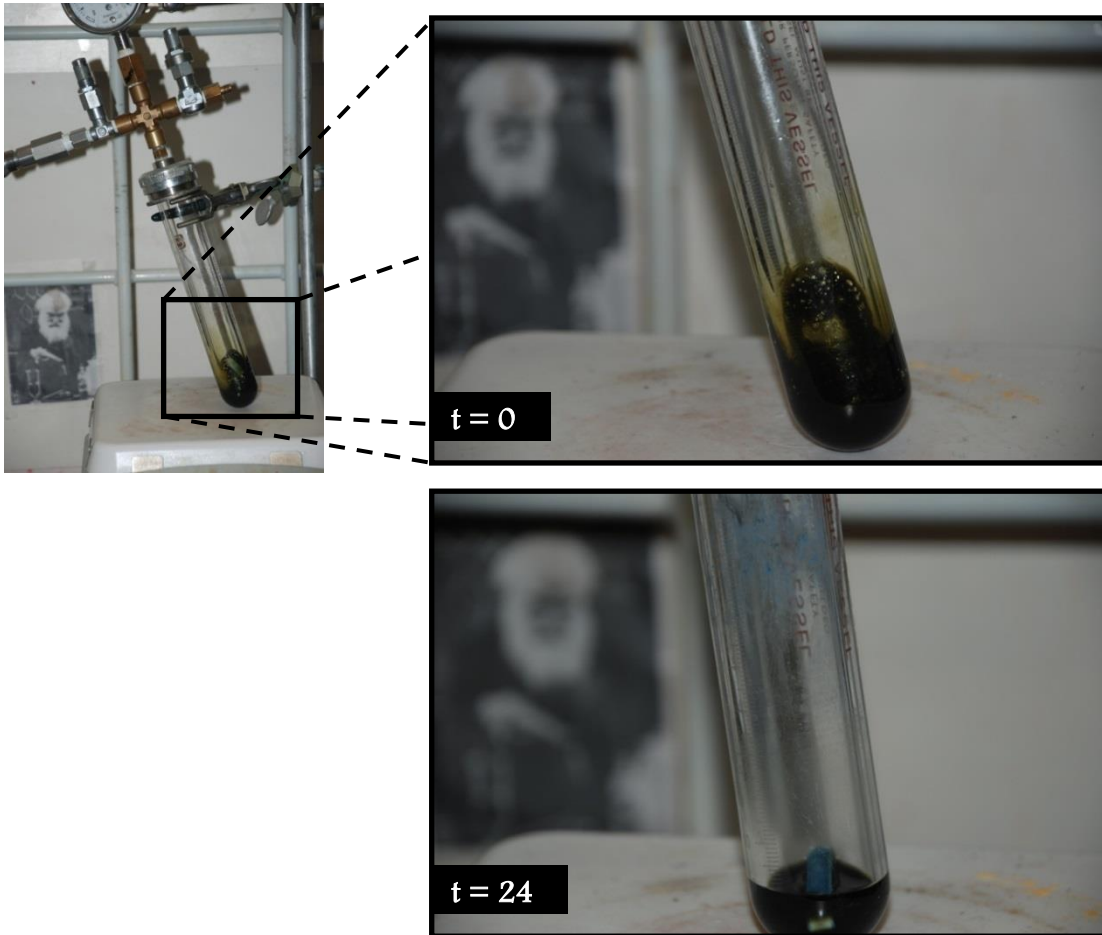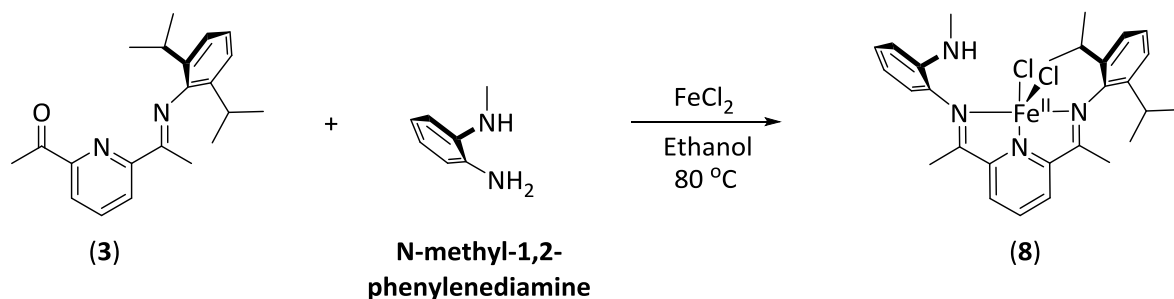
142

Figure 6.5. Picture of CO_2 reduction of **4** at t = 0 h and t = 24 h.

www.manaraa.com

Preparation of ^{MeNH}PDIFeCl$_2$ (8)

(3)   +   **N-methyl-1,2-phenylenediamine** $\xrightarrow[\text{80 °C}]{\begin{array}{c}\text{FeCl}_2\\\text{Ethanol}\end{array}}$ (8)

In an oven-dried 100 mL Schlenk flask, [(ArN=C(CH$_3$))C$_2$H$_3$N((CH$_3$)C=O] (Ar= 2,6-^{i}Pr-C$_6$H$_3$) (0.500 g, 1.55 mmol) and FeCl$_2$ (0.197 g, 1.55 mmol) was dissolved in ethanol (20 mL) producing a purple solution. While stirring, the solution was heated at 60 °C for 30 min under N$_2$ gas. A solution of N-methyl-1,2-phenylenediamine (0.187 g, 1.55 mmol) in 10 mL of methanol was syringed into the Schlenk flask and heated at 80 °C for 12 h under N$_2$ gas. The solvent was removed in vacuo and brought back into the glove box to be re-dissolved in methylene chloride and filtered through a pipette packed with glass wool and celite. Recrystallization from methylene chloride and diethyl ether layer afforded black crystals identified as ^{MeNH}PDIFeCl$_2$ (8) (69%).

FTIR (ATR): ν(N-H) 3318 cm^{-1}.

^{1}**H NMR** (CDCl$_3$): δ = 82.0 (s, 1 H, *p*-pyr), 78.2 (s, 1 H, *o*-pyr), 74.9 (s, 1 H, *o*-pyr), 54.5 (s, 1 H, ^{MeNH}Ar), 25.0 (s, 1 H, <u>H</u>NCH$_3$), 22.1 (s, 1 H, ^{MeNH}Ar), 19.3 (s, 1 H, ^{MeNH}Ar), 14.9 (s, 1 H, *o*-^{iPr}Ar), 10.3 (s, 1 H, *o*-^{iPr}Ar), -1.54 (s, 3 H, C<u>H</u>$_3$NH), -4.26 (s, 12 H, (C<u>H</u>$_3$)$_2$CH), -6.66 (s, 1 H, ^{MeNH}Ar), -8.96 (s, 1 H, *p*-^{iPr}Ar), -10.6 (s, 1H, C<u>H</u>(CH$_3$)$_2$), -12.7 (s, 3 H, (CH$_3$)C=N-^{MeNH}Ar), -45.5 (s, 3 H, (CH$_3$)C=N-^{iPr}Ar).

Evan's Method: μ_{eff} = 4.93 μ_B (solution), 5.11 μ_B (solid).

Elemental: C$_{28}$H$_{34}$Cl$_2$FeN$_4$•CH$_2$Cl$_2$ (636.10): calcd. C, 54.57; H, 5.68; N, 8.78; found C, 55.33; H, 5.86; N, 8.76.
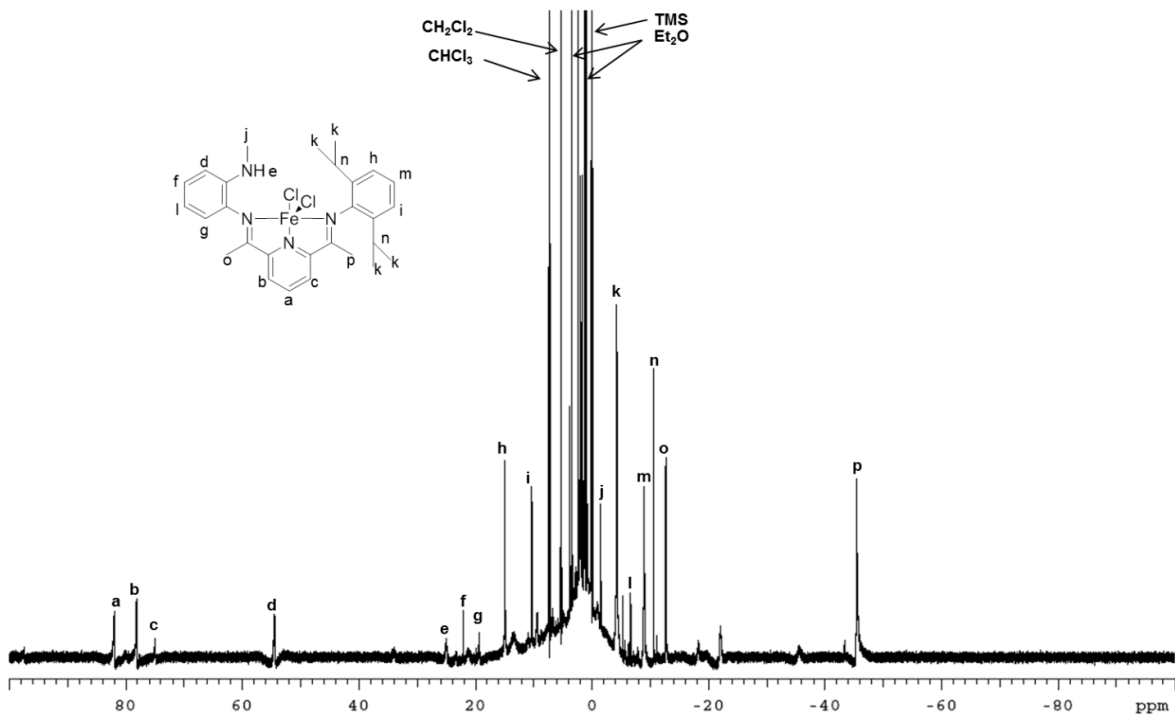
Figure 6.6. ^{1}H NMR spectrum of **8**, 500 MHz, CDCl$_3$.

Preparation of $^{\text{Me2N}}$PDIFeCl$_2$ (9)
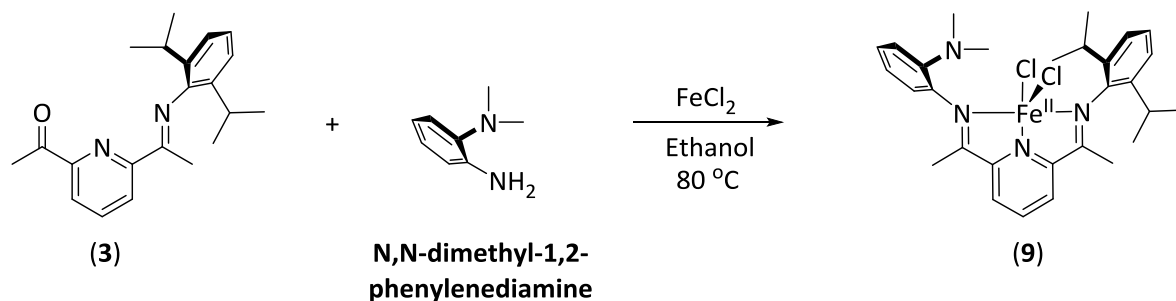
(3)   +   N,N-dimethyl-1,2-phenylenediamine $\xrightarrow[\text{80 }^{\text{o}}\text{C}]{\text{FeCl}_2 \quad \text{Ethanol}}$ (9)

In an oven-dried 100 mL Schlenk flask, [(ArN=C(CH$_3$))C$_2$H$_3$N((CH$_3$)C=O] (Ar= 2,6-$^{\text{i}}$Pr-C$_6$H$_3$) (0.500 g, 1.55 mmol) and FeCl$_2$ (0.197 g, 1.55 mmol) was dissolved in ethanol (20 mL) producing a purple solution. While stirring, the solution was heated at 60 °C for 30 min under N$_2$ gas. A solution N,N-dimethyl-1,2-phenylenediamine (0.211 g, 1.55 mmol) in 10 mL of methanol was syringed into the Schlenk flask and heated at 80 °C for 12 h under N$_2$ gas. The solvent was removed in vacuo and brought back into the glove box to be re-dissolved in methylene chloride and filtered through a pipette packed with glass wool and celite. Recrystallization from methylene chloride and diethyl ether layer afforded black crystals identified as $^{\text{Me2N}}$PDIFeCl$_2$ (9) (58%).

^{1}**H NMR (CDCl$_3$):** δ = 79.9 (s, 1 H, p-pyr), 77.4 (s, 1 H, o-pyr), 75.9 (s, 1 H, o-pyr), 17.3 (s, 4 H, o,m,p-$^{\text{(Me)2N}}$Ar), 16.1 (s, 6 H, (CH$_3$)$_2$N), 6.9 (s, 1 H, o-$^{\text{iPr}}$Ar), 5.8 (s, 1 H, o-$^{\text{iPr}}$Ar), -4.9 (s, 12 H, (C$\underline{\text{H}}_3$)$_2$CH), -8.4 (s, 1 H, p-$^{\text{iPr}}$Ar), -11.0 (s, 2 H, C$\underline{\text{H}}$(CH$_3$)$_2$), -32.7 (s, 3 H, (CH$_3$)C=N-$^{\text{(Me)2N}}$Ar), -40.4 (s, 3 H, (CH$_3$)C=N-$^{\text{iPr}}$Ar)

Evan's Method: μ_{eff} = 4.99 μ_B (solution), 5.01 μ_B (solid).

Elemental: C$_{29}$H$_{36}$Cl$_2$FeN$_4$ (567.37): calcd. C, 61.39; H, 6.40; N, 9.87; found C, 60.48; H, 6.88; N, 9.47.
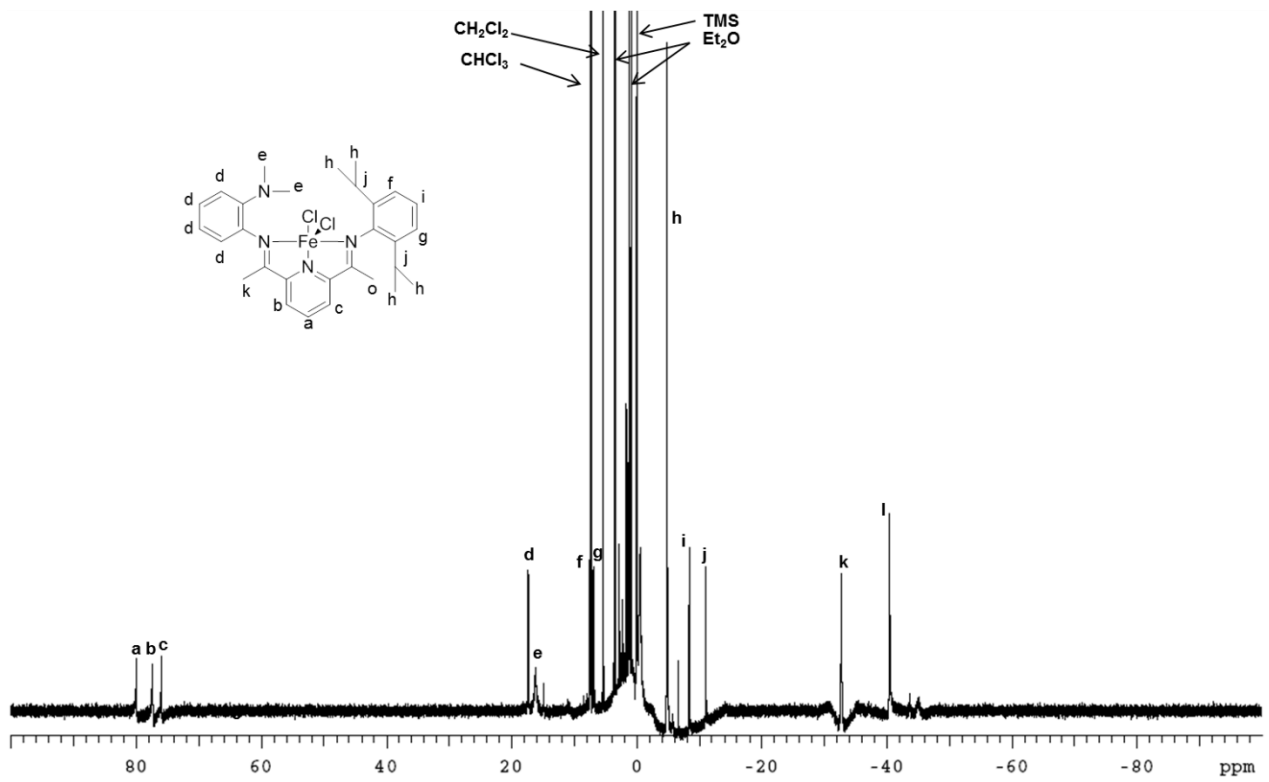
Figure 6.7. ^{1}H NMR spectrum of **9**, 500 MHz, CDCl$_3$.

147

Preparation of ^{Bpin}PDIFeCl$_2$ (10)
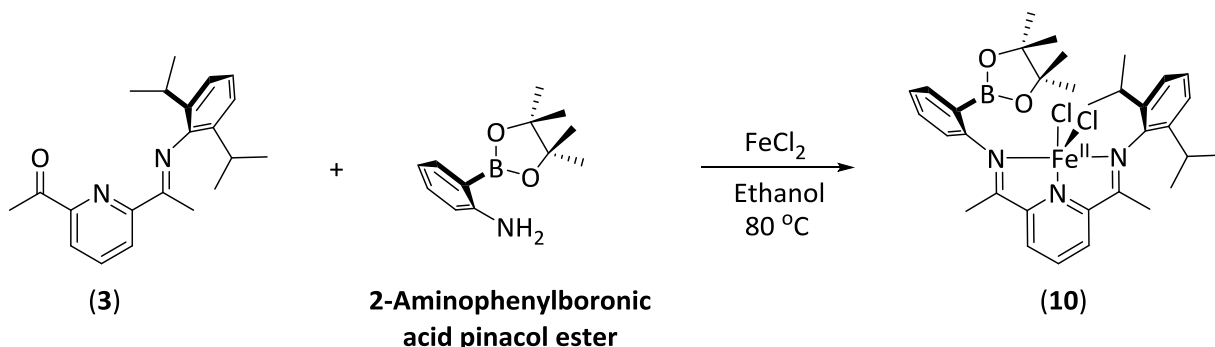
(3) + 2-Aminophenylboronic acid pinacol ester $\xrightarrow[\text{80 °C}]{\text{FeCl}_2 \text{ Ethanol}}$ (10)

In an oven-dried 100 mL Schlenk flask, [(ArN=C(CH$_3$))C$_2$H$_3$N((CH$_3$)C=O] (Ar= 2,6-^{i}Pr-C$_6$H$_3$) (0.500 g, 1.55 mmol) and FeCl$_2$ (0.197 g, 1.55 mmol) was dissolved in ethanol (20 mL) producing a purple solution. While stirring, the solution was heated at 60 °C for 30 min under N$_2$ gas. A solution of 2-aminophenylboronic acid pinacol ester in ethanol (10 mL) was syringed into the Schlenk flask and heated at 80 °C for 12 h under N$_2$ gas. The solvent was removed in vacuo and brought back into the glove box to be re-dissolved in acetonitrile and filtered through a pipette packed with glass wool and celite. A slow vapor diffusion of diethyl ether into an acetonitrile solution of ^{Bpin}PDIFeCl$_2$ afforded blue crystals identified as ^{Bpin}PDIFeCl$_2$ (10) (78%).

^{1}H NMR (CDCl$_3$): δ = 83.4 (s, 1 H, p-pyr), 80.0 (s, 1 H, o-pyr), 44.3 (s, 1 H, o-pyr), 24.9 (s, 1 H, ^{Bpin}Ar), 22.7 (s, 1 H, ^{Bpin}Ar), 15.8 (s, 1 H, ^{Bpin}Ar), 13.5 (s, 1 H, ^{Bpin}Ar), 10.0 (s, 1 H, o-^{iPr}Ar), 9.86 (s, 1 H, o-^{iPr}Ar), -3.10 (s, 1 H, p-^{iPr}Ar), -7.90 (s, 12 H, Bpin(CH$_3$)$_2$), -16.9 (s, 12 H, (C$\underline{H}_3$)$_2$CH), -17.6 (s, 2H, C$\underline{H}$(CH$_3$)$_2$), -25.5 (s, 3 H, (CH$_3$)C=N-^{Bpin}Ar), -29.9 (CH$_3$)C=N-^{iPr}Ar).

^{11}B{^{1}H} NMR (CDCl$_3$): δ = 38.2 (s, Bpin).

Evan's Method: μ_{eff} = 4.65 μ_B (solution), 4.73 μ_B (solid).

Elemental: C$_{33}$H$_{42}$BCl$_2$FeN$_3$O$_2$ (650.27): calcd. C, 60.95; H, 6.51; N, 6.46; found C, 59.47; H, 6.35; N, 6.47.

148
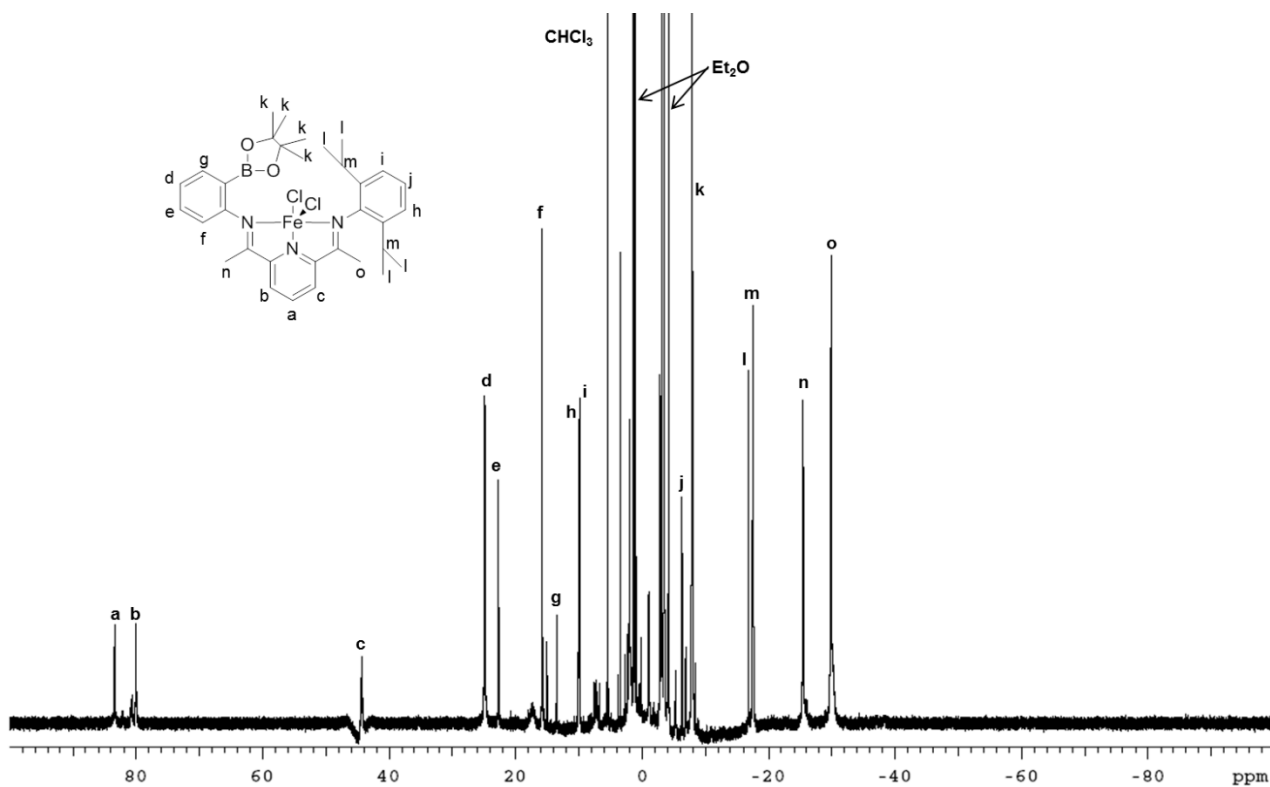
Figure 6.8. ^{1}H NMR spectrum of **10**, 500 MHz, CDCl$_3$.

Preparation of ^{MeNH}PDIFe(CO)₂ (11)

Preparation of ^{MeNH}PDIFe(CO)$_2$ (11)

(**8**) → CO 1 atm / 5 NaHg / DCM → (**11**)
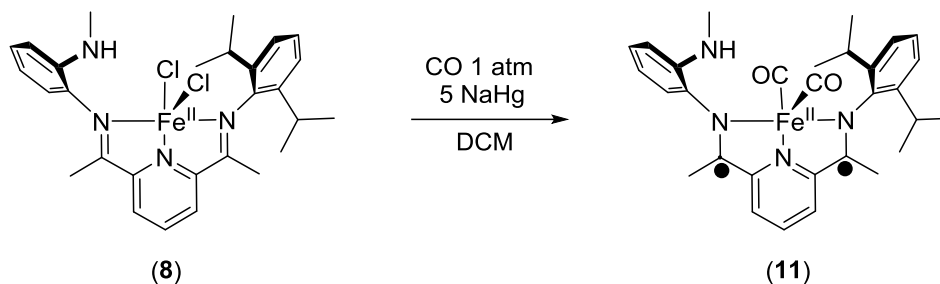
An 88 mL Fisher-Porter tube was charged with **8** (0.100 g, 0.181 mmol), sodium mercury amalgam (0.416 g), methylene chloride (10 mL) and CO gas (1 atm). The mixture was allowed to stir for 2 d, producing a green solution. The solvent was removed in vacuo and brought back into the glove box to be re-dissolved in diethyl ether and filtered through a pipette packed with glass wool and celite. Slow evaporation of the diethyl ether afforded green crystals identified as **^{MeNH}PDIFe(CO)$_2$ (11)** (76%).

FTIR (ATR): v(N-H) 3389 cm^{-1}, v(CO) 1945 and 1883 cm^{-1}.

^{1}H NMR (CD$_2$Cl$_2$): δ = 8.15 (dd, J = 7.3, 1.8 Hz, 2 H, o-pyr), 7.57 (t, J = 7.3 Hz, 1 H, p-pyr), 7.20 (m, 4 H, o,m,p-^{MeNH}Ar), 6.93 (dd, J = 7.9, 1.2 Hz, 1 H, o-^{iPr}Ar), 6.75 (t, J = 6.7 Hz, 1 H, p-^{iPr}Ar), 6.71 (d, J = 7.9 Hz, 1 H, o-^{iPr}Ar), 3.27 (q, J = 4.9 Hz, 1 H, NH), 2.74 (septet, J = 6.7 Hz, 1 H, C$\underline{H}$(CH$_3$)$_2$), 2.65 (d, J = 4.8 Hz, 3 H, NCH$_3$), 2.38 (s, 3 H, (CH$_3$)C=N), 2.35 (s, 3 H, (CH$_3$)C=N), 2.18 (septet, J = 6.7 Hz, 1 H, C$\underline{H}$(CH$_3$)$_2$), 1.27 (d, J = 6.7 Hz, 3 H, (C$\underline{H}_3$)$_2$CH), 1.09 (d, J = 6.7 Hz, 3 H, (C$\underline{H}_3$)$_2$CH), 1.06 (d, J = 6.7 Hz, 3 H, (C$\underline{H}_3$)$_2$CH), 0.92 (d, J = 6.7 Hz, 3 H, (C$\underline{H}_3$)$_2$CH).

^{13}C{^{1}H} NMR (CD$_2$Cl$_2$): δ = 217.5, 210.6 (2 s, Fe(CO)$_2$), 157.1, 150.1, 145.8, 142.2, 141.0, 140.0, 127.3, 126.7, 124.0, 123.5, 122.5, 121.8, 121.5, 118.2, 116.6, 111.0, 66.2, 30.8, 28.8, 27.8, 25.2, 24.9, 23.5, 23.1, 22.7, 16.8, 15.6, 15.5 ppm.

Elemetnal: C$_{30}$H$_{34}$FeN$_4$O$_2$ (538.46): calcd. C, 66.92; H, 6.36; N, 10.40; found C, 66.34; H, 6.98; N, 10.18.

Preparation of ^{Me2N}PDIFe(CO)$_2$ (12)
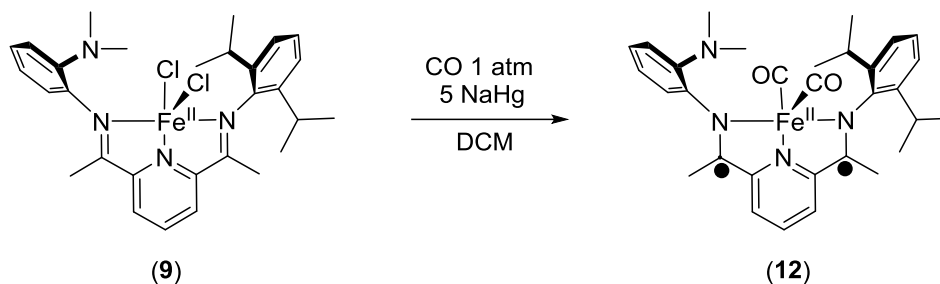
An 88 mL Fisher-Porter tube was charged with **9** (0.100 g, 0.176 mmol), sodium mercury amalgam (0.405 g), methylene chloride (10 mL) and CO gas (1 atm). The mixture was allowed to stir for 2 d, producing a green solution. The solvent was removed in vacuo and brought back into the glove box to be re-dissolved in diethyl ether and filtered through a pipette packed with glass wool and celite. Slow evaporation of the diethyl ether afforded green crystals identified as ^{Me2N}PDIFe(CO)$_2$ **(12)** (65%).

FTIR (ATR): ν(CO) 1951 and 1892 cm^{-1}.

^{1}H NMR (CD$_2$Cl$_2$): δ = 8.09 (dd, J = 7.8, 2.44 Hz, 2 H, o-pyr), 8.45 (t, J = 7.8 Hz, 1 H, p-pyr), 7.22 (m, 4 H, o,m,p-$^{(Me)2N}$Ar), 7.08 (dd, J = 5.9, 2.9 Hz, 1 H, o-^{iPr}Ar), 7.10 (dt, J = 7.8, 1.5 Hz, 1 H, p-^{iPr}Ar), 6.97 (dd, J = 7.8, 1.5 Hz, 1 H, p-^{MeO}Ar), 2.88 (septet, J = 6.8 Hz, 1 H, C$\underline{H}$(CH$_3$)$_2$), 2.40 (s, 3 H, (CH$_3$)C=N), 2.36 (s, 6 H, N(CH$_3$)$_2$), 2.33 (s, 3 H, (CH$_3$)C=N), 1.97 (septet, J = 6.8 Hz, 1 H, C$\underline{H}$(CH$_3$)$_2$), 1.35 (d, J = 6.4 Hz, 3 H, (CH$_3$)$_2$CH), 1.15 (d, J = 6.8 Hz, 3 H, (C$\underline{H}_3$)$_2$CH), 0.90 (d, J = 6.8 Hz, 3 H, (C$\underline{H}_3$)$_2$CH), 0.85 (d, J = 6.8 Hz, 3 H, (C$\underline{H}_3$)$_2$CH).

^{13}C{^{1}H} NMR (CD$_2$Cl$_2$): δ = 219.1, 209.1 (2 s, Fe(CO)$_2$), 156.2, 155.4, 149.8, 147.0, 145.8, 145.5, 145.2, 141.1, 139.2, 126.3, 126.0, 125.0, 123.4, 123.3, 121.2, 121.1, 118.3, 117.8, 65.7, 41.9, 27.4, 27.3, 25.3, 24.8, 23.9, 22.9, 15.9, 15.4, 15.2.

Elemental: C$_{31}$H$_{36}$FeN$_4$O$_2$•0.5C$_4$H$_{10}$O (589.26): calcd. C 67.23, H 7.01, N 19.50; found C, 67.15; H, 7.44; N, 9.34.

Preparation of ^{Bpin}PDIFe(CO)₂ (13)

Preparation of ᴮᵖⁱⁿPDIFe(CO)₂ (13)

(10)   (13)
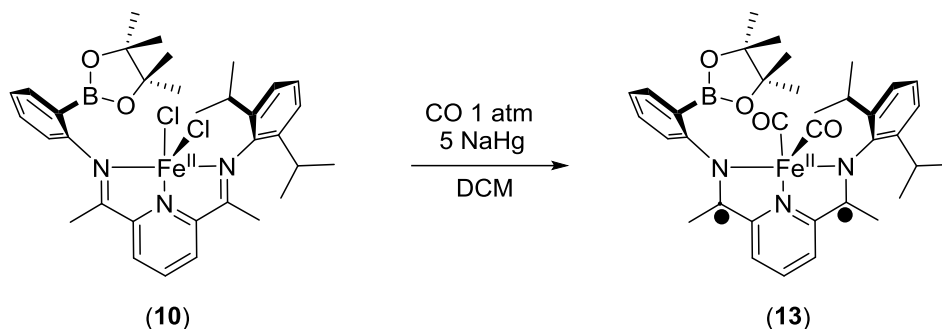
An 88 mL Fisher-Porter tube was charged with **10** (0.100 g, 0.154 mmol), sodium mercury amalgam (0.354 g), methylene chloride (10 mL) and CO gas (1 atm). The mixture was allowed to stir for 2 d, producing a green solution. The solvent was removed in vacuo and brought back into the glove box to be re-dissolved in diethyl ether and filtered through a pipette packed with glass wool and celite. Slow evaporation of the diethyl ether afforded green crystals identified as **ᴮᵖⁱⁿPDIFe(CO)₂ (13)** (61%).

FTIR (ATR): v(CO) 1950 and 1888 cm⁻¹.

¹H NMR (CD₂Cl₂): δ = 8.13 (dd, J = 7.9 Hz, 2 H, o-pyr), 7.69 (dd, J = 7.3, 1.2 Hz, 1 H, o-ⁱᴾʳAr), 7.56 (t, J = 7.3 Hz, 1 H, p-pyr), 7.48 (dt, J = 7.9, 1.22 Hz, 1 H, p-ⁱᴾʳAr), 7.22 (m, 5 H, o,m,p-ᴮᵖⁱⁿAr), 2.59 (septet, J = 6.7 Hz, 1 H, C$\underline{H}$(CH₃)₂), 2.54 (septet, J = 6.7 Hz, 1 H, C$\underline{H}$(CH₃)₂), 2.43 (s, 3 H, (CH₃)C=N), 2.36 (s, 3 H, (CH₃)C=N), 1.26 (d, J = 6.7 Hz, 3 H, (C$\underline{H}$₃)₂CH), 1.40 (d, J = 6.7 Hz, 3 H, (C$\underline{H}$₃)₂CH), 1.06 (d, J = 6.7 Hz, 3 H, (C$\underline{H}$₃)₂CH)), 1.02 (s, 6 H, Bpin(CH₃)₂), 0.92 (d, J = 7.3 Hz, 3 H, (C$\underline{H}$₃)₂CH), 0.86 (s, 6 H, Bpin(CH₃)₂.

¹³C{¹H} NMR (CD₂Cl₂): δ = 216.3, 213.1 (2 s, Fe(CO)₂), 159.9, 157.4, 155.6, 150.4, 145.4, 140.9, 140.8, 134.9, 131.1, 128.5, 126.5, 125.2, 124.0, 123.9, 123.4, 121.2, 120.9, 117.9, 83.6, 27.9, 27.8, 27.7, 25.2, 25.1, 24.9, 24.8, 24.8, 24.7, 24.2, 17.1, 16.8, 16.3, 14.4.

¹¹B{¹H} NMR (CD₂Cl₂): δ = 33.6 (s, Bpin).

Elemental: C₃₅H₄₂BFeN₃O₄•C₄H₁₀O (709.33): calcd. C, 66.16; H, 6.66; N, 6.61; found C, 65.83; H, 7.58; N, 6.11.

6.2 References

1. Bianchini, C.; Mantovani, G.; Meli, A.; Migliacci, F.; Zanobini, F.; Laschi, F.; Sommazzi, A. *Eur. J. Inorg.   Chem.* **2003**, 1620-1631.

2. P. Ren, O. Vechorkin, Z. Csok, I. Salihu, R. Scopelliti, X. Hu, *Dalton Trans*. **2011**, 40, 8906- 8911.

3. Sur, S. K. *J. Mag. Res.* **1988**, *82*, 169-173.

4. Berry. J. J. *J. Chem. Ed.* **2008**, *85*, 532-536.

5. Sheldrick, G. M. (1998). *Siemens Area Detector Absorption Correction Program*, Bruker 6. AXS Inc., Madison, WI, USA.

6. Van der Sluis, P.; Spek, A. L.; *Acta Cryst.* **1990**, A46, 194-201.

7. SHELXTL-6.10 "*Program for Structure Solution, Refinement and Presentation*" Bruker AXS Inc., 5465 East Cheryl Parkway, Madison, WI, USA

8. Bruker (2007) APEX2 (Version 2.1-4), SAINT (version 7.34A), SADABS (version 2007/4), 9. BrukerAXS Inc, Madison, Wisconsin, USA.

9. (a) Altomare, A.; Burla, C.; Camalli, M.; Cascarano, G. L.; Giacovazzo, C.; Guagliardi, A.; Moliterni, A.G.G.; Polidori, G.; Spagna, R. *J. Appl. Cryst.* **1999**, 32, 115-119. (b) Altomare, A.; Cascarano, G. L.; Giacovazzo, C.; Guagliardi, A. *J. Appl. Cryst.* **1993**, 26, 343-350.

10. Sheldrick, G.M. (1997) SHELXL-97, *Program for the Refinement of Crystal Structures*. University of Göttingen, Germany.

11. Mackay, S.; Edwards, C.; Henderson, A.; Gilmore, C.; Stewart, N.; Shankland, K.; Donald, A. (1997) MaXus: *a computer program for the solution and refinement of crystal structures from diffraction data*. University of Glasgow, Scotland.

12. Waasmaier, D.; Kirfel, A. *Acta Cryst*. **1995**, 51, 416-430.

13. Braun, S.; Kalinowski, H.-O.; Berger, S. *100 and More Basic NMR Experiments*. VCH: New York, 1996; pp 231-233